Louisiana State University
LSU Digital Commons

LSU Doctoral Dissertations | Graduate School

1-16-2018

Biomedical Applications of Hydrogels and GUMBOS

Kelsey Elizabeth McNeel
Louisiana State University and Agricultural and Mechanical College

Follow this and additional works at: https://digitalcommons.lsu.edu/gradschool_dissertations

 Part of the Analytical Chemistry Commons, and the Materials Chemistry Commons

Recommended Citation

McNeel, Kelsey Elizabeth, "Biomedical Applications of Hydrogels and GUMBOS" (2018). *LSU Doctoral Dissertations*. 4198.
https://digitalcommons.lsu.edu/gradschool_dissertations/4198

This Dissertation is brought to you for free and open access by the Graduate School at LSU Digital Commons. It has been accepted for inclusion in LSU Doctoral Dissertations by an authorized graduate school editor of LSU Digital Commons. For more information, please contactgradetd@lsu.edu.

BIOMEDICAL APPLICATIONS OF HYDROGELS AND GUMBOS

A Dissertation

Submitted to the Graduate Faculty of the
Louisiana State University and
Agricultural and Mechanical College
in partial fulfillment of the
requirements for the degree of
Doctor of Philosophy

in

The Department of Chemistry

by
Kelsey Elizabeth McNeel
B.S., Florida State University, 2011
May 2018

To my love for making each day better.

To my parents, the love and support you have given me through the years has made all the difference.

To all my friends and family for everything.

ACKNOWLEDGEMENTS

I would like to recognize the following people for their support:

Prof. Isiah Warner for his encouragement and support throughout my PhD process. I appreciate your help in making me my best. Thank you for the opportunity to work in your group.
Doctoral committee members: Profs. Doug Gilman, John Pojman, Cristina Sabliov, and (formerly) Daniel Hayes for the helpful discussions and suggestions throughout my time here.

Profs. Ioan Negulescu and Paul Russo and Dr. Rafael Cueto for use of their instrumentation and helpful discussions regarding my analyses.

Drs. Noureen Siraj, Susmita Das, and Pratap Chhotaray for the immense amount of help, support, and guidance.

Drs. Andre Striegel, Mallory Morris, Steven Rowland, and Dustin Richard for a good foundation and continued support.

Drs. Atiya Jordan, Jon Dumke, Leonard Moore, and Sergio De Rooy for helping me navigate the waters of graduate school.

The entire Warner research group, past and present, for support, criticism, helpful discussions, and friendship.

Funding agencies: National Science Foundation and Louisiana Board of Regents Fellowship

TABLE OF CONTENTS

LIST OF TABLES

LIST OF FIGURES

ABBREVIATIONS

γCD	gamma-cyclodextrin
λ	wavelength
A	absorbance
ANS	8-anilino-1-naphthalenesulfonic acid
AOT	bis(2-ethylhexyl) sulfosuccinate
b	pathlength
c	concentration
d	distance
DSC	differential scanning calorimetry
ε	molar extinction coefficient
F	fluorescence
G’	elastic or storage modulus
G”	viscous or loss modulus
G*	complex modulus
GUMBOS	Group of Uniform Materials Based on Organic Salts
HMT	1,1′,3,3,3′,3′-hexamethylindotricarbocyanine
I	transmitted light
I_0	incident light
IC	internal conversion
ISC	intersystem crossing
LMW	low molecular weight
NIR	near infrared
NaDC	sodium deoxycholate
Ntf_2	bis(trifluoromethane)sulfonimide

P	phosphorescence
Phe	phenylalanine
POM	polarized optical microscopy
Prodan	6-propionyl-2-(dimethylamino)naphthalene
φ	quantum yield
r	anisotropy
T	transmission
TEM	transmission electron microscopy
TRIS	tris(hydroxymethyl)aminomethane
TPB	tetraphenylborate
Trp	tryptophan
UV-vis	ultraviolet-visible
XRD	X-ray diffraction

ABSTRACT

Sodium deoxycholate (NaDC) is a small bile salt that was used in this dissertation to produce gelation of tris(hydroxymethyl)amino-methane (TRIS) solutions above, below, and near the pKa of NaDC. These solutions respectively yielded a neutral gelator, a charged gelator, and a mixture of each. Impacts of ionic interactions on gel formation were studied in detail and showed that pH can be used to modify many hydrogel properties including sol-gel temperature, crystallinity, and mechanical strength. It was also observed that pH modification of the hydrogels affected nanoparticle formation. Nanoparticles derived from a Group of Uniform Materials Based on Organic Salts (nanoGUMBOS), specifically cyanine-based NIR dyes, were templated within the hydrogel network for potential applications in tissue imaging. These nanoGUMBOS were found to be size-tunable, although material dependent.

Several hydrogel formulations yielded a unique rheological finding of two stable regions of elastic modulus. Release of different solutes was investigated under different hydrogel conditions and at variable shear rate. Temperature, solute size, hydrogel formulation, and shear rate were all found to impact solute release. This suggests that NaDC/TRIS hydrogels can be used as injectable, topical, or patch-type drug delivery vehicles or as solute delivery vehicles in applications such as fertilizers and packaging.

Enantiopreferential drug release from these hydrogels was also examined. Native gels exhibited significant release preference. This is of great importance to pharmaceutical applications due to the prevalence of racemic drugs. It was found that with facile modification, the enantiopreferential release could be inverted. Further

understanding of NaDC/TRIS gelation has broadened the tunability and multidimensional applications of these tailored hydrogel systems.

A three-component GUMBOS derived from fluorescein, rhodamine B, and tetradecyltrihexyl phosphonium was synthesized and characterized. Nanoparticles prepared from this GUMBOS exhibited dual-wavelength fluorescence. Ratiometric analysis of these two emission bands revealed changes with pH, specifically between the biologically relevant values of pH 5 and pH 7. Thus, fluorescence microscopy was employed to image cancerous and normal breast cells incubated with nanoGUMBOS. Higher uptake of nanoGUMBOS and more pervasive fluorescence intensity were found in comparison to normal cells, showing great potential for fast, visual determination of cancer cells.

CHAPTER 1.
INTRODUCTION

1.1. Classifications and properties of hydrogels

"The colloidal condition, the 'gel,' is one which is easier to recognize than define." This immortal quote of Jordan Lloyd in 1926 is a statement that still holds true today.[1] Hydrogels are prevalent in many areas of science and our everyday lives. For example, they are used as sensors,[2,3] in soft electronics,[4,5] and in drug delivery[6,7] in addition to use in shampoo, diapers, and contact lenses. For this reason, many tests and definitions have been developed for gel determination; yet all are incomplete or not fully inclusive.[1,8] One qualitative determination is the bubble rise test, in which a possible gel is bubbled with air. If the bubbles move through the sample on the timescale of the experiment, the sample is not a gel.[9] On the other hand, more quantitative tests, such as the modulus comparison test, rely on rheology.[8] A common definition of a hydrogel (a gel composed primarily of water or an aqueous solution) is a three-dimensional polymer network capable of retaining large amounts water.[10] This definition is, however, incomplete. An important distinction must be made between polymeric hydrogels and molecular hydrogels. The primary difference is the type of gelator, the molecule immobilizing the water, as named. While there are many common characteristics between these two classes, there are also many impactful differences.

Hydrogels of both classes tend to be viscoelastic, solid-like at low stress, and primarily composed of water.[11] It should be noted that there is a vast array of gelators with an equivalent variety of properties. Polymeric gels can be composed of a covalently crosslinked network of synthetic or biological polymers and generally have relatively

high mechanical strength. Molecular gels are often formed by noncovalent interactions such as hydrogen bonding, π-π stacking, and hydrophobic interactions. However, some molecular gels are covalently bound.[12] The gelator of a molecular gel is often a low molecular weight (LMW) molecule such as certain porphyrins[13] or bile acids. Therefore, these molecular gels are often referred to as LMW or physical hydrogels. Benefits of such gels include biocompatibility, simple and inexpensive synthesis, thermoreversibility, and stimuli response.[15] Each of these benefits is largely due to the lack of chemical crosslinking.[16] Polymeric hydrogels have vast applicability and benefits (such as high mechanical strength), and will be discussed briefly in this work. However, the focus of this dissertation will be on LMW hydrogels.

1.2. Development and types of molecular hydrogels

Of the currently known LMW hydrogelators, almost all have been discovered in the past 20 years.[12,17] Early examples were primarily found through serendipity. It is only in recent years that they have been strategically designed. Design of LMW hydrogelators began by formulating molecules with structural similarities to those found serendipitously.[12] For example, amphiphilic moieties and hydrogen bonding sites are prevalent in gelator design. The ability to rationally design a gelator has increased the application of hydrogels, because properties can be chosen to fit specific requirements.

The earliest known discovery of an LMW hydrogelator, uric acid, was documented in an 1841 paper by Lipowitz.[18] In 1892, Brenzinger found that dibenzoyl cysteine could be used as an LMW hydrogelator.[19] It has been suggested that such systems were not of interest until recent years due to the lack of terminology to describe and technology to understand the hydrogels.[20,21] Several classes of molecules,

including amino acids,[22,23] carbohydrates,[24,25] and surfactants,[26,27] were found to contain hydrogelators. With an increasing number of LMW hydrogelators discovered and the use of microscopy for visualization of gel structure, the 1900s saw a drastic increase in attention towards LMW hydrogels.[8] As a result, the natural desire to design LMW hydrogelators increased as well.

Rational design of small molecule hydrogelators began by mimicking and modifying organogelators (molecules known to gelate organic solvents) and hydrogelators that had previously been found serendipitously.[12,17] Common to most hydrogelators are hydrophobic domains, such as the tails of many surfactants, and hydrogen bonding sites, as in the hydroxyl groups of carbohydrates.[12] It can be expected then that any small molecule designed to be a hydrogelator might have one or both of these properties. In 1999 and 2000, the Hamilton group, for example, converted an organogelator to a series of hydrogelators by carboxylating and alkylating bis-urea.[28] A few years later, the Hanabusa group similarly converted a group of L-lysine based bis-amide organogelators to hydrogelators with the introduction of an ionic moiety, e.g. a cationic nitroaromatic group.[29] Once a hydrogelator was discovered, similar molecules were often broadly screened for other hydrogelators. For example, a collection of naphthalene-dipeptide hydrogelators was developed by the Adams group in 2010 by varying three different substituent groups.[30] As the library of LMW hydrogelators increases, so does the number of potential applications and consequently the number of hydrogelators designed for such specific functions.

Applications of hydrogels can be listed endlessly. This vast array includes drug delivery,[31,32] food (including processing and end-product),[33,34] cosmetics,[35] tissue

scaffolding,[36,37] material templating,[38,39] sensing,[40-42] soft electronics,[43,4] and optical devices.[44,45] It is important to realize that each application, even within the same category of use, requires a discrete set of properties of the chosen hydrogel. For instance, in tissue scaffolding applications the mechanical strength required of a gel can vary greatly depending on the type of tissue being mimicked.[46] It is for this reason that tunability is a strong benefit. Tunability can come from either modifications to the gelator as discussed, e.g. carboxylation or other functionalization, or from the addition of a modifier to the hydrogel formulation. Either mode of tunability, or indeed a combination of both, can provide the necessary characteristics for numerous applications.

While rational design of LMW hydrogelators began as an exploratory function, focus has now shifted to the intentional development of molecules with desired properties for use in a particular application. This approach has recently been aimed toward the development of stimuli-responsive hydrogels.

1.3. Stimuli-responsive hydrogels

Stimuli-responsive hydrogels are gels that change characteristics, or "respond," when introduced to a stimulus. Common stimuli of interest include pH, light, and ion concentration.[47] Sol-gel transitions are the most commonly exploited change in stimuli-responsive hydrogels.[14] However, volume changes,[48] optical properties,[49] swelling kinetics,[50] and conductivity[51] can also be affected by stimuli. These responsive hydrogels have gained recent interest because a change in physical or chemical properties in response to specified stimuli can be useful in many applications. For example, sensing and drug delivery can each be enhanced with stimuli-responsive materials.

LMW, physical hydrogels are particularly suited for development into stimuli-responsive materials based on three characteristics as described by Jan van Esch and colleagues[12] First, the absence of covalent bonds between gelator molecules facilitates reversible gelation. This can be exploited in response to various triggers. Second, if it is well understood which moieties of the molecule participate in gelation, the gelator can be modified to have varied and tunable properties. For example, alkyl chains are often added for enhanced aggregation in aqueous media. Changes in chain length may be used to change physical properties. Finally, gelator molecules self-assemble into highly ordered patterns. These characteristics allow for the design of LMW hydrogels as stimuli-responsive materials.

Sol-gel transitions that depend on pH are important in biological applications due to the specific pH of different parts of the body and caused by different conditions, such as the relative acidity of bacterial infections and cancer sites.[47] Polypeptides have been explored for these purposes by several groups.[52-54] The sequence of amino acids can be chosen such that sol-gel transitions take place at a wide range of pH values. A group of LMW hydrogelators based on N-(fluorenyl-9-methoxycarbonyl)-D-alanine-D-alanine have been shown to have a completely reversible sol-gel transition with change in pH.[55] In addition to full sol-gel transitions, some hydrogel materials have been developed to have pH-dependent shrinking and swelling.[52,56,57] This can be exceptionally useful for continued release in response to desired pH, rather than a single use system. A common theme in the design of pH-responsive systems for drug delivery applications is the use of pH-dependent moieties such as amines and carboxylic acids.[6] In every case, the ability to tune the transition pH for a desired application is ideal.

Response to temperature is another useful characteristic in hydrogels for drug delivery.[58] Among other uses, the most common is to employ a temperature induced gel-to-sol transition to release drugs within the body or a sol-to-gel transition for facilitated processing with the desired properties of a gel in vivo. Thus far, most work towards temperature-responsive hydrogels has been with polymeric gelators. Poly(*N*-isopropylacrylamide) seems to be the most popular material base for this type of application.[59,60] Other common thermoresponsive gelators include similar structures such as poly(*N,N*-diethylacrylamide)[61,62] and copolymers including one or both of these.[6] In addition to phase transitions, thermally triggered volume changes (i.e. swelling and shrinking) can also be useful in drug delivery. An interpenetrating network of poly(acrylic acid) and polyacrylamide, for example, swells in response to increased temperature, thereby changing the drug release rate.[63,64] It is ideal if modifications (such as changes in component ratio) can be made to the hydrogel system to modify these responses to best fit individual applications. As more is understood about LMW hydrogels, work with temperature response will follow.

While pH and temperature are common triggers for stimuli-responsive hydrogels, response to other stimuli is gaining interest as well. Response to biomolecules is rapidly gaining attention due to its specificity, especially systems for insulin release triggered by glucose concentration.[6] Hydrogels can also be designed to be responsive to light,[65,66] mechanical stress,[67] electrical field,[68,69] and salt composition or concentration.[70,71] The utility of hydrogels is demonstrated by the multitude of hydrogel phase transition and volume change triggers studied and a correspondingly high number of hydrogel materials. It also further illustrates that the vast array of hydrogel applications requires

an equal array of hydrogel systems to choose from; ergo, the design of new, specifically tunable, hydrogels is of the utmost importance.

1.4. Hydrogels in drug delivery

Hydrogels have long been investigated as drug delivery vehicles for two primary reasons. First, their inherent similarities to biological membranes make them suitable for such applications. Second, the wide range of hydrogel systems allows for diverse use across many types of delivery. For these two reasons, hydrogels have been applied in delivery systems ranging from wound dressings and topical applications to ocular and gastrointestinal deliveries.[32]

The general similarity of hydrogels to biological membranes is a many-faceted resemblance that can be made even stronger with intentional modifications. Arguably the most important similarities are those of high water content and high porosity.[72] The combination of these two properties facilitates diffusion of oxygen, nutrients, and drugs into sites of interest and diffusion of waste, heat, and dead cells out of the site.[31] Furthermore, specific gelators can be chosen or designed for increased biocompatibility and biodegradability. The development of stimuli-responsive hydrogels can be exploited to further enhance drug delivery. The benefits and diversity of hydrogel systems allow their broad application in several different types of drug delivery systems.

1.4.1. Modes of drug delivery

The requirements of drug delivery applications are at least as diverse and ever-changing as the large number of systems currently available, if not more so. Therefore, it is of great importance that new drug delivery vehicles are continually being designed

and explored. Different modes of delivery, such as gastrointestinal and ocular delivery, as well as their corresponding requirements of a delivery system will be discussed briefly as an example of the extent of this diversity.

Gastrointestinal environments are common targets of oral drug delivery.[73] Robust hydrogels are required for this type of application, because they need to protect drugs from harsh digestive processes until the desired site of application is reached. In addition to being robust, orally administered drug delivery vehicles also need to be nontoxic.[32] Polymeric gelators such as pectin,[74] cellulose acetate,[75] and other biopolymers are often chosen for this reason. Because each section of the digestive tract has a distinct pH,[76] hydrogels responsive to pH are particularly useful for gastrointestinal delivery.[51] For example, a system can be designed such that it degrades or swells at the pH value of the desired application site to release a drug. LMW gelators such as chitosan and alginate gels have both been used in such cases.[77,78]

Ocular delivery is a particularly challenging type of delivery due to the efficient disposal processes and protective barriers of the eye. Topical applications to the eye are often washed away or diluted due to the 75% loss of ophthalmic solution.[79] Membranes such as the conjunctiva and three layers of the cornea inhibit passage of foreign substances into the eyes and each has different requirements (e.g. polarity) for transportation to occur.[80] Injectable devices are one way to overcome these obstacles. P(NIPAAm-co-Dex-Lactate HEMA) hydrogels, for example, were developed for significant release when injected into the subconjuctival space of the eyes. Such

administration circumvents the eye's barriers, and the high release allows for sufficient dosing after dilution processes.[81]

Transdermal delivery of substances to the body can be speculated to date back to the body painting of our prehistoric ancestors.[82] Modern use of transdermal delivery began with a motion sickness patch in 1979 and has grown to include smoking cessation aids, hormone therapy, birth control, and many other uses. It was estimated in 2008 that over one billion transdermal patches were produced per year.[83] Transdermal delivery overcomes the discomfort and expense of injectable drug delivery vehicles. This type of delivery can also be used to avoid premature metabolism and harmful side effects that may be encountered with oral drug delivery vehicles. As with ocular delivery, the difficulty with transdermal application is the natural barriers that have evolved to keep exogenous substances out.[84] Hydrogels have been useful in the design of transdermal patches due to the broad flexibility of their design,[85] their ability to contour to the application site, and their ability to be coupled with iontophoresis (a method of applying an electric field to induce transport across the membrane).[86] Poloxamer 407 gels were found to release peptide drugs such as insulin transdermally, enhanced by coupling with iontophoresis. This study exhibits an additional benefit of using a gel system in that chemical enhancers can be loaded within a gel system to further facilitate drug transport through the skin.

Subcutaneous delivery has become a popular approach used to completely bypass the skins natural barriers. Lee et al. designed triblock PEG copolymers for subcutaneous antibody delivery.[87] For subcutaneous delivery, it is desirable that hydrogels be injectable at ambient conditions for facile administration. In many cases,

however, hydrogel materials are not injectable at ambient conditions, making thermoresponsive properties desirable for subcutaneous applications. For that reason, it is desirable to design hydrogels with sol-to-gel transition at body temperature for subcutaneous injection, such as the chitosan/polyelectrolyte gels designed by Matanovic et al. for heparin release.[88]

1.4.2. LMW benefits of hydrogels for drug delivery

As has been previously mentioned, LMW hydrogels can provide significant enhancements in drug delivery applications. In many ways the synthesis of LMW hydrogels, specifically, is superior to that of polymeric hydrogels when used for drug delivery applications. For example, LMW hydrogels typically do not require harsh initiation triggers because they are self-assembled.[89,90] A common problem with polymeric systems is the high probability of the presence of unreacted monomer, typically a toxic molecule.[91,92] The small molecules used to gelate aqueous solutions are typically nontoxic, thereby eliminating this complication. Synthesis of LMW hydrogels are often less expensive than comparable polymeric systems due simply to the reduction of steps. Initiation, subsequent polymerization, and removal of unreacted monomer and crosslinker are typically not required steps in the synthesis of LMW hydrogels. Simple and inexpensive synthesis means that such materials can be used in a multitude of more common applications in addition to vital or sophisticated applications.

The absence of a chemical crosslinker in and of itself provides a multifaceted advantage. Firstly, crosslinkers tend to be toxic, so any unreacted excess will be a deficiency.[72] Most importantly, however, are the properties resulting from the absence of

chemical crosslinking, namely thixotropy and thermoreversibilty.[93] Agitation and temperature can each temporarily disturb the physical interactions immobilizing an LMW hydrogel. However, the reestablishment of hydrogen bonding, π-π stacking, hydrophobic interactions, etc. will occur over time, thereby gelating again. Because this "physical crosslinking" is more easily perturbed than a chemical crosslink, biodegradation and excretion from the body are typically superior in LMW hydrogels.[17]

As with all hydrogel applications, it is important to note that different properties are beneficial for different types of drug delivery applications. Drug delivery can be categorized by the route of delivery. Wound dressing, subcutaneous, ocular, oral, and surgical implantations are a few representative types of delivery, each with specific needs from a delivery system. Hydrogels used as wound dressings for example, should have maximum porosity for removal of waste and transfer or oxygen, drugs, and nutrients.[94,95,96] They should also be deformable, as opposed to a rigid gel, in order to increase contact area (thereby facilitating molecular and heat diffusion further), and to provide a physical barrier to microbes and physical damage.[97,98] Ocular delivery, on the other hand, requires a hydrogel that can withstand the rapid degradation processes of the eyes. This can be attained through use of a more rigid contact lens.[99]

LMW hydrogels exhibit properties that make them beneficial for many types of drug delivery.[31,32,100] Facile, inexpensive synthesis makes them widely applicable, while the absence of chemical crosslinking provides additional benefits. Thermoreversibility, thixotropy, simple biodegradation, and biocompatibility all enhance LMW hydrogels toward drug delivery applications. The wide variety of available LMW gelators also

allows for selection of properties suited for a specific desired application. Bile salts are one example of LMW gelator and will be explored further in this dissertation.

1.5. Bile salt gels

Bile salts are a class of molecules found in the liver of most vertebrates. Their ability to form micelles contributes to digestion, dietary fat absorption, cholesterol elimination, and other metabolic processes.[101] This type of salt comprises a large family of molecules, but all are derived from cholesterol and consequently share some of its characteristics. Cholesterol and all bile acids have a steroid backbone. This includes three six-membered rings and one five-membered ring (see Figure 1.1) and a five- or eight- carbon side chain often ending in a carboxyl group. Variation between different members of this class can be due to varied hydroxylation and leads to different properties and, consequently, functions.

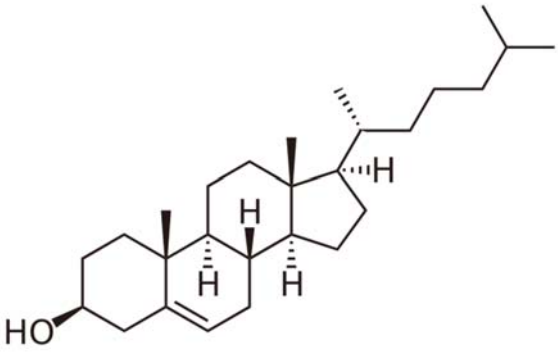

Figure 1.1. Structure of cholesterol.

Bile salt media is used to distinguish pneumococcus (the pneumonia-causing bacteria) from other cocci (spherically-shaped bacteria) based on dissolution.[102,103] The serendipitous discovery of bile salt hydrogelation was first documented through this use. Harry Sobotka and Nina Czeczowiczka were consulted about this discovery and, in

1958, published the first study investigating bile salt hydrogels.[104] The gelation of deoxycholic, cholic, glycocholic, and lithocholic acid was explored. They found that deoxycholic and lithocholic acid each formed gels while the others did not. A cholic acid trimer (tripodal cholamide), however, was found by Uday Maitra and colleagues to gelate water and aqueous solutions.[105] As is found throughout the literature, this is an indication of the sensitivity of LMW physical hydrogels. For gelation to occur there must be a delicate balance between the hydrophobic and hydrophilic moieties and between the physical interactions immobilizing the network.[17] Moreover, even molecules that do exhibit the needed balance require certain conditions for gelation. With bile acids for instance, a relatively low pH is often needed to increase the aggregation number sufficiently for gelation.

Gelation by these molecules can be attributed to several of their characteristics.[11,106] Bile acids have a relatively hydrophilic convex face due to the presence of hydroxyl groups. They also have a relatively hydrophobic concave face due to the presence of aliphatic groups. This results in a facial amphiphilicity that imparts hydrophobic interactions and, consequently, aggregation. Additionally, hydroxyl groups can participate in hydrogen bonding, further ordering a bile salt solution.

Despite the fact that bile salt gels have been around for several decades, significant work is still being done on their development. This widespread interest is due in part to the fact that bile salts are highly derivitizable.[14] This means that systems can be facilely designed and tuned for specific applications. Applications of bile acid gels are widespread and include everything from sensing materials to nanoelectronics to drug delivery systems.

From about 1958-1960, Blow and Rich did pioneering work on the understanding of the gelation mechanism of bile salts, specifically sodium deoxycholate.[107,108] It was found that gelation of deoxycholate solutions is related to the surfactant properties of the molecule and the resultant micelle formation. Unlike typical micelles, deoxycholate molecules form "huge," helical micelles with regular intervals. The large helices (determined to be 36 Å) are relatively rigid and, most importantly, have a large degree of molecular specificity in relation to typical micellar systems. That is to say, small changes to the deoxycholate structure can result in a complete destruction of the complexing process. Another important distinction between a typical micelle and deoxycholate hydrogels is the observation of crystalline spacing. While soap solutions are determined to be "liquid,"[109] deoxycholate gels exhibit a definite crystalline spacing when analyzed by X-ray diffraction. These findings were critical for the further understanding, development, and application of deoxycholate hydrogels.

Uday Maitra is a leader in the field of bile acid gels. His group has done work with several different bile acid gelators under many sets of conditions. [105,106,110,111,112] Goals of this group include development of a broad array of systems for various applications in addition to further understanding the properties of the gel, including structure and dynamics. The Maitra group employed a battery of techniques in order to characterize these materials. This includes spectroscopy techniques (e.g. steady-state and time-resolved fluorescence, dynamic light scattering), mechanical techniques (e.g. rheology, viscometry), and other techniques such as electron microscopy and neutron scattering.

Bile acid gels have a long history of development that still continues in current research, as evidenced by the continual publication of research articles, books, and

review papers. Gelators have been designed and discovered with neutral, cationic, and anionic side chains.[72,113,114] Gelation has been found to be influenced by many factors. One such factor is the pH value of the aqueous solution to be immobilized.[115] In almost all cases, a more acidic solution enhanced strength and speed of gelation. Salt concentration was also found to influence many systems. However, this is a more complicated factor. In some cases, salt enhances gelation[116] while in others, it disrupts or inhibits it.[117] As previously mentioned, the most important thing to note about such varied systems is that each profile of properties can be suited toward specific applications.

The applications of bile acid gels are as many and varied as the number of systems available. Common applications can be categorized into groups including use as rigid platforms, molecular recognition devices, separation membranes, synthesis templates, use in optoelectronics, and biological applications. Some examples will be described herein; however, there are many review articles that discuss these applications in detail. [118-122]

Rigid platforms, such as a hydrogel, can be used to direct molecular orientation and immobilize molecules within a network. The Shinkai group, for example, utilizes this immobilization for use as a fluorescence-based pH sensor.[123] A fluorescent moiety, 1,10-phenanthroline, was incorporated into a cholesterol-based gel. Both fluorescence intensity and emission wavelength were found to change with proton concentration in this study. Due to the immobilization properties of the hydrogel network, the rigid platform can also be used for the promotion of electronic energy transfer.[110]

An emerging use of bile acid hydrogels is for the templating of nanomaterials synthesized within the hydrogel network. Bhattacharya, a leader in the field of bile acid gels, used stearic acid-based hydrogels for controlled templating of silver nanoparticles.[124] Bile acid hydrogels are well suited for nanotemplating because of their well-defined and easily tunable properties. Bhat and Maitra have also used thiolated cholic acid-based hydrogels to template and stabilize gold nanoparticles.[111] This is an important application of hydrogel materials due to the many uses of metal nanoparticles.

Bile acid hydrogels are particularly well-suited for biological applications due to their high water content, porosity, and biocompatibility. Drug delivery will be discussed in detail in the following sections. Other biological applications include use as artificial tissues[125] and cell immobilization. Cell immobilization not only utilizes, but requires, the high porosity and rigid mesh network of a hydrogel. Cells are large enough that they are "macroencapsulated" within the gel network.[126-128] The porosity allows for diffusion of nutrients and oxygen into the cells and waste and heat out of the cells.[46]

Regardless of the category of application, stimuli-responsive bile gels can be used for enhancement. As discussed with other stimuli-responsive materials, bile gels have been designed to respond to external stimuli such as light,[129] temperature[130,112] and pH with changes in phase, color, or volume. The Kolehmainen group, for example, has designed a stigmasterol-based hydrogelator that has a sol-gel transition triggered by acidification.[131] Conversely, Liu et al. designed a cholesteryl glycinate-based hydrogelator that has a sol-gel transition with the addition of a base.[132] The multitude of

bile acid gelators and their endless tunability provide potential for design of many stimuli-responsive bile gel materials.

1.5.1. Bile salt gels in drug delivery

Thus far, bile gel drug delivery has not been exhaustively explored, although some important work has been published indicating great potential. The Bernkop-Schnürch group was the first to evaluate sodium deoxycholate hydrogels for their use as drug delivery vehicles.[133] Release of the model drug rutin was examined and determined to be affected by sugars such as mannitol. Deoxycholate hydrogels were found to enhance permeation in this case. This property can be extremely beneficial for increasing drug uptake. Due to the many potential benefits of bile salt hydrogels and the lack of research using them, there is a significant opportunity for exploration in this field.

1.5.2. Benefits of NaDC/TRIS hydrogels

The primary focus of this dissertation is the development and exploration of sodium deoxycholate (NaDC)/tris(hydroxymethyl)aminomethane (TRIS) hydrogels. These hydrogels are LMW and physically crosslinked, meaning that they have all the advantages associated with such systems as previously described. In addition to thixotropy, thermoreversibility, biocompatibility, etc., they also exhibit a host of other benefits that make them suitable for drug delivery and other applications. These beneficial properties will be discussed and demonstrated at length in the following chapters. In summary, NaDC/TRIS hydrogels are highly tunable with facile modifications, injectable at room temperature, optically transparent, and can be loaded

with drugs or other materials concurrent with gelation. Therefore, NaDC/TRIS hydrogels are exceptional candidates for a multitude of applications.

1.6. Group of Uniform Materials Based on Organic Salts for biomedical applications

Hydrogels are only one example of interesting materials for biomedical applications. A *G*roup of *U*niform *M*aterials *B*ased on *O*rganic *S*alts (GUMBOS) also show great promise and utility in the field of biomedicine. The term GUMBOS refers to organic salt materials with a melting point range of 25 to 250 °C renowned for tunability and broad applicability.[134-138] In some respects, GUMBOS may be thought of as solid phase ionic liquids since the same counterions are often used in both. Primary differences lie in the melting point range of these organic salts. While applications of ionic liquids are extensive due to longer existence, GUMBOS have more recently proven useful in applications as varied as solar cell sensitization[139] and molar mass sensing of volatile organic compounds by use of quartz crystal microbalance.[140] This dissertation will involve discussion and application of GUMBOS for biomedical applications. Thus far, GUMBOS have been used in at least three notable ways toward this field. Li et al. exploited the facile tunability of GUMBOS to incorporate luminescent and paramagnetic properties into several GUMBOS found to selectively target cancer cells *in vitro*.[141] The inhibition of growth in tumor cells was attributed to a cation choice of aryltriphenylphosphonium. Tunability of GUMBOS has also been exploited by Magut et al., demonstrating an improvement in selective cytotoxicity toward cancer cells with a simple change in anion.[142] Das et al. have investigated the intersection of two exciting materials, GUMBOS and LMW hydrogels.[143] In that study, LMW hydrogels were shown to provide a tunable template for nanoGUMBOS synthesis. Nanoparticle size and

spectral properties were found to be tunable in ways pertinent for a variety of biomedical applications. For example, fluorescence emission wavelength was tuned with slight modification to the hydrogels. These exceptional materials, GUMBOS and hydrogels, show great potential for biomedical applications ranging from imaging to drug delivery vehicles to active drugs. Both will be explored further in this dissertation.

1.7. Instrumentation

1.7.1. Ultraviolet-visible spectroscopy

Ultraviolet-visible (UV-vis) spectroscopy is an analytical technique used for qualification and quantification of molecules that absorb light in the UV-vis range of the electromagnetic spectrum, from about 200-800 nm. UV-vis spectrophotometers are typically comprised of a light source, monochromator, sample holder, and detector (Figure 1.2). Light from the source is passed through a monochromator so that absorption can be measured at distinct wavelengths. The filtered light reaches the sample, and a portion of the light is transmitted through the sample and measured by the detector, typically a photomultiplier tube or a photodiode. Transmission (T) is the ratio of incident light (I_0) to transmitted light (I), and absorbance (A) is calculated as the negative natural log of transmission.

$$T = \frac{I}{I_0} \qquad A = -lnT$$

Beer-Lambert's law can be used to calculate sample concentration from absorbance using the equation A=εbc, where ε is the molar absorptivity coefficient characteristic of a molecule, b is the pathlength of the light through the sample, and c is the concentration of the molecule in the sample.

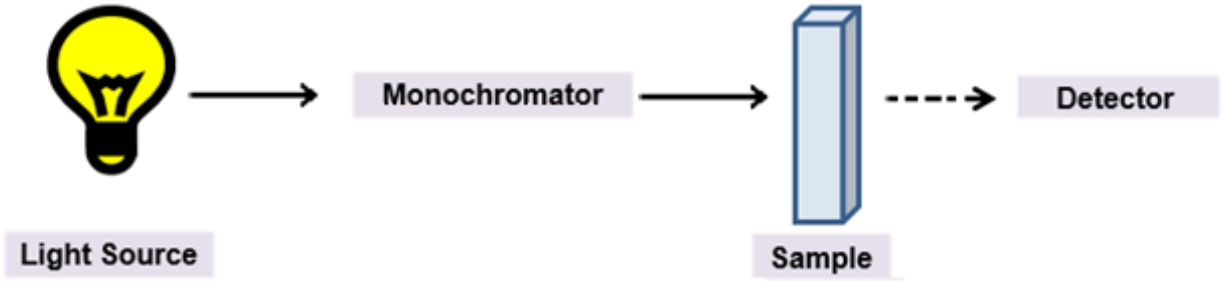

Figure 1.2. Schematic representation of a UV-vis absorbance instrument.

1.7.2. Fluorescence spectroscopy

Fluorescence is a phenomenon associated with radiative transitions of a molecule between energy states of the same multiplicity, for example from the excited S_1 singlet state to the ground S_0 singlet state. Fluorescence spectroscopy is a technique used to measure and analyze the radiative light emitted during this phenomenon. For aromatic hydrocarbons, fluorescence occurs on a timescale of 10^{-9} seconds. A proportionality constant called quantum yield (φ_f) can be used to describe the ratio of photons that fluoresce to the number that was absorbed:

$$\varphi_f = \frac{\#\ of\ molecules\ that\ fluoresce}{\#\ of\ molecules\ that\ absorb\ light}$$

Fluorescence and related processes are commonly illustrated in a Jablonski diagram (Figure 1.3). Absorbance (A) and fluorescence (F) are depicted along with the competing processes of internal conversion (IC), intersystem crossing (ISC), and phosphorescence (P). IC is a nonradiative decay between two coupled vibrational states of different energy levels. ISC is also a nonradiative transition occurring between two states of different multiplicities, promoting phosphorescence. Phosphorescence

occurs after ISC to a different multiplicity (e.g. singlet to triplet). It typically occurs on a much slower time scale than fluorescence because it is a kinetically unfavored transition.

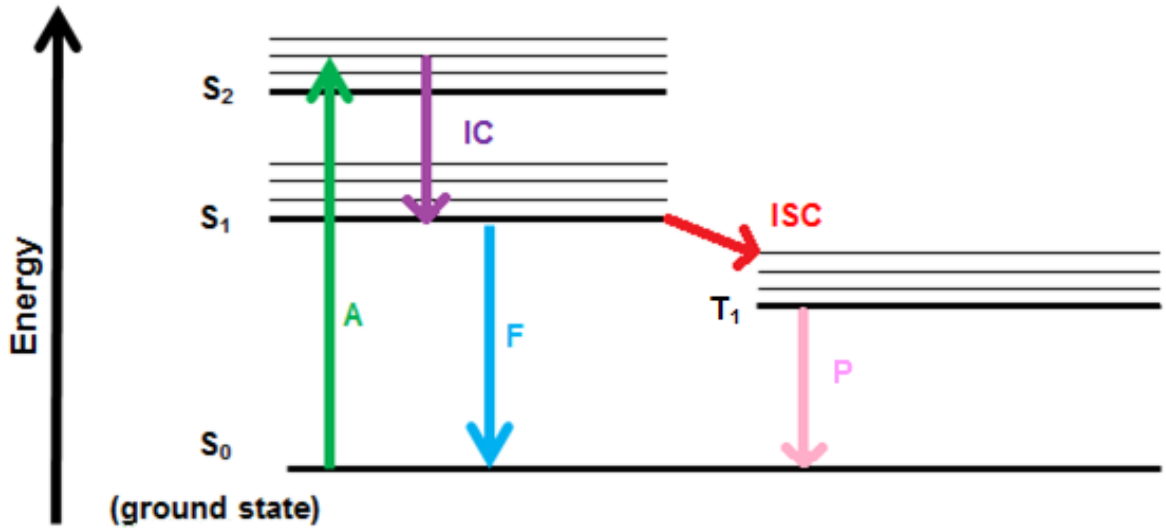

Figure 1.3. Jablonski diagram depicting absorbance (A), fluorescence (F), and competing processes (IC, ISC, P).

Instrumentation for fluorescence spectroscopy is typically configured in a right angle geometry (Figure 1.4) Typical light sources include mercury or xenon arc lamps. Light passes through a monochromator before reaching the sample. Light emitted at 90° from the incident light is primarily passed through a second monochromator and collected. Photomultiplier tubes are often used for signal amplification before data is sent to the computer for processing.

1.7.3. Differential scanning calorimetry

Differential scanning calorimetry is a type of thermal analysis in which the difference in heat flow between a sample and a reference is measured as a function of temperature. Small aluminum pans containing the sample and reference materials are

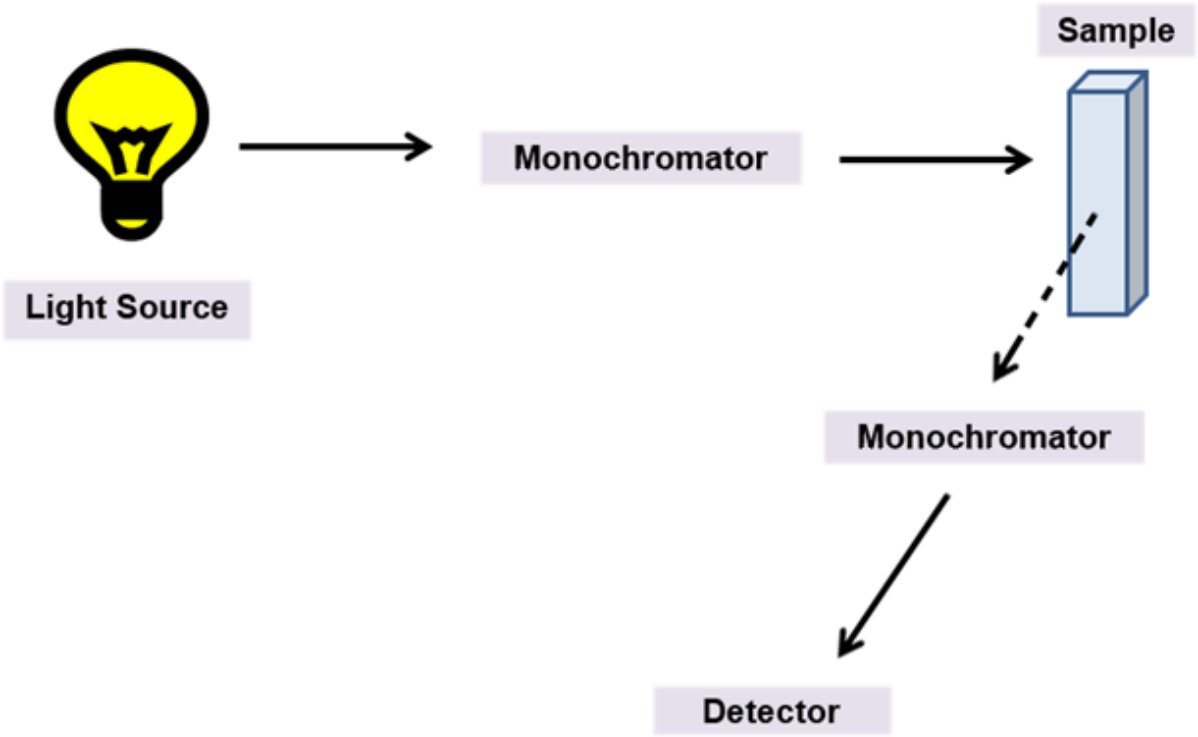

Figure 1.4. Schematic diagram of a fluorescence spectrophotometer.

heated concurrently in a sample chamber. Typically, heating is computer controlled and linear at a specified rate, for example 5 °C/minute. Thermocouple junctions are used to quantify the differential heat flow of the sample and reference. The resulting output from the computer is a thermogram (Figure 1.5), a plot of temperature versus differential heat flow.

Applications of DSC often include investigation of transitions. For example, melting point onset and maximum melting temperature can be found through DSC. Similarly, DSC can be used to determine the glass transition temperature. For amorphous materials, this is the temperature at which the material reversibly transitions between a flexible state and a brittle state. Through integration of thermogram curves,

the enthalpies of transitions can be found as well. DSC can also be used to obtain information on crystallization such as degree of crystallization and changes in crystalline phase, such as with dissolution. Similarly, formation of liquid crystals or eutectic points can be determined as well. The many applications of DSC have been used in industries such as pharmaceuticals for determination of drug purity and food industries for processing and packaging temperatures. Any event, chemical or physical, that results in a change of heat flow (exo- or endo-thermic) can be considered for DSC evaluation.

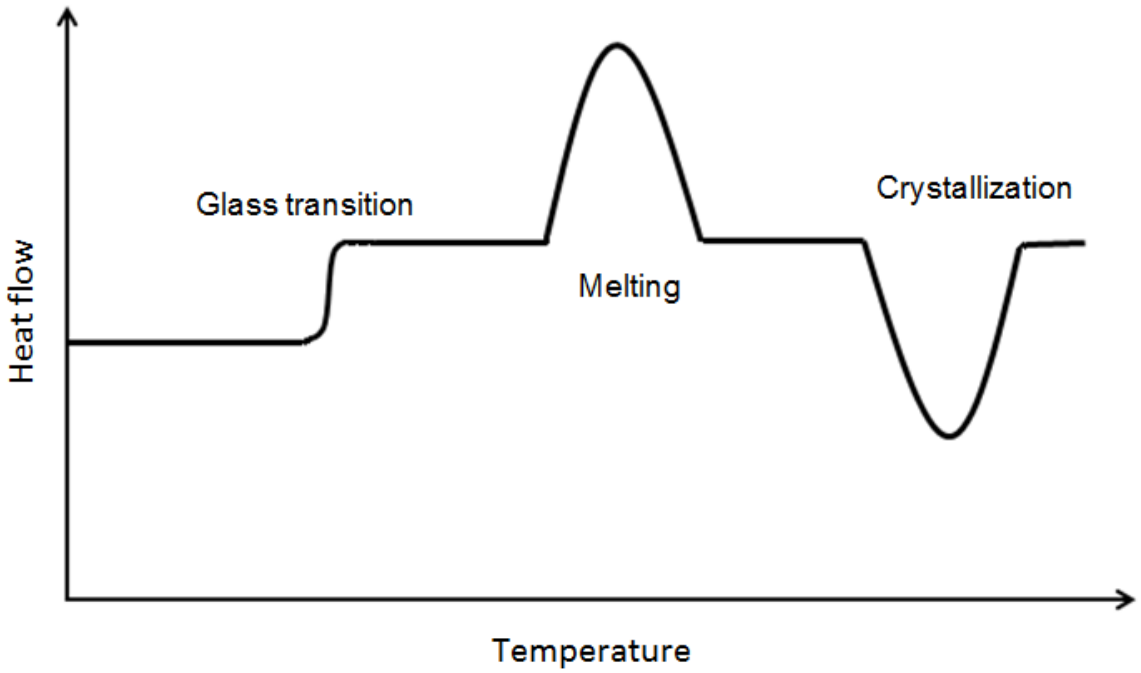

Figure 1.5. Depiction of a thermogram including typical transitions. Note that in a thermogram, endothermic transitions may be represented as “up” or “down” with exothermic transitions being the opposite.

1.7.4. Polarized optical microscopy

Polarized optical microscopy (POM), also called cross-polarized light microscopy, is a technique used for visualization of birefringence, typically giving information about

the crystallinity of a material. The apparatus is that of a typical optical microscope with the addition of a pre-sample polarizer and a post-sample polarizer, often called an analyzer. The unfiltered light source vibrates at all angles along an axis until it reaches the first polarizer, reducing the vibration to one plane. The second polarizer is set at 90° (hence “cross-polarized”), so that only light that has been split from the original plane is observed. Birefringence is an indication of crystallinity. Therefore, the images obtained reveal the organization and geometry of a material’s crystal packing. A sample that does not exhibit birefringence, such as an amorphous material, will result in a dark image.

1.7.5. X-Ray diffraction

X-Ray diffraction (XRD) is an analytical technique based on diffraction of x-rays in a crystalline sample. Bragg’s law describes a condition of scattering in which:

$$n\lambda = 2d \sin\theta.$$

where n is an integer, λ is the incident wavelength, d is the distance between planes of the sample crystal, and θ is the beam angle. In order to fit this law, the interplanar distance must be approximately equal to the incident wavelength. Resulting diffraction patterns can give information on the phase of the sample material, the spatial arrangement of atoms within a crystal, and, with use of a database, the chemical makeup of a sample. Degree of crystallinity can also be determined using the intensity of scattering. The instrumentation is parallel to any spectroscopic method in that there is a source, a filter or monochromator, a sample holder, a detector, and a processor (Figure 1.6). X-rays are typically produced by a cathode ray tube. When the incident

beam reaches the sample, any crystallinity that obeys Bragg's law will result in a diffracted beam. The pattern is typically processed as 2θ versus electron counts and can be used as a fingerprint for a particular substance.

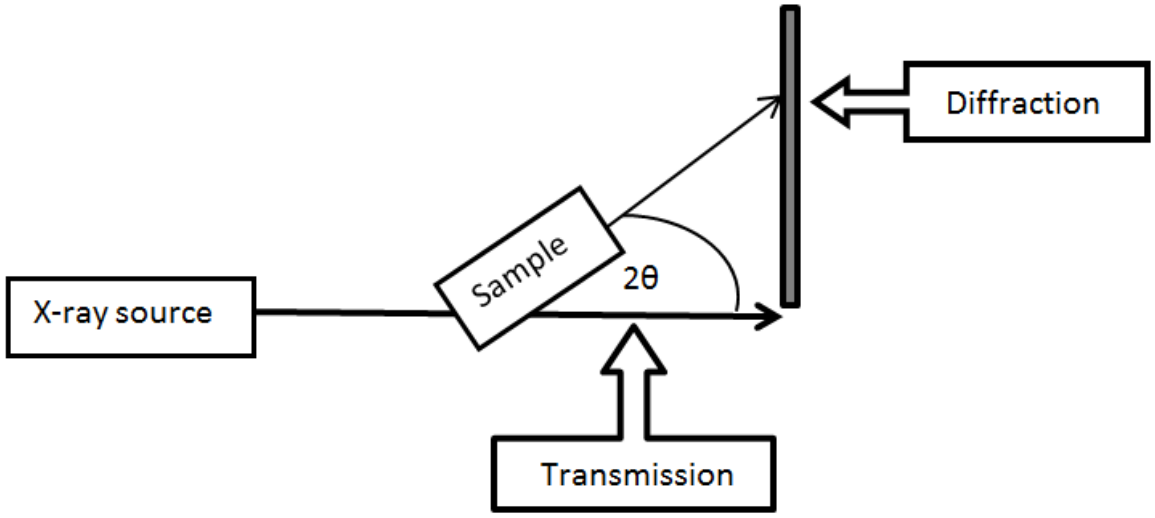

Figure 1.6. Schematic diagram of an x-ray diffractometer. An x-ray source bombards a sample, and the diffraction pattern is recorded.

1.7.6. Transmission electron microscopy (TEM)

Electron microscopy is a technique used to overcome the resolution limitations of typical optical microscopes by using an electron beam under vacuum instead of a light beam. Due to the enhanced magnification, electron microscopy has become a valuable tool for the visualization of nanoscale materials. An electron gun generates an electron beam that is focused on the sample using a series of lenses (Figure 1.7). Samples are thinly coated onto a grid often composed of carbon-coated copper. In transmission electron microscopy (TEM), the electrons transmitted by the sample are captured as an image by a phosphorescent screen and a charge-coupled device (CCD). Consequently,

areas of the sample that are denser result in a darker image, while areas that are less dense result in a brighter image.

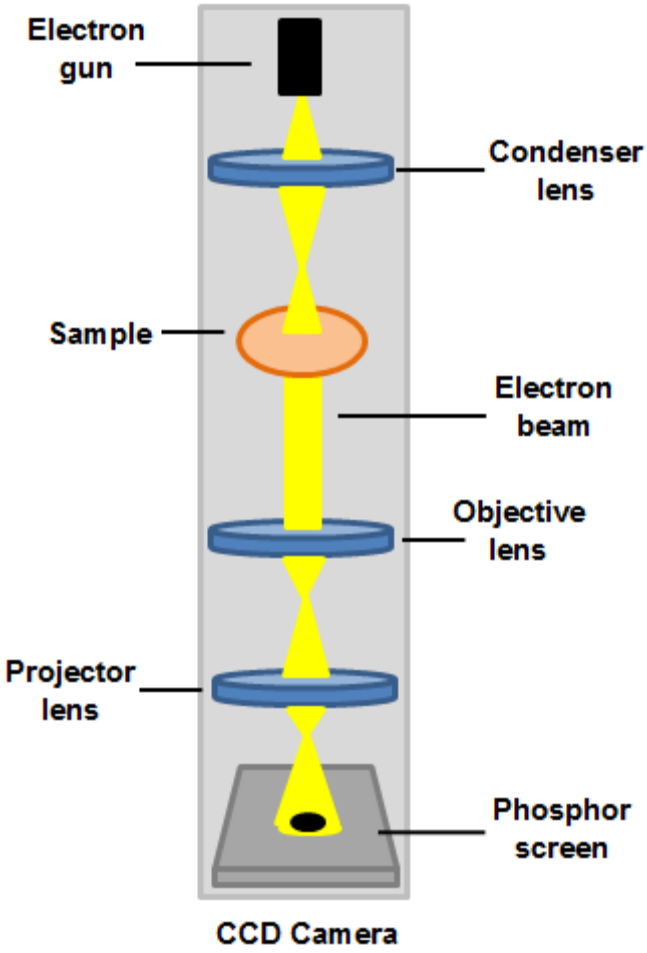

Figure 1.7. Schematic diagram of a transmission electron microscope. The yellow represents the path of the electron beam through sample and lenses.

1.7.7. Rheology

Rheology is the study of the flow properties of a material. In a typical experiment, stress is applied to a material while the resulting strain is measured. One type of instrumentation does this with a parallel plate geometry (Figure 1.8). This analytical technique can be used to gain understanding of complex structures such as colloids and suspensions. Behaviors such as thixotropy, shear thinning, or shear thickening can

be analyzed by rheology as well. Essentially, rheology is useful for viscoelastic materials, those that exhibit both fluid-like and solid-like responses to stress. Viscoelasticity is represented by the complex modulus, G*. The complex modulus is composed of two moduli, the viscous or loss modulus (denoted G") and the elastic or storage modulus (denoted G'). The terms viscous and elastic refer to the solid- or liquid-like behavior of the material. The terms loss or storage refer to whether energy is stored in the material or released as heat. The scope of applications of this technique is extremely broad and varied. Within this dissertation, rheology is used to determine the mechanical strength of hydrogel materials as determined through examination of the elastic modulus and for a controlled rate of shearing.

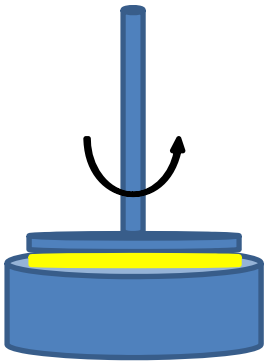

Figure 1.8. Diagram of a plate geometry rheometer. The sample of interest (yellow) is pressed between a sample holder and an oscillating plate.

1.8. Scope of the dissertation

In this dissertation, I explore the use of two new materials in a variety of biomedical applications – NaDC/TRIS-based hydrogels and two different GUMBOS. Chapters 2 and 3 are an examination of the characteristics and delivery applications of a new class of materials, sodium deoxycholate/TRIS-based hydrogels. In Chapter 2, the

effects of modifications to the pH and concentration of the buffer solution on the properties of the resultant hydrogel were evaluated. A broad range of analyses including thermal and mechanical measurements was performed to better understand the characteristics of these materials. These materials were also evaluated for their use in templating organic nanoparticles derived from GUMBOS. Preliminary studies also probed the use of NaDC/TRIS hydrogels for use as injectable drug delivery vehicles. In the third chapter of this dissertation, several formulations of NaDC/TRIS hydrogels were evaluated as sustained release devices. The effect of shearing was tested to determine the utility of the materials as injectable or spreadable drug delivery devices compared to implanted or dressing applications. The effects of drug size, temperature, and loaded drug concentration were also examined. The use of NaDC/TRIS hydrogels for enantioselective drug release is also investigated in this chapter. In addition to preferential release of one enantiomer in the native state, modifications were also found to switch the preferential release to the other enantiomer. Chapter 4 is a description of the synthesis of a three component GUMBOS derived from fluorescein, rhodamine B, and tetradecyltrihexyl phosphonium. Nanoparticles of this material were explored as a ratiometric, FRET-based pH sensor with particular sensitivity between the biologically relevant pH values of 5 and 7. Fluorescence microscopy of these nanoGUMBOS varied greatly between cancer and normal cells, indicating incredible potential for use of these nanoGUMBOS in visual diagnosis of cancer

1.9. References

1. Nishinari, K., Some thoughts on the definition of a gel. In *Gels: Structures, Properties, and Functions*, Springer: 2009; pp 87-94.

2. Shin, J.; Han, S. G.; Lee, W., Dually tunable inverse opal hydrogel colorimetric sensor with fast and reversible color changes. *Sensors and Actuators B: Chemical* **2012,** *168*, 20-26.

3. Manandhar, P.; Calvert, P. D.; Buck, J. R., Elastomeric ionic hydrogel sensor for large strains. *Sensors Journal, IEEE* **2012,** *12* (6), 2052-2061.

4. Kishi, R.; Kubota, K.; Miura, T.; Yamaguchi, T.; Okuzaki, H.; Osada, Y., Mechanically tough double-network hydrogels with high electronic conductivity. *Journal of Materials Chemistry C* **2014,** *2* (4), 736-743.

5. Ding, H.; Zhong, M.; Kim, Y. J.; Pholpabu, P.; Balasubramanian, A.; Hui, C. M.; He, H.; Yang, H.; Matyjaszewski, K.; Bettinger, C. J., Biologically Derived Soft Conducting Hydrogels Using Heparin-Doped Polymer Networks. *ACS nano* **2014,** *8* (5), 4348-4357.

6. Qiu, Y.; Park, K., Environment-sensitive hydrogels for drug delivery. *Advanced drug delivery reviews* **2012,** *64, Supplement* (0), 49-60.

7. Park, H.; Park, K.; Shalaby, W. S., *Biodegradable hydrogels for drug delivery*. CRC Press: 2011.

8. Weiss, R. G., The Past, Present, and Future of Molecular Gels. What Is the Status of the Field, and Where Is It Going? *Journal of the American Chemical Society* **2014,** *136* (21), 7519-7530.

9. Raghavan, S. R.; Cipriano, B. H., Gel formation: phase diagrams using tabletop rheology and calorimetry. Springer: 2006; pp 241-252.

10. Peppas, N.; Mikos, A., Preparation methods and structure of hydrogels. *Hydrogels in medicine and pharmacy* **1986,** *1*, 1-27.

11. Bhattacharya, S. M., U.; Mukhopadhyay, S.; Srivastava, A., Advances in molecular hydrogels. In *Molecular Gels. Materials with Self-Assembly Fibrillar Networks*, 1 ed.; Springer: New York, 2006; pp 613-4.

12. de Loos, M.; Feringa, B. L.; van Esch, J. H., Design and Application of Self-Assembled Low Molecular Weight Hydrogels. *European Journal of Organic Chemistry* **2005,** *2005* (17), 3615-3631.

13. Huang, H.; Song, W.; Chen, G.; Reynard, J. M.; Ohulchanskyy, T. Y.; Prasad, P. N.; Bright, F. V.; Lovell, J. F., Pd-Porphyrin-Cross-Linked Implantable Hydrogels with Oxygen-Responsive Phosphorescence. *Advanced healthcare materials* **2014,** *3* (6), 891-896.

14. Svobodova, H.; Noponen, V.; Kolehmainen, E.; Sievaenen, E., Recent advances in steroidal supramolecular gels. *RSC Adv.* **2012,** *2* (12), 4985-5007.

15. Sangeetha, N. M.; Maitra, U., Supramolecular gels: functions and uses. *Chemical Society Reviews* **2005,** *34* (10), 821-836.

16. Hennink, W.; Van Nostrum, C. F., Novel crosslinking methods to design hydrogels. *Advanced drug delivery reviews* **2012,** *64*, 223-236.

17. Estroff, L. A.; Hamilton, A. D., Water gelation by small organic molecules. *Chemical reviews* **2004,** *104* (3), 1201-1218.

18. Lipowitz, v. A., Versuche und Resultate über die Löslichkeit der Harnsäure. *Justus Liebigs Annalen der Chemie* **1841,** *38* (3), 348-355.

19. Brenzinger, K., Zur Kenntniss des Cystins und des Cystëins.(Mitgetheilt von E. Baumann.). *Zeitschrift für physiologische Chemie* **1892,** *16* (6), 552-588.

20. Weiss, R. G.; Terech, P., Molecular gels. *SpringerBerlin, Germany* **2006**.

21. Cheremisinoff, N. P., *Handbook of polymer science and technology*. CRC Press: 1989; Vol. 4.

22. Sutton, S.; Campbell, N. L.; Cooper, A. I.; Kirkland, M.; Frith, W. J.; Adams, D. J., Controlled release from modified amino acid hydrogels governed by molecular size or network dynamics. *Langmuir* **2009,** *25* (17), 10285-10291.

23. Kiyonaka, S.; Sugiyasu, K.; Shinkai, S.; Hamachi, I., First thermally responsive supramolecular polymer based on glycosylated amino acid. *Journal of the American Chemical Society* **2002,** *124* (37), 10954-10955.

24. Kobayashi, H.; Friggeri, A.; Koumoto, K.; Amaike, M.; Shinkai, S.; Reinhoudt, D. N., Molecular design of “super” hydrogelators: understanding the gelation process of azobenzene-based sugar derivatives in water. *Organic letters* **2002,** *4* (9), 1423-1426.

25. Jung, J. H.; John, G.; Masuda, M.; Yoshida, K.; Shinkai, S.; Shimizu, T., Self-assembly of a sugar-based gelator in water: Its remarkable diversity in gelation ability and aggregate structure. *Langmuir* **2001,** *17* (23), 7229-7232.

26. Lin, Y.; Qiao, Y.; Yan, Y.; Huang, J., Thermo-responsive viscoelastic wormlike micelle to elastic hydrogel transition in dual-component systems. *Soft Matter* **2009,** *5* (16), 3047-3053.

27. Imae, T.; Takahashi, Y.; Muramatsu, H., Formation of fibrous molecular assemblies by amino acid surfactants in water. *Journal of the American Chemical Society* **1992,** *114* (9), 3414-3419.

28. Estroff, L. A.; Hamilton, A. D., Effective Gelation of Water Using a Series of Bis-urea Dicarboxylic Acids. *Angewandte Chemie International Edition* **2000,** *39* (19), 3447-3450.

29. Suzuki, M.; Yumoto, M.; Kimura, M.; Shirai, H.; Hanabusa, K., A Family of Low-Molecular-Weight Hydrogelators Based on L-Lysine Derivatives with a Positively Charged Terminal Group. *Chemistry – A European Journal* **2003,** *9* (1), 348-354.

30. Chen, L.; Revel, S.; Morris, K.; Serpell, L. C.; Adams, D. J., Effect of Molecular Structure on the Properties of Naphthalene-Dipeptide Hydrogelators. *Langmuir* **2010,** *26* (16), 13466-13471.

31. Hoare, T. R.; Kohane, D. S., Hydrogels in drug delivery: Progress and challenges. *Polymer* **2008,** *49* (8), 1993-2007.

32. Vashist, A.; Vashist, A.; Gupta, Y. K.; Ahmad, S., Recent advances in hydrogel based drug delivery systems for the human body. *J. Mater. Chem. B* **2014,** *2* (2), 147-166.

33. Gregorova, A.; Saha, N.; Kitano, T.; Saha, P., Hydrothermal effect and mechanical stress properties of carboxymethylcellulose based hydrogel food packaging. *Carbohydrate polymers* **2015,** *117*, 559-568.

34. Wu, B.-c.; Degner, B.; McClements, D. J., Soft matter strategies for controlling food texture: formation of hydrogel particles by biopolymer complex coacervation. *Journal of Physics: Condensed Matter* **2014,** *26* (46), 464104.

35. Kanlayavattanakul, M.; Lourith, N., Biopolysaccharides for Skin Hydrating Cosmetics. In *Polysaccharides*, Springer: 2014; pp 1-23.

36. Daniele, M. A.; Adams, A. A.; Naciri, J.; North, S. H.; Ligler, F. S., Interpenetrating networks based on gelatin methacrylamide and PEG formed using concurrent thiol click chemistries for hydrogel tissue engineering scaffolds. *Biomaterials* **2014,** *35* (6), 1845-1856.

37. Cheung, H. K.; Han, T. T. Y.; Marecak, D. M.; Watkins, J. F.; Amsden, B. G.; Flynn, L. E., Composite hydrogel scaffolds incorporating decellularized adipose tissue for soft tissue engineering with adipose-derived stem cells. *Biomaterials* **2014,** *35* (6), 1914-1923.

38. Lu, Y.; Sturek, M.; Park, K., Microparticles produced by the hydrogel template method for sustained drug delivery. *International journal of pharmaceutics* **2014,** *461* (1), 258-269.

39. Li, Z.; Wen, T.; Su, Y.; Wei, X.; He, C.; Wang, D., Hollow hydroxyapatite spheres fabrication with three-dimensional hydrogel template. *CrystEngComm* **2014,** *16* (20), 4202-4209.

40. Hamilton, G. R.; Fullerton, L.; McCaughan, B.; Donnelly, R. F.; Callan, J. F., A ratiometric fluorescent hydrogel sensor for zinc (II) based on a two fluorophore approach. *New Journal of Chemistry* **2014,** *38* (7), 2823-2830.

41. Wu, R.; Zhang, S.; Lyu, J.; Lu, F.; Yue, X.; Lv, J., A visual volumetric hydrogel sensor enables quantitative and sensitive detection of copper ions. *Chemical communications* **2015,** *51* (38), 8078-8081.

42. Carmona, D.; Martinez, J.; Londoño, M. E.; Montoya, Y.; Torres, R. In *Novel Sensor Based on Polyvinyl Alcohol Hydrogel*, VI Latin American Congress on Biomedical Engineering CLAIB 2014, Paraná, Argentina 29, 30 and 31 October 2014, Springer: 2015; pp 39-42.

43. Chen, B.; Bai, Y.; Xiang, F.; Sun, J. Y.; Mei Chen, Y.; Wang, H.; Zhou, J.; Suo, Z., Stretchable and transparent hydrogels as soft conductors for dielectric elastomer actuators. *Journal of Polymer Science Part B: Polymer Physics* **2014,** *52* (16), 1055-1060.

44. Choi, M.; Humar, M.; Kim, S.; Yun, S. H., Step-Index Optical Fiber Made of Biocompatible Hydrogels. *Advanced Materials* **2015**.

45. Monteiro, J. P.; Predabon, S. M.; Pereira da Silva, C. T.; Radovanovic, E.; Girotto, E. M., Plasmonic device based on a PAAm hydrogel/gold nanoparticles composite. *Journal of Applied Polymer Science* **2015**.

46. Jen, A. C.; Wake, M. C.; Mikos, A. G., Review: hydrogels for cell immobilization. *Biotechnol. Bioeng.* **1996,** *50* (4), 357-364.

47. González-Alvarez, M.; González-Alvarez, I.; Bermejo, M., Hydrogels: an interesting strategy for smart drug delivery. *Therapeutic delivery* **2013,** *4* (2), 157-160.

48. Zhou, L.; Chen, M.; Guan, Y.; Zhang, Y., Multiple responsive hydrogel films based on dynamic Schiff base linkages. *Polymer Chemistry* **2014**.

49. Lim, S.; Song, J. E.; La, J. A.; Cho, E. C., Gold Nanospheres Assembled on Hydrogel Colloids Display a Wide Range of Thermoreversible Changes in Optical Bandwidth for Various Plasmonic-Based Color Switches. *Chemistry of Materials* **2014,** *26* (10), 3272-3279.

50. Li, D.; Yang, H.; Emmerich, H., Phase field model simulations of hydrogel dynamics under chemical stimulation. *Colloid and Polymer Sci* **2011,** *289* (5-6), 513-521.

51. Schmaljohann, D., Thermo-and pH-responsive polymers in drug delivery. *Advanced drug delivery reviews* **2006,** *58* (15), 1655-1670.

52. Zhou, S.-L.; Matsumoto, S.; Tian, H.-D.; Yamane, H.; Ojida, A.; Kiyonaka, S.; Hamachi, I., pH-Responsive Shrinkage/Swelling of a Supramolecular Hydrogel Composed of Two Small Amphiphilic Molecules. *Chemistry – A European Journal* **2005,** *11* (4), 1130-1136.

53. Hartgerink, J. D.; Beniash, E.; Stupp, S. I., Self-assembly and mineralization of peptide-amphiphile nanofibers. *Science* **2001,** *294* (5547), 1684-1688.

54. Aggeli, A.; Bell, M.; Carrick, L. M.; Fishwick, C. W.; Harding, R.; Mawer, P. J.; Radford, S. E.; Strong, A. E.; Boden, N., pH as a trigger of peptide β-sheet self-assembly and reversible switching between nematic and isotropic phases. *Journal of the American Chemical Society* **2003,** *125* (32), 9619-9628.

55. Zhang, Y.; Gu, H.; Yang, Z.; Xu, B., Supramolecular Hydrogels Respond to Ligand-Receptor Interaction. *J. Am. Chem. Soc.* **2003,** *125* (45), 13680-13681.

56. Saito, H.; Taguchi, T.; Aoki, H.; Murabayashi, S.; Mitamura, Y.; Tanaka, J.; Tateishi, T., pH-responsive swelling behavior of collagen gels prepared by novel crosslinkers based on naturally derived di-or tricarboxylic acids. *Acta biomaterialia* **2007,** *3* (1), 89-94.

57. Gemeinhart, R. A.; Chen, J.; Park, H.; Park, K., pH-sensitivity of fast responsive superporous hydrogels. *Journal of Biomaterials Science, Polymer Edition* **2000,** *11* (12), 1371-1380.

58. Bromberg, L. E.; Ron, E. S., Temperature-responsive gels and thermogelling polymer matrices for protein and peptide delivery. *Advanced drug delivery reviews* **1998,** *31* (3), 197-221.

59. Serres, A.; Baudyš, M.; Kim, S. W., Temperature and pH-sensitive polymers for human calcitonin delivery. *Pharmaceutical research* **1996,** *13* (2), 196-201.

60. Yong-Hee, K.; Bae, Y. H.; Kim, S. W., pH/temperature-sensitive polymers for macromolecular drug loading and release. *Journal of controlled release* **1994,** *28* (1), 143-152.

61. Peppas, N. A.; Khare, A. R., Preparation, structure and diffusional behavior of hydrogels in controlled release. *Advanced drug delivery reviews* **1993,** *11* (1), 1-35.

62. Panayiotou, M.; Freitag, R., Synthesis and characterisation of stimuli-responsive poly (N, N′-diethylacrylamide) hydrogels. *Polymer* **2005,** *46* (3), 615-621.

63. Aoki, T.; Kawashima, M.; Katono, H.; Sanui, K.; Ogata, N.; Okano, T.; Sakurai, Y., Temperature-responsive interpenetrating polymer networks constructed with poly (acrylic acid) and poly (N, N-dimethylacrylamide). *Macromolecules* **1994,** *27* (4), 947-952.

64. Shibanuma, T.; Aoki, T.; Sanui, K.; Ogata, N.; Kikuchi, A.; Sakurai, Y.; Okano, T., Thermosensitive Phase-Separation Behavior of Poly (acrylic acid)-g raft-poly (N, N-dimethylacrylamide) Aqueous Solution. *Macromolecules* **2000,** *33* (2), 444-450.

65. Zhao, Y.-L.; Stoddart, J. F., Azobenzene-Based Light-Responsive Hydrogel System. *Langmuir* **2009,** *25* (15), 8442-8446.

66. Mamada, A.; Tanaka, T.; Kungwatchakun, D.; Irie, M., Photoinduced phase transition of gels. *Macromolecules* **1990,** *23* (5), 1517-1519.

67. Zhong, X.; Wang, Y.-X.; Wang, S.-C., Pressure dependence of the volume phase-transition of temperature-sensitive gels. *Chemical Engineering Science* **1996,** *51* (12), 3235-3239.

68. Sawahata, K.; Hara, M.; Yasunaga, H.; Osada, Y., Electrically controlled drug delivery system using polyelectrolyte gels. *Journal of Controlled Release* **1990,** *14* (3), 253-262.

69. Yoshida, R.; Sakai, K.; Okano, T.; Sakurai, Y., Pulsatile drug delivery systems using hydrogels. *Advanced drug delivery reviews* **1993,** *11* (1–2), 85-108.

70. Park, T. G.; Hoffman, A. S., Sodium chloride-induced phase transition in nonionic poly(N-isopropylacrylamide) gel. *Macromolecules* **1993,** *26* (19), 5045-5048.

71. Starodoubtsev, S. G.; Khokhlov, A. R.; Sokolov, E. L.; Chu, B., Evidence for Polyelectrolyte/Ionomer Behavior in the Collapse of Polycationic Gels. *Macromolecules* **1995,** *28* (11), 3930-3936.

72. Ganji, F.; Vasheghani-Farahani, E., Hydrogels in controlled drug delivery systems. *Iranian Polymer Journal* **2009,** *18* (1), 63-88.

73. Rouge, N.; Buri, P.; Doelker, E., Drug absorption sites in the gastrointestinal tract and dosage forms for site-specific delivery. *International journal of pharmaceutics* **1996,** *136* (1), 117-139.

74. Yan, F.; Cao, H.; Cover, T. L.; Washington, M. K.; Shi, Y.; Liu, L.; Chaturvedi, R.; Peek, R. M.; Wilson, K. T.; Polk, D. B., Colon-specific delivery of a probiotic-derived soluble protein ameliorates intestinal inflammation in mice through an EGFR-dependent mechanism. *The Journal of Clinical Investigation* **2011,** *121* (6), 2242-2253.

75. Bajpai, S. K.; Banger, P., Photopolymerized pH-sensitive semi-IPN: Synthesis, water uptake analysis, and preliminary drug release study. *Polymer Engineering and Science* **2013,** *53* (10), 2129-2140.

76. Florence, A. T.; Attwood, D., *Physicochemical principles of pharmacy*. pharmaceutical press: 2011.

77. Fajardo, A. R.; Silva, M. B.; Lopes, L. C.; Piai, J. F.; Rubira, A. F.; Muniz, E. C., Hydrogel based on an alginate–Ca 2+/chondroitin sulfate matrix as a potential colon-specific drug delivery system. *RSC Advances* **2012,** *2* (29), 11095-11103.

78. George, M.; Abraham, T. E., Polyionic hydrocolloids for the intestinal delivery of protein drugs: Alginate and chitosan — a review. *Journal of Controlled Release* **2006,** *114* (1), 1-14.

79. Schoenwald, R. D., Ocular pharmacokinetics. Lippincott-Raven: Philadelphia, PA, USA: 1997; pp 119-138.

80. Kuno, N.; Fujii, S., Recent advances in ocular drug delivery systems. *Polymers* **2011,** *3* (1), 193-221.

81. Misra, G. P.; Singh, R. S. J.; Aleman, T. S.; Jacobson, S. G.; Gardner, T. W.; Lowe, T. L., Subconjunctivally implantable hydrogels with degradable and thermoresponsive properties for sustained release of insulin to the retina. *Biomaterials* **2009,** *30* (33), 6541-6547.

82. Ochoa, M.; Mousoulis, C.; Ziaie, B., Polymeric microdevices for transdermal and subcutaneous drug delivery. *Advanced drug delivery reviews* **2012,** *64* (14), 1603-1616.

83. Prausnitz, M. R.; Langer, R., Transdermal drug delivery. *Nature Biotechnology* **2008,** *26* (11), 1261-1268.

84. Wertz, P.; Downing, D., In Transdermal Drug Delivery. *Development Issues and Research Initiatives, Hadgraft, JJ, Guy R H. Eds. Marcel Dekker Inc, New York* **1989,** *35*, 1-22.

85. Prausnitz, M. R.; Mitragotri, S.; Langer, R., Current status and future potential of transdermal drug delivery. *Nature Reviews Drug Discovery* **2004,** *3* (2), 115-124.

86. Pillai, O.; Panchagnula, R., Transdermal delivery of insulin from poloxamer gel: ex vivo and in vivo skin permeation studies in rat using iontophoresis and chemical enhancers. *Journal of Controlled Release* **2003,** *89* (1), 127-140.

87. Lee, A. L. Z.; Ng, V. W. L.; Gao, S.; Hedrick, J. L.; Yang, Y. Y., Injectable Hydrogels from Triblock Copolymers of Vitamin E-Functionalized Polycarbonate and

Poly(ethylene glycol) for Subcutaneous Delivery of Antibodies for Cancer Therapy. *Advanced Functional Materials* **2014,** *24* (11), 1538-1550.

88. Radivojša Matanović, M.; Grabnar, I.; Gosenca, M.; Ahlin Grabnar, P., Prolonged subcutaneous delivery of low molecular weight heparin based on thermoresponsive hydrogels with chitosan nanocomplexes: Design, in vitro evaluation, and cytotoxicity studies. *International journal of pharmaceutics* **2015,** *488* (1–2), 127-135.

89. Li, J.; Li, X.; Ni, X.; Wang, X.; Li, H.; Leong, K. W., Self-assembled supramolecular hydrogels formed by biodegradable PEO–PHB–PEO triblock copolymers and α-cyclodextrin for controlled drug delivery. *Biomaterials* **2006,** *27* (22), 4132-4140.

90. Tang, Y.; Heaysman, C. L.; Willis, S.; Lewis, A. L., Physical hydrogels with self-assembled nanostructures as drug delivery systems. *Expert opinion on drug delivery* **2011,** *8* (9), 1141-1159.

91. Gatenholm, P.; Holmström, C.; Maki, J. S.; Kjelleberg, S., Toward biological antifouling surface coatings: marine bacteria immobilized in hydrogel inhibit barnacle larvae. *Biofouling* **1995,** *8* (4), 293-301.

92. Andrade-Vivero, P.; Fernandez-Gabriel, E.; Alvarez-Lorenzo, C.; Concheiro, A., Improving the loading and release of NSAIDs from pHEMA hydrogels by copolymerization with functionalized monomers. *Journal of pharmaceutical sciences* **2007,** *96* (4), 802-813.

93. Li, X.; Li, J., Supramolecular hydrogels based on inclusion complexation between poly (ethylene oxide)-b-poly (ε-caprolactone) diblock copolymer and α-cyclodextrin and their controlled release property. *Journal of Biomedical Materials Research Part A* **2008,** *86* (4), 1055-1061.

94. Kickhöfen, B.; Wokalek, H.; Scheel, D.; Ruh, H., Chemical and physical properties of a hydrogel wound dressing. *Biomaterials* **1986,** *7* (1), 67-72.

95. Nayak, S.; Kundu, S. C., Sericin-carboxymethyl cellulose porous matrices as cellular wound dressing material. *Journal of Biomedical Materials Research, Part A* **2014,** *102A* (6), 1928-1940.

96. Yoo, H.-J.; Kim, H.-D., Synthesis and properties of waterborne polyurethane hydrogels for wound healing dressings. *Journal of Biomedical Materials Research, Part B* **2008,** *85B* (2), 326-333.

97. Drury, J. L.; Mooney, D. J., Hydrogels for tissue engineering: scaffold design variables and applications. *Biomaterials* **2003,** *24* (24), 4337-4351.

98. Kumar, P. T. S.; Lakshmanan, V.-K.; Anilkumar, T. V.; Ramya, C.; Reshmi, P.; Unnikrishnan, A. G.; Nair, S. V.; Jayakumar, R., Flexible and microporous chitosan

hydrogel/nano ZnO composite bandages for wound dressing: in vitro and in vivo evaluation. *ACS Applied Materials and Interfaces* **2012,** *4* (5), 2618-29.

99. Gaudana, R.; Jwala, J.; Boddu, S. H. S.; Mitra, A. K., Recent Perspectives in Ocular Drug Delivery. *Pharmaceutical Research.* **2009,** *26* (5), 1197-1216.

100. Boucard, N.; Viton, C.; Domard, A., New Aspects of the Formation of Physical Hydrogels of Chitosan in a Hydroalcoholic Medium. *Biomacromolecules* **2005,** *6* (6), 3227-3237.

101. Hofmann, A. F., The function of bile salts in fat absorption. The solvent properties of dilute micellar solutions of conjugated bile salts. *Biochemical Journal* **1963,** *89* (1), 57-68.

102. Neufeld, F., Ueber eine specifische bakteriolytische Wirkung der Galle. *Zeitschr. f. Hygiene.* **1900,** *34* (1), 454-464.

103. Dash, M. STREPTOCOCCUS PNEUMONIAE. National Institute of Technology Rourkela, 2013.

104. Sobotka, H.; Czeczowiczka, N., The gelation of bile salt solutions. *Journal Colloid Science.* **1958,** *13*, 188-91.

105. Maitra, U.; Mukhopadhyay, S.; Sarkar, A.; Rao, P.; Indi, S. S., Hydrophobic Pockets in a Nonpolymeric Aqueous Gel: Observation of such a Gelation Process by Color Change. *Angewandte Chemie International Edition* **2001,** *40* (12), 2281-2283.

106. Mukhopadhyay, S.; Maitra, U., Chemistry and biology of bile acids. *Current Science* **2004,** *87* (12), 1666-1683.

107. Rich, A. B., D.M., Formation of a helical steroid complex. *Nature* **1958,** *182* (4633), 423-426.

108. Blow, D.; Rich, A., Studies on the formation of helical deoxycholate complexes1, 2. *Journal of the American Chemical Society* **1960,** *82* (14), 3566-3571.

109. Luzzati, V.; Mustacchi, H.; Skoulios, A., The structure of the liquid-crystal phases of some soap+ water systems. *Discussions of the Faraday Society.* **1958,** *25*, 43-50.

110. Terech, P.; Sangeetha, N. M.; Maitra, U., Molecular hydrogels from bile acid analogues with neutral side chains: network architectures and viscoelastic properties. Junction zones, spherulites, and crystallites: Phenomenological aspects of the gel metastability. *The Journal of Physical Chemistry B* **2006,** *110* (31), 15224-15233.

111. Bhat, S.; Maitra, U., Nanoparticle−Gel Hybrid Material Designed with Bile Acid Analogues. *Chemistry of Materials* **2006,** *18* (18), 4224-4226.

112. Babu, P.; Sangeetha, N. M.; Maitra, U. In *Supramolecular chemistry of bile acid derivatives: formation of gels*, Macromolecular Symposia, Wiley Online Library: 2006; pp 60-67.

113. Sahiner, N.; Singh, M.; De Kee, D.; John, V. T.; McPherson, G. L., Rheological characterization of a charged cationic hydrogel network across the gelation boundary. *Polymer* **2006,** *47* (4), 1124-1131.

114. Kim, B.; Shin, Y., pH-sensitive swelling and release behaviors of anionic hydrogels for intelligent drug delivery system. *Journal of Applied Polymer Science* **2007,** *105* (6), 3656-3661.

115. ISHIOROSHI, M.; JIMA, K. S.; YASUI, T., Heat-induced gelation of myosin: factors of pH and salt concentrations. *Journal of Food Science* **1979,** *44* (5), 1280-1284.

116. Li, J.; Fan, K.; Niu, L.; Li, Y.; Song, J., Effects of Salt on the Gelation Mechanism of a d-Sorbitol-Based Hydrogelator. *The Journal of Physical Chemistry B* **2013,** *117* (19), 5989-5995.

117. Kimura, M.; Fukumoto, K.; Watanabe, J.; Ishihara, K., Hydrogen-bonding-driven spontaneous gelation of water-soluble phospholipid polymers in aqueous medium. *Journal of Biomaterials Science, Polymer Edition* **2004,** *15* (5), 631-644.

118. Byrne, M. E.; Park, K.; Peppas, N. A., Molecular imprinting within hydrogels. *Advanced Drug Delivery Reviews* **2002,** *54* (1), 149-161.

119. Simhadri, J. J.; Stretz, H. A.; Oyanader, M.; Arce, P. E., Role of nanocomposite hydrogel morphology in the electrophoretic separation of biomolecules: a review. *Industrial and Engineering Chemistry Research* **2010,** *49* (23), 11866-11877.

120. Fujimoto, C.; Fujise, Y.; Matsuzawa, E., Fritless packed columns for capillary electrochromatography: separation of uncharged compounds on hydrophobic hydrogels. *Analytical Chemistry* **1996,** *68* (17), 2753-2757.

121. Richter, A.; Paschew, G.; Klatt, S.; Lienig, J.; Arndt, K.-F.; Adler, H.-J. P., Review on hydrogel-based pH sensors and microsensors. *Sensors* **2008,** *8* (1), 561-581.

122. Hoffman, A. S., Hydrogels for biomedical applications. *Advanced drug delivery reviews* **2012,** *64, Supplement* (0), 18-23.

123. Sugiyasu, K.; Fujita, N.; Takeuchi, M.; Yamada, S.; Shinkai, S., Proton-sensitive fluorescent organogels. *Organic and Biomolecular Chemistry* **2003,** *1* (5), 895-899.

124. Basit, H.; Pal, A.; Sen, S.; Bhattacharya, S., Two-Component Hydrogels Comprising Fatty Acids and Amines: Structure, Properties, and Application as a

Template for the Synthesis of Metal Nanoparticles. *Chemistry – A European Journal* **2008,** *14* (21), 6534-6545.

125. Lee, K. Y.; Mooney, D. J., Hydrogels for Tissue Engineering. *Chemical Reviews. (Washington, D. C.)* **2001,** *101* (7), 1869-1879.

126. Lim, F.; Sun, A. M., Microencapsulated islets as bioartificial endocrine pancreas. *Science* **1980,** *210* (4472), 908-910.

127. Dai, W.; Barbari, T., Gel-impregnated pore membranes with mesh-size asymmetry for biohybrid artificial organs. *Biomaterials* **2000,** *21* (13), 1363-1371.

128. Wang, W.; Gu, Y.; Hori, H.; Sakurai, T.; Hiura, A.; Sumi, S.; Tabata, Y.; Inoue, K., Subcutaneous transplantation of macroencapsulated porcine pancreatic endocrine cells normalizes hyperglycemia in diabetic mice1. *Transplantation* **2003,** *76* (2), 290-296.

129. Murata, K.; Aoki, M.; Suzuki, T.; Harada, T.; Kawabata, H.; Komori, T.; Ohseto, F.; Ueda, K.; Shinkai, S., Thermal and light control of the sol-gel phase transition in cholesterol-based organic gels. Novel helical aggregation modes as detected by circular dichroism and electron microscopic observation. *Journal of the American Chemical Society* **1994,** *116* (15), 6664-6676.

130. Terech, P.; Dourdain, S.; Bhat, S.; Maitra, U., Self-Assembly of Bile Steroid Analogues: Molecules, Fibers, and Networks. *The Journal of Physical Chemistry B* **2009,** *113* (24), 8252-8267.

131. Svobodova, H.; Nonappa; Wimmer, Z.; Kolehmainen, E., Design, synthesis and stimuli responsive gelation of novel stigmasterol-amino acid conjugates. *Journal of Colloid and Interface Science* **2011,** *361* (2), 587-93.

132. Liu, K.; Yan, N.; Peng, J.; Liu, J.; Zhang, Q.; Fang, Y., Supramolecular gels based on organic diacid monoamides of cholesteryl glycinate. *Journal of Colloid and Interface Science* **2008,** *327* (1), 233-242.

133. Valenta, C.; Nowack, E.; Bernkop-Schnurch, A., Deoxycholate-hydrogels: novel drug carrier systems for topical use. *International Journal of Pharmaceutics* **1999,** *185* (1), 103-11.

134. Warner, I. M.; El-Zahab, B.; Siraj, N., Perspectives on Moving Ionic Liquid Chemistry into the Solid Phase. *Analytical Chemistry.* **2014**.

135. Siraj, N.; Hasan, F.; Das, S.; Kiruri, L. W.; Steege Gall, K. E.; Baker, G. A.; Warner, I. M., Carbazole-Derived Group of Uniform Materials Based on Organic Salts: Solid State Fluorescent Analogues of Ionic Liquids for Potential Applications in Organic-Based Blue Light-Emitting Diodes. *Journal of Physical Chemistry* **2014**, 118 (5), 2312-2320.

136. Tesfai, A.; El-Zahab, B.; Kelley, A. T.; Li, M.; Garno, J. C.; Baker, G. A.; Warner, I. M. *ACS Nano* **2009**, 3, 3244−3250.

137. de Rooy, S. L.; El-Zahab, B.; Li, M.; Das, S.; Broering, E.; Chandler, L.; Warner, I. M. *Chemical Communications*. **2011**, 47, 8916−8918.

138. Galpothdeniya, W. I. S.; Regmi, B. P.; McCarter, K. S.; de Rooy, S. L.; Siraj, N.; Warner, I. M., Virtual Colorimetric Sensor Array: Single Ionic Liquid for Solvent Discrimination. *Analytical Chemistry* **2015**, 87 (8), 4464-4471.

139. Jordan, A. N.; Das, S.; Siraj, N.; de Rooy, S. L.; Li, M.; El-Zahab, B.; Chandler, L.; Baker, G. A.; Warner, I. M., Anion-controlled morphologies and spectral features of cyanine-based nanoGUMBOS--an improved photosensitizer. *Nanoscale* **2012**, 4 (16), 5031-8.

140. Regmi, B. P.; Monk, J.; El-Zahab, B.; Das, S.; Hung, F. R.; Hayes, D. J.; Warner, I. M., A novel composite film for detection and molecular weight determination of organic vapors. *Journal of Materials Chemistry* **2012**, 22 (27), 13732-13741.

141. Li, M., Ganea, G. M., Lu, C., De Rooy, S. L., El-Zahab, B., Fernand, V. E., Warner, I. M., Lipophilic phosphonium–lanthanide compounds with magnetic, luminescent, and tumor targeting properties. *Journal of Inorganic Biochemistry* **2012**, 107(1), 40-46.

142. Magut, P. K. S.; Das, S.; Fernand, V. E.; Losso, J.; McDonough, K.; Naylor, B. M.; Aggarwal, S.; Warner, I. M., Tunable Cytotoxicity of Rhodamine 6G via Anion Variations. *Journal of the American Chemical Society* **2013**, 135 (42), 15873-15879.

143. Das, S.; de Rooy, S. L.; Jordan, A. N.; Chandler, L.; Negulescu, II; El-Zahab, B.; Warner, I. M., Tunable size and spectral properties of fluorescent nanoGUMBOS in modified sodium deoxycholate hydrogels. *Langmuir* **2012,** *28* (1), 757-65.

CHAPTER 2.
SODIUM DEOXYCHOLATE HYDROGELS: EFFECTS OF MODIFICATIONS ON GELATION, DRUG RELEASE, AND NANOTEMPLATING*

2.1. Introduction

Bile acids such as sodium deoxycholate (NaDC) have long been known as hydrogelators.[1,2] However, it is only during the past couple of decades that low molecular weight (LMW) gelators, such as some steroids, have been studied extensively.[3] Steroids (including bile acids) are composed of a tetracyclic ring system with functional groups often including hydroxyl groups and an aliphatic side chain.[4] The rigidity of the steroid backbone and the stereochemistry of hydroxyl functionalities result in facial amphiphilicity in NaDC, thereby enhancing formation of aqueous pools immobilized by a hydrophobic gel network.[5] In pure water, the gelation mechanism of NaDC is considered to result from primarily entangled micellization,[6] forming an overall helical structure.[1] The addition of a modifier such as TRIS[7] or mannitol[8] has been shown to contribute hydrogen bonding to this gelation mechanism.

In addition to NaDC, LMW gelators include chitosan,[9] azo dyes,[10] nucleoside derivatives,[11] and many others.[12] The myriad of LMW gelators allow a broad array of applications such as nanofabrication,[13,14] biomedical engineering,[15] separation science,[16] and sensing.[17] Development of a more diverse group of gels through mechanical and thermal experimentation is essential due to such broad applicability.[18,19]

---

*This chapter previously appeared as “McNeel, K. E.; Das, S.; Siraj, N.; Negulescu, I. I.; Warner, I. M., Sodium Deoxycholate Hydrogels: Effects of Modifications on Gelation, Drug Release, and Nanotemplating”. Reproduced with permission from *The Journal of Physical Chemistry B 119* (27), 8651-8659. Copyright 2015 American Chemical Society.

It has been established that polymeric hydrogels are typically stronger in durability due to covalently cross-linked polymerization, making them more useful for actuators and other material applications.[20] The physicochemical interactions of LMW hydrogels are much weaker in terms of durability; thus an increase in mechanical strength may be desirable, especially for bioengineering.

Gels with variable mechanical strengths are expected to provide variable templating capabilities for nanoparticle fabrication. The ability to develop a hydrogel with a designable template is of importance to nanoscience due to the many useful properties of nanoparticles dictated by particle size.[21,22] These properties have been found to include surface control and interaction with cells and other physiological media making nanoparticles applicable in biosensors, drug delivery systems, and bioengineering.[22,23] Nanoparticles derived from a **G**roup of **U**niform **M**aterials **B**ased on **O**rganic **S**alts (GUMBOS), i.e. nanoGUMBOS, have previously been formed by use of a variety of methods.[24,25,26] This class of materials, GUMBOS, are solid phase materials with tunable properties similar to ionic liquids. However, GUMBOS differ from ionic liquids in that they are primarily used in the solid state and have melting points between 25 and 250 °C.[21] An exponentially increasing number of applications[27] including optical electronics,[21-30] biological imaging,[24] solar cell sensitizing,[31] cancer targeting,[21,32] antibacterial,[33] and molecular weight sensing functions[34,35] make GUMBOS an interesting class of materials to study. Das et al. have recently studied NaDC/TRIS hydrogels as templates for size-tunable preparation of organic GUMBOS nanoparticles.[7] In their method, hydrophobic nanoGUMBOS are formed similarly to a reverse micelle synthesis without a surfactant.[7,36] The GUMBOS of greatest interest are

in a water miscible solution (e.g. ethanol). Thus, the solvated GUMBOS preferentially moves to hydrophilic pockets consequently forming nanoGUMBOS. Thus far, neither the composition of GUMBOS nor the pH of the hydrogel have been shown to affect the resultant size of nanoGUMBOS templated by these materials.

In this study, I desire to further understand the modified gelation mechanism and expand the applicability of NaDC/TRIS hydrogels by investigating new materials under previously unknown conditions. Herein, I report the pH dependence of gelation at various TRIS concentrations through investigations of two distinctly different pH values: pH 5.5 well below the pKa of NaDC[2, 37] and pH 7.4, the physiological pH, which is above the pKa of NaDC. An intermediate pH value of 6.8, i.e. near the pKa of NaDC, was also investigated. Each pH value was found to yield different properties in the resultant hydrogels indicating that ionic interactions are an important factor contributing to the gelation process. Through investigation of gelation, several properties were found to be tunable towards desired applications including sol-gel temperature, mechanical strength, templating capabilities, and viscoelasticity. NanoGUMBOS derived from three different NIR dyes were synthesized, and it was determined that hydrogel conditions and GUMBOS composition influenced particle size. Unique viscoelastic properties were found that prompted further investigations of small molecule release. Namely, two stable regions were found in the elastic modulus of several formulations, indicating great potential as injectable drug delivery vehicles. In order to demonstrate the utility of this property, fluorescein release was examined in gels that had and had not been sheared.

2.2. Experimental details

2.2.1. Materials

Sodium deoxycholate (NaDC), tris(hydroxymethyl)aminomethane (TRIS), 6-propionyl-2-(dimethylamino)naphthalene (Prodan), 8-anilino-1-naphthalenesulfonic acid (ANS), 1,1′,3,3,3′,3′-hexamethylindotricarbocyanine (HMT) iodide (97%), bis(trifluoromethane)sulfonimide (NTf2) lithium salt, and bis(2-ethylhexyl) sulfosuccinate (AOT) sodium salt (≥ 99%), were purchased from Sigma Aldrich and used as received. Sodium tetraphenylborate (TPB) was purchased from TCI America and used as received. Ultrathin Carbon Type-A copper grids (CF400-Cu; Ted Pella, Inc.; Redding, CA) were used for TEM imaging. Triply deionized water (18 MΩ cm) was obtained from an Aries Filterworks high purity water system and used for all experiments.

2.2.2. Selection of hydrogels

TRIS buffer solutions were prepared at concentrations of 25, 50, 100, 200, 250, 300, 400, and 500 mM. By use of concentrated and/or dilute hydrochloric acid, each concentration was adjusted from an initial pH value greater than 10 to each of four pH values: 5.5, 6.0, 6.8, and 7.4, generating a total of 32 individual samples. Solid NaDC was added to each solution to provide a concentration of 20 mM, followed immediately by 30 seconds of vortexing. Each sample was then bath sonicated for 20 minutes. The samples were allowed to stabilize at 5 °C overnight before analyses. Hydrophobicity studies using the fluorescent probe Prodan were employed for determining which of the 32 samples would be pursued for further study (Table 2.1).

Table 2.1. Concentrations of TRIS buffer at each pH value selected for study.

	TRIS concentration (mM)
pH 5.5	25, 100, 200, 250, 300, and 500
pH 6.0	25, 100, 200, 300, and 500
pH 6.8	50, 100, 200, and 400
pH 7.4	25, 100, 200, 300, and 500

2.2.3. Characterization of hydrogels

Hydrogels were characterized using several techniques. X-ray diffraction studies were performed on air-dried hydrogels using a Brüker/Siemens D5000 automated powder X-ray diffractometer, and diffraction patterns were analyzed using MDI Jade 9.4.5 software. An Olympus BH polarizing optical microscope with an MD 1900 camera was used to obtain POM micrographs. The polarizer was set to 90°, and the analyzer was set to 0°. The hydrogels were drop-cast onto pre-cleaned glass slides and left to dry, with a thin layer remaining after solvent evaporation. A Thermal Analysis (TA) differential scanning calorimeter 2920 was used to determine sol-gel temperatures. Samples were heated in hermetic pans from 10 °C to 80 °C at a rate of 2 °C per minute. A TA AR 1000 rheometer (TA Instruments, Inc., Waters Corp., New Castle, DE) with stainless steel plate geometry was used to determine the rheological properties of the hydrogels, specifically the G' and G" moduli. The fluorescent probe ANS was used to characterize the rigidity of hydrogel fibers and size of aqueous pools through fluorescence anisotropy (r) measurements. Fluorescence anisotropy is a measure of the average angular displacement of a fluorophore, i.e. ANS in this study, which is given by the equations:

$$r = \frac{I_{vv} - GI_{vh}}{I_{vv} + 2GI_{vh}}, G = \frac{I_{hv}}{I_{hh}}.$$

Anisotropy values can vary between -0.2 and 0.4, where -0.2 indicates free rotation and 0.4 indicates completely restricted rotation. To acquire these measurements, the light source is polarized either vertically (*v*) or horizontally (*h*) before absorption, and the emission is polarized either parallel or perpendicular to the source polarization. In my studies, ANS was excited at 360 nm, and values of fluorescence anisotropy were calculated at 430 and 520 nm.

2.2.4. Synthesis and characterization of [HMT][NTf_2] and [HMT][TPB] GUMBOS

The GUMBOS [HMT][NTf_2], [HMT][TPB], and [HMT][AOT] were synthesized using a metathesis reaction, commonly referred to as an anion exchange method.[24] Characterizations of GUMBOS were performed using ^{1}H (Bruker Avance 400, $CDCl_3$) and ^{19}F NMR (Bruker DPX 250, $CDCl_3$).

2.2.5. Synthesis of nanoGUMBOS in NaDC hydrogels

After addition of 20 mM NaDC to each TRIS solution, a 1 mM ethanolic solution of [HMT][NTf_2] was injected to achieve a final concentration of 20 μM. The solution was then vortexed for 30 seconds, and followed immediately with 20 minutes of bath sonication. The hydrogel samples were then allowed to stabilize overnight at 5 °C before further study.

2.2.6. Characterization of NanoGUMBOS: Size and Morphology

A JEM-1011 (JEOL USA, Inc., Peabody, MA) transmission electron microscope was used to obtain micrographs in order to examine the morphology of the prepared nanoGUMBOS. Each hydrogel sample was drop-cast (100 μL) onto a TEM grid. Upon drying, the grids were washed with water to remove the hydrophilic gels leaving behind the hydrophobic nanoparticles. The grids were left to dry before obtaining TEM

micrographs. ImageJ was used to determine statistical data on the particles including average sizes and standard deviations.

2.3. Results and discussion

2.3.1. Characterization of hydrogels

In order to investigate the use of modified NaDC hydrogels as templates for synthesis of nanoGUMBOS and to determine their potential for other applications, including material applications, physical characterizations were necessary. Using visual observation, it was clear that the hydrogels varied in structural integrity after various modifications to TRIS concentration and pH of the medium (Figure 2.1). For example, a gel with 25 mM TRIS demonstrated “gel-like” behavior when at pH 5.5. However, the same concentration of TRIS at pH 7.4 displayed significant fluidity, or a more “liquid-like” behavior. In addition, a gel with 300 mM TRIS at pH 7.4 demonstrated “gel-like” behavior. Lowering the pH value has been shown to increase NaDC aggregation, thereby aiding gelation.[38] Therefore, gelation has mostly been reported in acidic environments. However, this study demonstrates gelation at the physiological pH for higher TRIS concentrations. Thus, it is evident from this study that TRIS is not only modifying the gel microenvironment in acidic pH, but is also capable of inducing gelation at physiological pH, i.e. above the pKa of NaDC. The morphology and microenvironment, as well as thermal and mechanical properties were investigated in more detail and are further discussed below.

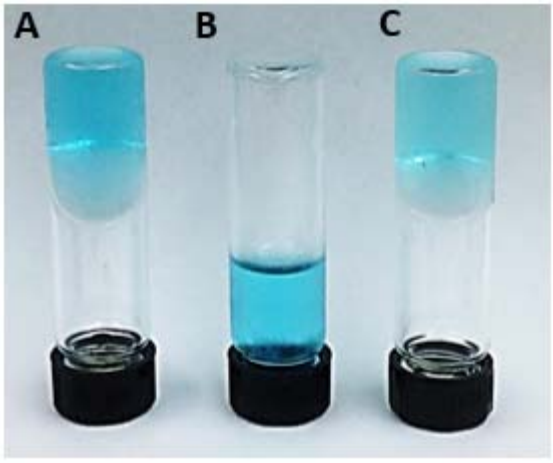

Figure 2.1. Visual comparison of structural integrity of transparent NaDC hydrogels containing blue [HMT][NTf_2] nanoparticles prepared at (A) pH 5.5, 25 mM TRIS; (B) pH 7.4, 25 mM TRIS; and (C) pH 7.4, 300 mM TRIS.

2.3.2. Hydrophobicity and anisotropy studies with fluorescent probes

Prodan is a neutral, fluorescent, and hydrophobic probe used to evaluate the microenvironments of these modified hydrogels. Prodan exhibits a fluorescence maximum at about 400 nm in a hydrophobic environment and a maximum at about 530 nm in a hydrophilic environment.[39] Determining the hydrophobicity of the hydrogel microenvironment provides information regarding structural changes from one hydrogel to another. Examination of the fluorescence spectra of 10 μM Prodan within the hydrogels (Figure 2.2), suggested differences in microenvironments. Among hydrogels with similar hydrophobicity (as exhibited by the fluorescence spectra) one was selected for further studies (Table 2.1). In general, the hydrophilicity of the microenvironment experienced by Prodan increased with increasing TRIS concentration. Given the mode of gelation, this shows that increasing TRIS concentration leads to an increase in the size of aqueous pools formed between the hydrophobic fibers of the hydrogel. This trend was not observed for pH 7.4, however, at which each concentration of TRIS had approximately the same hydrophobicity with slight variations in intensities. Based on this

observation, I suggest that the gel microenvironments at various TRIS concentrations are not significantly different at pH 7.4. Based on these data, one TRIS concentration was selected from each cluster of intensities for further investigation.

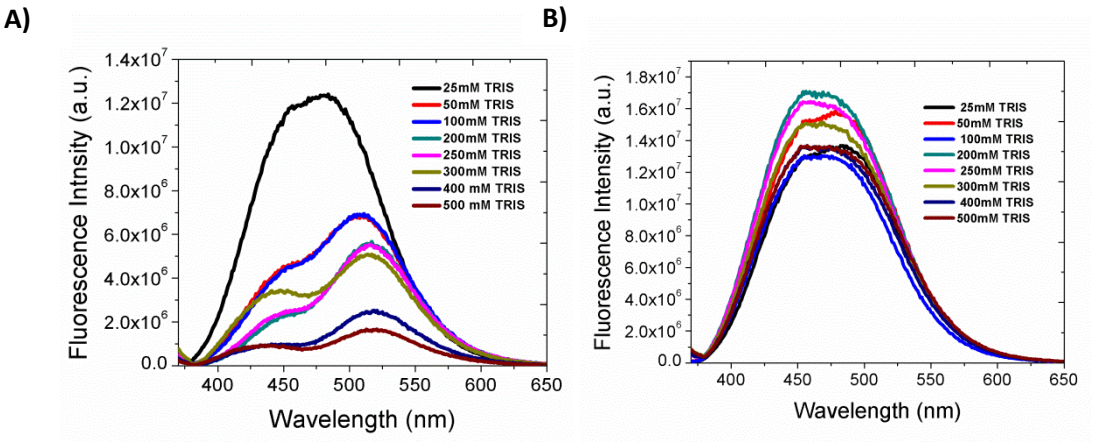

Figure 2.2. Emission spectra of the fluorescent probe Prodan in hydrogels at A) pH 5.5 and B) pH 7.4. Samples were excited at λ_{ex} = 360 nm.

The hydrophobicity probe ANS was used to determine the degree of anisotropy, or restricted rotation, in each hydrogel. This probe exhibits emission maxima near 430 nm and 520 nm in hydrophobic and hydrophilic environments, respectively.[40] The anisotropy of each hydrogel was calculated for both the hydrophobic and hydrophilic wavelengths in order to determine the restriction of ANS rotation in the hydrophobic gel fibers and the aqueous pools (Figure 2.3). Higher anisotropy values in a hydrophobic environment suggest higher rigidity of gel fibers, and higher anisotropy values in a hydrophilic environment indicate a smaller water pool between the fibers. This rationalization is the result of both a more rigid network and a smaller water pool each decreasing the free rotation of a fluorophore, thereby increasing anisotropy.

Anisotropy studies at 430 nm aid in examining the rigidity of the hydrogel fibers, where an increase in anisotropy indicates an increase in rigidity. The anisotropy, and therefore rigidity, within the fibrous network of pH 5.5 hydrogel was found to increase

with increasing TRIS concentration from -0.23 in the 25 mM TRIS hydrogel to 0.057 in the 500 mM TRIS hydrogel. The rigidity of the pH 6.8 gel fibers was also found to increase with TRIS concentration with an anisotropy increase from -0.11 to 0.11 from the hydrogel with 25 mM TRIS to that with 500 mM TRIS. However, hydrogel fibers at the physiological pH value of 7.4 were observed to produce no significant change in rigidity with varying TRIS concentration, while exhibiting an average anisotropy of 0.028 ± 0.004. Except at pH 7.4, an increase in TRIS concentration resulted in an increase in hydrogel fiber rigidity.

The sizes of the aqueous pools within the hydrogel network were estimated from the anisotropy values at 530 nm. A smaller anisotropy indicated greater rotational diffusion of the excited state of the fluorophore and therefore larger pool sizes. Examination of these results suggested that the size of the aqueous pools within the pH 5.5 hydrogels increased at lower TRIS concentrations and decreased at higher TRIS concentrations. The 25 mM TRIS and 100 mM TRIS hydrogels exhibited anisotropies of -0.058 and -0.029 respectively at the hydrophilic wavelength of ANS. From 200 to 500 mM TRIS, the anisotropy was found to decrease from -0.033 to -.075. The size of the aqueous pools within the hydrogel network at pH 6.8 was found to increase with TRIS concentrations. The anisotropy values decreased from 0.10 to 0.062 with increasing TRIS concentration from 25 mM to 500 mM. At a pH value of 7.4 with 25, 100, and 200 mM TRIS, anisotropy of ANS in the aqueous pools of the hydrogels had an average value of 0.021 ± 0.008. The higher concentrations of 300 and 500 mM TRIS resulted in larger pool size with an average anisotropy of -0.014 with insignificant deviation. In

general, an increase in TRIS concentration resulted in formation of larger water pools after gelation.

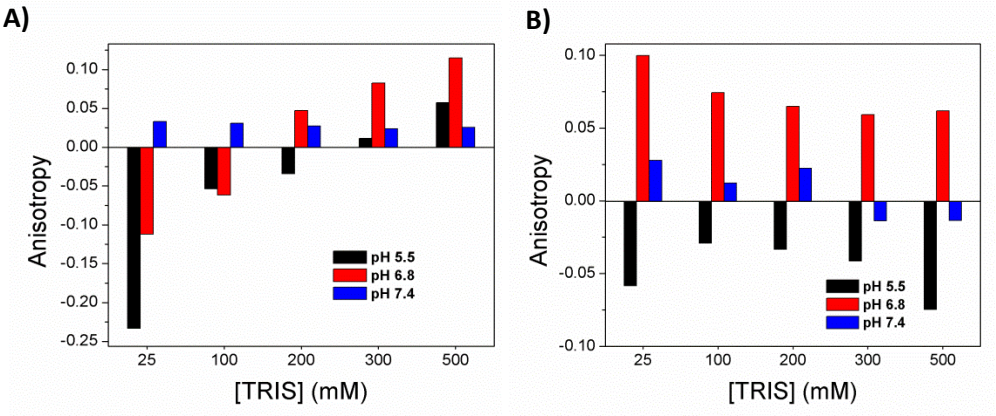

Figure 2.3. Calculated anisotropies at A) hydrophobic wavelength (430 nm) and B) hydrophilic wavelength (520 nm).

2.3.3. Polarized optical microscopy (POM) of modified hydrogels

The morphology and crystallinity of these hydrogels were characterized by use of POM, which is often employed for studies of birefringent materials. This characterization yields important information for potential applications of the materials. For example, morphology and crystallinity may impact thermal stability, ability to form tough materials, use in sensing applications, and use in soft electronics. Figure 2.4 is a compilation of polarized optical micrographs of hydrogels at pH 5.5, 6.8, and 7.4 with increasing concentrations of TRIS. Hydrogels of pH 5.5 with 25 mM and 200 mM TRIS exhibited fibrous structures, while hydrogels with 500 mM TRIS displayed spherulite crystalline domains. The increased rigidity of the hydrogels and the appearance of spherulite like microstructures at higher TRIS concentrations may be attributed to increased crystallinity of the modified hydrogels. This increased crystallinity with increasing TRIS concentration was found within each pH level studied. By increasing the TRIS

concentration, the concentrations of structured hydrogen bond donors and acceptors also increased, producing more stability and alignment for the hydrogel network.

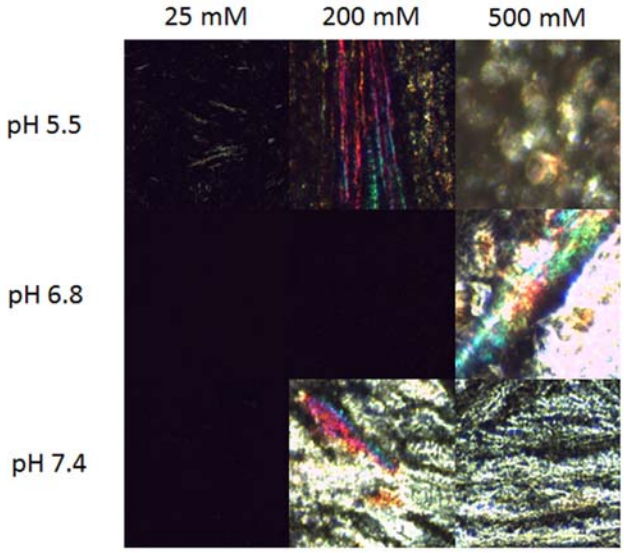

Figure 2.4. POM micrographs of pH 5.5, 6.8, and 7.4 hydrogels each with 25, 200, and 500 mM TRIS. Crystallinity is represented by brightness, and domains were found to be amorphous, fibrous, or spherulite in morphology. At pH 6.8 25 and 200 mM and pH 7.4 25 mM the micrographs were completely black with no apparent crystallinity.

2.3.4. XRD studies

X-ray diffraction (XRD) studies in conjunction with circular dichroism and quasi-elastic light scattering have been previously used to show that the structure and arrangement of NaDC molecules depend on several conditions including concentration, temperature, and salt concentration.[38,41] These studies showed that deoxycholate aggregates in cylindrical, helical, or spherical patterns are strongly induced as a result of hydrogen bonding. XRD studies were performed on hydrogels with 25, 200, and 500 mM TRIS at each of the three pH values (Figure 2.5) in order to quantify the crystallinity of these modified hydrogel structures. Counts obtained through XRD measurements have a direct relationship to crystallinity: Higher counts indicate higher crystallinity.

Examination of data from these studies confirmed that, in general, the crystallinity of the hydrogel increased with TRIS concentration, as visualized using POM.

For a pH value of 5.5, 25 mM TRIS produced a fairly amorphous hydrogel lacking any significant crystalline domains. Evaluation of the 200 mM TRIS hydrogel showed relatively intense crystalline planes at 2θ = 10.86° (5877 counts) and 21.7° (4594 counts). Peaks at these angles correspond to short range spacings of 8.3 and 4.1 nm, respectively. The 500 mM hydrogel exhibited several less intense (by an order of magnitude, ranging between 100 and 600 counts) crystalline planes between 2θ = 40° and 70°.

At pH 6.8, hydrogels with 25 and 200 mM TRIS had similar planes of crystallinity each at 2θ ≈ 10.7° and 21.5° with about 3300 and 2000 intensity counts, respectively. The intensities of these peaks were increased in the 500 mM hydrogel (13000 and 14400 counts respectively), where several less intense planes also resulted.

The XRD profile of the 25 mM gel at pH 7.4 revealed an amorphous hydrogel. This result is closely aligned with the liquid-like appearance of the hydrogel. The 200 and 500 mM hydrogels again showed peaks at 2θ ≈ 10.8° and 21.7°, although the intensities do not follow the trend observed at other pH values. The intensities of the peaks exhibited by the 200 mM hydrogel (27000 and 24000 counts at 10.8° and 21.7°, respectively) were about twice as intense as those exhibited by the 500 mM hydrogel (about 13000 and 9700 counts at 10.8° and 21.7°, respectively). A pH of 7.4 is well above the pKa of NaDC (6.6), resulting in charged, less hydrophobic molecules. This is expected to reduce the hydrogen bonding interactions as well as the hydrophobic interactions. It is evident from these results that hydrogen bonding is an extremely

important factor for increased gel rigidity. Based on these results, it follows that hydrogels with different planes of crystallinity should provide different templates for nanoparticle synthesis and thus can be exploited for such applications.

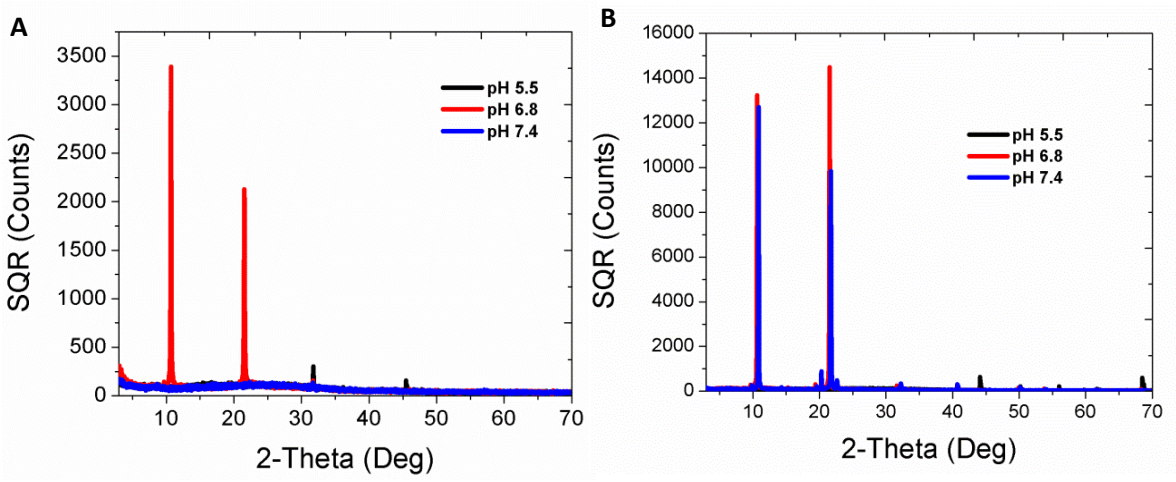

Figure 2.5. X-ray diffraction patterns of A) 25 mM TRIS and B) 500 mM TRIS, where increased counts indicate increased crystallinity.

2.3.5. DSC studies

Sol-gel transitions are endothermic events and can, therefore, be measured using DSC.[42] Endothermic transitions are represented by a significant decrease in measured heat flow. The sol-gel temperature of this system was found to increase with TRIS concentration, which is considered the result of increased crystallinity and network stability.[43] In this study, the sol-gel transition temperatures of the hydrogels were tuned from about 35 °C to about 65 °C (Table 2.2). Such a property could be extremely useful for *in situ* applications in that a hydrogel system could be selected to undergo or to avoid a sol-gel transition during an experiment. For example, a sol-gel temperature above 37 °C would allow a hydrogel to be used *in vivo* as artificial tissue or an implantable drug delivery device.[44]

Table 2.2. Sol-gel transition temperatures of gels as measured by differential scanning calorimetry. (Note: Due to the high water content and lack of covalent bonding, specific protocols were developed for each sample. An appropriate methodology could not be found for DSC analysis of these (*,**) gels. However, a sol-gel transition was visually observed between 50 and 60 °C for each of the three * samples and slightly above room temperature for the single ** sample.)

	concentration (mM)	approximate sol-gel temperature (°C)
pH 5.5	25	37
	100	49
	200	*
	250	*
	300	*
	500	63
pH 6.8	50	36
	100	47
	200	51
	400	54
pH 7.4	25	**
	100	50
	200	51
	300	61
	500	57

Measurements provided by use of DSC were also confirmed by visual observations of the gels in a water bath of gradually increasing temperature. An approximate temperature was recorded when a sample no longer appeared to have a gelatinous consistency. For example, the visually observed sol-gel temperature for pH 6.8, 50 mM (as seen in Table 2.2) was about 35 °C, compared to the DSC measurement of 36 °C (Figure 2.6). Increased sol-gel temperature with increased TRIS concentration confirmed the XRD and POM findings of increased crystallinity and rigidity under such conditions.

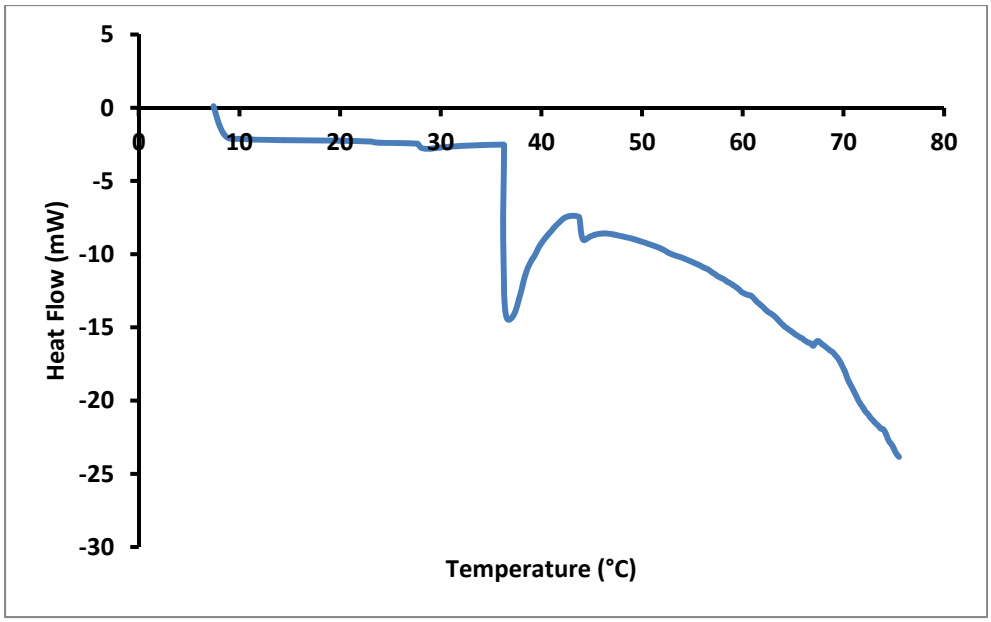

Figure 2.6. DSC thermogram of a hydrogel of pH 6.8 and 50 mM TRIS. The sharp decrease at 36 °C indicates a sol-gel transition. This closely corresponds to a visually observed transition at approximately 35 °C.

2.3.6. Rheology

Rheological studies are typically performed in order to examine the viscoelasticity of hydrogels.[45] Such studies are important for understanding the utility of these gels for various applications. For instance, high mechanical strength hydrogels can be useful for materials applications.[46] The storage modulus (G') and the loss modulus (G") were determined for each sample as a function of angular frequency (rad/s). Each hydrogel of this study had a particular shear rate after which the G' and G" showed erratic behavior. This is the shear rate at which there is enough mechanical stress placed on the structure of the gel such that it began to have greatly increased fluidity. This is commonly referred to as "breaking" the gel.[47] For pH values of 6.8 and 7.4, both the G' and G" showed a break at shear rates that increased with increasing concentrations of TRIS. This further supports the theory that increasing the TRIS concentration increases the internal structural rigidity of the hydrogels. At pH 5.5, the G" follows the observed

trend as well, with the breaking rate increasing from 28.6 rad s^{-1} to > 63 rad s^{-1} when the TRIS concentration increases from 25 to 500 mM. However, the G' does not follow an observable trend, which suggests a more complicated gelation mechanism. This observation is also complementary to fluorescence anisotropy results for the hydrophobic gel fibers where no regular trend was observed at this pH. The increase in fluidity that occurs during breaking lends to potential use of these hydrogels as drug delivery systems.[48] In addition, gels with high rigidity have potential utility for use in biotechnology applications such as artificial tissues.[49]

Under shear stress, a unique behavior was observed in several of the hydrogels in this study, namely pH 5.5: 200, 250, and 300 mM TRIS; pH 6.8: 200 mM TRIS; and pH 7.4: 300 mM TRIS (Figure 2.7 A-E). A plot of storage modulus versus shear frequency yielded two stable regions as opposed to the generally observed single region. In cases where no data are shown between the two stable regions (Figure 2.7 B, C, and E), the G' exhibits an erratic behavior indicative of a broken gel in the omitted region. Presence of two stable regions in the elastic modulus indicated that there are two ranges of shear frequency in which the hydrogels form stable structures. To the best of our knowledge, such a behavior has not been previously observed and yields exceptional potential for applications in injectable drug delivery.[50,51] Preliminary work was done to investigate this potential, and both hydrogel formulation and shearing seem to significantly affect drug release (Figure 2.7 F), warranting further investigation.

2.3.7. Characterization of hydrogel-templated nanoGUMBOS and microGUMBOS.

Modifications to the NaDC hydrogels, including changes in TRIS concentration and pH, led to tunable size variations of nano- and microGUMBOS formed therein

(Table 2.3). All nano- and microGUMBOS in this study are NIR dyes with potential applications in biological imaging. NanoGUMBOS formed in pH 5.5 hydrogel templates were relatively consistent in size at low TRIS concentrations with no specific trend

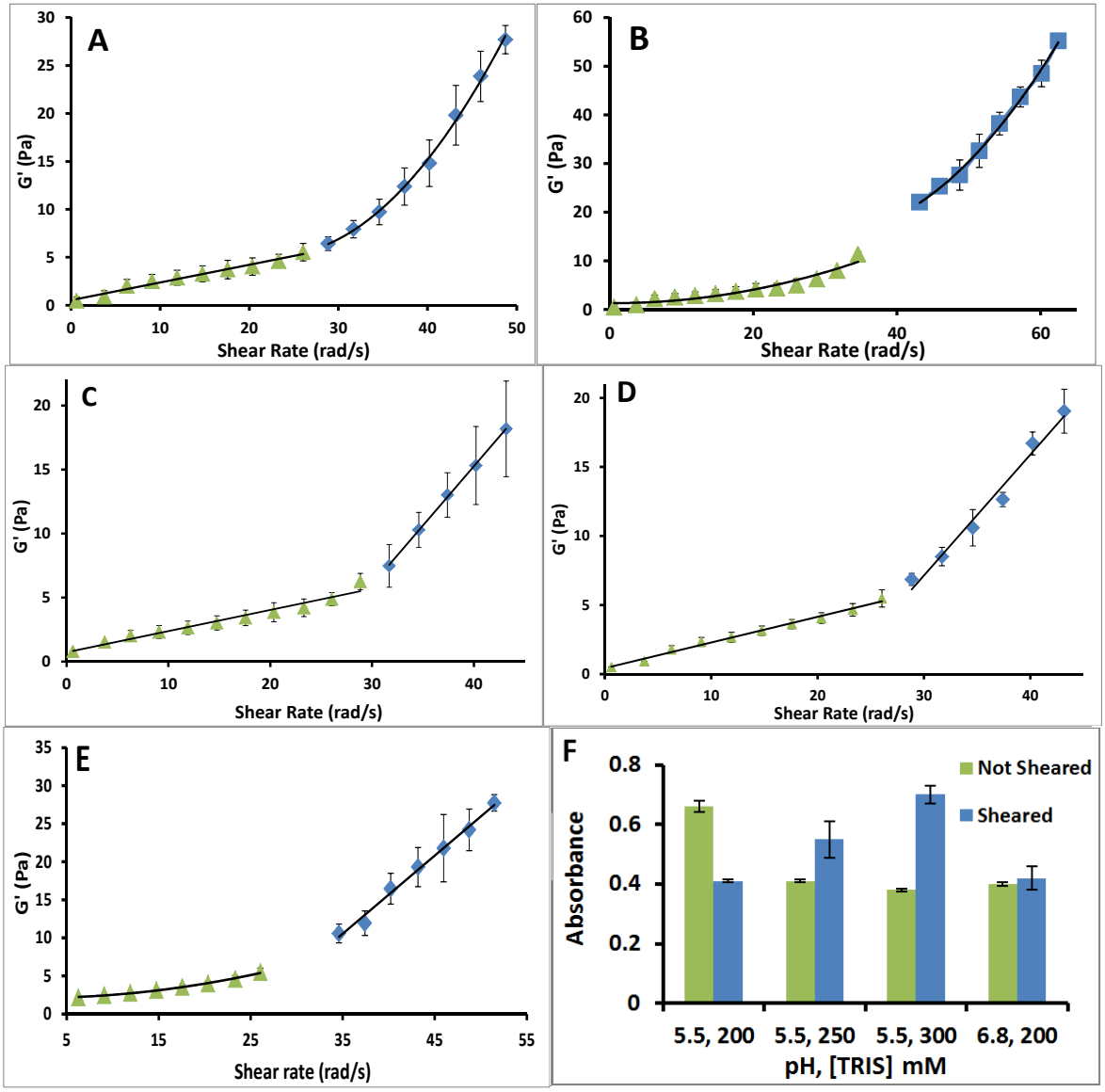

Figure 2.7. A-E: Rheograms (G') showing two distinct hydrogel structures at different ranges of shear rates. A) pH 5.5, 200 mM TRIS; B) pH 5.5, 250 mM TRIS; C) pH 5.5, 300 mM TRIS; D) pH 6.8, 200 mM TRIS; and E) pH 7.4, 300 mM TRIS. F: Release of fluorescein from several formulations. The green bars correspond to release from gels that had not been sheared and the blue to release from gels that had been sheared to 45 rad/s.

Table 2.3. Average size of [HMT][NTf2] nano- and microGUMBOS as measured from TEM micrographs.

pH	[TRIS] (mM)	size (nm)
5.5	25	57 ± 6
	100	46 ± 8
	200	44 ± 8
	250	72 ± 14
	300	809 ± 150
	500	8 ± 1
6	25	76 ± 6
	200	48 ± 11
	300	21 ± 4
	500	19 ± 4
6.8	50	33 ± 9
	100	62 ± 29
	200	209 ± 35
	400	30 ± 4
7.4	25	154 ± 26
	100	221 ± 58
	300	312 ± 58

observed with increasing TRIS concentration. For example, the size of [HMT][NTf_2] remained almost constant at 50 nm with increasing TRIS concentration between 25 and 200 mM. At 250 mM TRIS, such nanoGUMBOS slightly increased in size to 72 ± 14 nm

with even greater increases at 300 mM TRIS (microGUMBOS of 809 ± 150 nm). Additional increases in TRIS concentration to 500 mM led to a significant decrease in size of the nanoparticles to 8 ± 1 nm.

Hydrogels immobilized at pH 6.0 with 25 mM TRIS yielded [HMT][NTf_2] nanoparticles with an average size of 76 ± 6 nm (Figure 2.8A). This is effectively the same size as nanoparticles produced under similar conditions with the GUMBOS [HMT][AOT].[7] TRIS concentrations of 200 mM, 300 mM, and 500 mM resulted in respective particle sizes of 48 ± 11, 21 ± 4 nm, and 19 ± 4 nm (Figure 2.8 B-D). The size of the [HMT][NTf_2] nanoparticles were found to decrease with increasing TRIS concentration. This trend was the reverse of that found with [HMT][AOT] studies where particle size was found to increase with TRIS concentration.

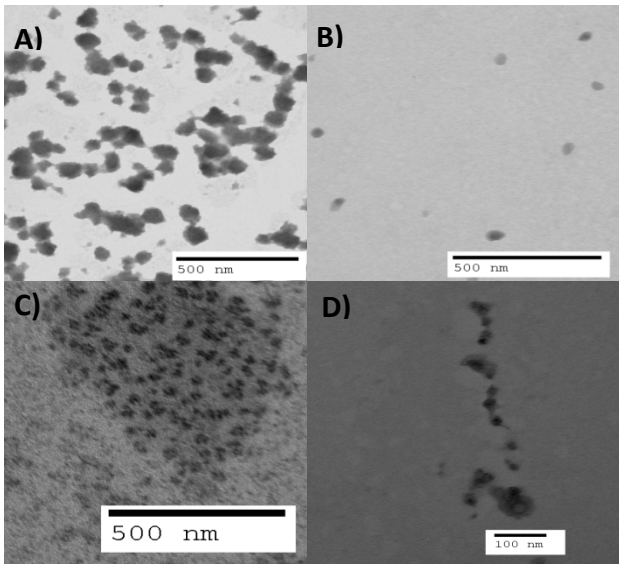

Figure 2.8. TEM micrographs of [HMT][NTf_2] nanoGUMBOS as templated by pH 6 hydrogels with A) 25 mM TRIS, B) 200 mM TRIS, C) 300 mM TRIS, and D) 500 mM TRIS. Under these conditions, particle size decreases with increasing TRIS concentration.

Contrasting trends found in nanoGUMBOS with [NTf_2] and [AOT] anions is believed to be a result of the relative hydrophobicities as determined by octanol/water partition coefficients ($P_{oct/wat}$). Hydrophobicity of [NTf_2] is significantly greater than that of [AOT] with respective $k_{oct/wat}$ values of 14.8 and 1.65. NanoGUMBOS with an even greater hydrophobicity ($k_{oct/wat}$=29.9), [HMT][TPB], were templated in pH 6.0 gels to confirm this theory. While the [HMT][TPB] nanoGUMBOS increased in size with an increase in TRIS, the particles had a wider range in size than did either of the other two GUMBOS investigated. From 25 to 500 mM TRIS, the [HMT][TPB] particles increased from 3.6 ± 0.5 to 257 ± 56 nm, indicating that particle size is material-dependent. However for a given material a definite trend in size was observed suggesting the applicability of these modified hydrogel systems for size-controlled synthesis of nanoparticles.

While the [HMT][NTf_2] nano- and microGUMBOS resulting from pH 6.8 templates did not follow an obvious trend in size, the sizes are consistent with the anisotropy studies performed on these gels. In smaller aqueous pools such as with 50 mM and 400 mM TRIS, the particles were 33 ± 9 nm and 30 ± 4 nm respectively. The largest aqueous pool of this pH formed the largest particles, i.e. 200 mM TRIS hydrogel forming 209 ± 35 nm particles. Pools of intermediate size, found in the 100 mM TRIS hydrogel, templated nanoGUMBOS of an intermediate size, i.e 62 ± 29 nm. This again suggests that the size of the aqueous pools is one of the governing factors for size control of the templated nanoparticles.

At pH 7.4, most particles were significantly larger than at other pH values and generally increased in size with increasing TRIS concentration from 154 ± 26 nm to 312 ± 58 nm with TRIS concentrations of 25-300 mM.

2.4. Conclusions

In conclusion, I have developed multiple new NaDC/TRIS hydrogel materials through variation of TRIS concentration within fixed pH values. These new materials were characterized and evaluated for nanosynthesis and drug delivery applications. Modification of the hydrogels led to a broad range of attainable properties. NanoGUMBOS of three NIR dyes were templated using hydrogels, and the resulting nanoparticle size was concluded to be material dependent and governed by the gel microstructure and rheological characteristics. As evidenced by anisotropy calculations, POM, and XRD characterization, pH and TRIS concentration within a given pH play an extremely important role towards crystallinity and structural rigidity of the hydrogels. Tunable crystallinity resulted in tunable sol-gel transition temperatures between slightly above room temperature and 63 °C, as measured by DSC and visually observed. Rheological studies showed that these designer hydrogels have tunable mechanical properties that could be suitable for bioengineering and drug delivery applications. Tunability was found in hydrogels immobilized at the physiological pH value, further demonstrating suitability in biological applications.

2.5. References

1. Rich, A.; Blow, D.M. Formation of a helical steroid complex. *Nature* 1958, *182*, 423-426.

2. Sobotka, H.; Czeczowiczka, N. The gelation of bile salt solutions. *Journal of Colloid Science.* 1958, *13*, 188-91.

3. Svobodova, H.; Noponen, V.; Kolehmainen, E.; Sievaenen, E. Recent advances in steroidal supramolecular gels. *RSC Advances.* 2012, *2*, 4985-5007.

4. Moss, G. P. Nomenclature of steroids. (Recommendations 1989). *Pure and Applied Chemistry.* 1989, *61*, 1783-822.

5. Terech, P.; Dourdain, S.; Maitra, U.; Bhat, S. Structure and Rheology of Cationic Molecular Hydrogels of Quinuclidine Grafted Bile Salts. Influence of the Ionic Strength and Counter-Ion type. *Journal of Physical Chemistry B* 2009, *113*, 4619-4630.

6. Jover, A.; Meijide, F.; Rodriguez, N. E.; Vazquez, T. J. Dynamic Rheology of Sodium Deoxycholate Gels. *Langmuir* 2002, *18*, 987-991.

7. Das, S.; de Rooy, S. L.; Jordan, A. N.; Chandler, L.; Negulescu, II; El-Zahab, B.; Warner, I. M. Tunable size and spectral properties of fluorescent nanoGUMBOS in modified sodium deoxycholate hydrogels. *Langmuir* 2012, *28*, 757-65.

8. Valenta, C.; Nowack, E.; Bernkop-Schnurch, A. Deoxycholate-hydrogels: novel drug carrier systems for topical use. *International Journal of Pharmaceutics.* 1999, *185*, 103-11.

9. Gan, Q.; Wang, T.; Cochrane, C.; McCarron, P. Modulation of surface charge, particle size and morphological properties of chitosan–TPP nanoparticles intended for gene delivery. *Colloids and Surfaces., B* 2005, *44*, 65-73.

10. Hamada, K.; Yamada, K.; Mitsuishi, M.; Ohira, M.; Miyazaki, K. Gelation of an aqueous fluorinated dye solution. *Journal of the Chemical Society, Chemical Communications* 1992, 7, 544-5.

11. Park, S. M.; Lee, Y. S.; Kim, B. H. Novel low-molecular-weight hydrogelators based on 2'-deoxyuridine. *Chemical Commununications (Cambridge, U. K.)* 2003, 23, 2912-2913.

12. van Esch, J. H. We Can Design Molecular Gelators, But Do We Understand Them? *Langmuir* 2009, *25*, 8392-8394.

13. Ferrer, M. L.; Del Monte, F. Enhanced emission of Nile red fluorescent nanoparticles embedded in hybrid sol-gel glasses. *Journal of Physical Chemistry B* 2005, *109*, 80-86.

14. Gutierrez, M. C.; Hortigueela, M. J.; Ferrer, M. L.; del Monte, F. Highly Fluorescent Rhodamine B Nanoparticles Entrapped in Hybrid Glasses. *Langmuir* 2007, *23*, 2175-2179.

15. Jensen, B. E. B.; Alves, M.-H.; Fejerskov, B.; Stadler, B.; Zelikin, A. N. Surface adhered poly(vinyl alcohol) physical hydrogels as tools for rational design of intelligent biointerfaces. *Soft Matter* 2012, *8*, 4625-4634.

16. Yamamichi, S.; Jinno, Y.; Haraya, N.; Oyoshi, T.; Tomitori, H.; Kashiwagi, K.; Yamanaka, M. Separation of proteins using supramolecular gel electrophoresis. *Chemical Communications* 2011, *47*, 10344-10346.

17. Wada, A.; Tamaru, S.-i.; Ikeda, M.; Hamachi, I. MCM−Enzyme−Supramolecular Hydrogel Hybrid as a Fluorescence Sensing Material for Polyanions of Biological Significance. *Journal of the American Chemical Society* 2009, *131*, 5321-5330.

18. Marler, J. J.; Guha, A.; Rowley, J.; Koka, R.; Mooney, D.; Upton, J.; Vacanti, J. P. Soft-tissue augmentation with injectable alginate and syngeneic fibroblasts. *Plastic and Reconstructive Surgery* 2000, *105*, 2049-58.

19. Yoshida, R.; Sakai, K.; Okano, T.; Sakurai, Y.; You Han, B.; Sung Wan, K. Surface-modulated skin layers of thermal responsive hydrogels as on-off switches: I. Drug release. *Journal of Biomaterials Science, Polymer Edition* 1992, *3*, 155-162.

20. Calvert, P. Hydrogels for Soft Machines. *Advanced Materials* 2009, *21*, 743-756.

21. de Rooy, S. L.; Das, S.; Li, M.; El-Zahab, B.; Jordan, A.; Lodes, R.; Weber, A.; Chandler, L.; Baker, G. A.; Warner, I. M. Ionically Self-Assembled, Multi-Luminophore One-Dimensional Micro- and Nanoscale Aggregates of Thiacarbocyanine GUMBOS. *Journal of Physical Chemistry C* 2012, *116*, 8251-8260.

22. Chen, J. H., C.M.; Lin, X.W.; Tang, Z.J.; Su, S.J. The research of silver nanoparticle dressing in the therapy of II burn wounds. *Chinese Journal of Surgery* 2006, *44*, 50-52.

23. Kim, K. J.; Sung, W. S.; Suh, B. K.; Moon, S. K.; Choi, J. S.; Kim, J. G.; Lee, D. G. Antifungal activity and mode of action of silver nano-particles on Candida albicans. *Biometals* 2009, *22*, 235-42.

24. Bwambok, D. K.; El-Zahab, B.; Challa, S. K.; Li, M.; Chandler, L.; Baker, G. A.; Warner, I. M. Near-infrared fluorescent nanoGUMBOS for biomedical imaging. *ACS Nano* 2009, *3*, 3854-60.

25. Tesfai, A.; El-Zahab, B.; Kelley, A. T.; Li, M.; Garno, J. C.; Baker, G. A.; Warner, I. M. Magnetic and nonmagnetic nanoparticles from a group of uniform materials based on organic salts. *ACS Nano* 2009, *3*, 3244-50.

26. Das, S.; Bwambok, D.; El-Zahab, B.; Monk, J.; de Rooy, S. L.; Challa, S.; Li, M.; Hung, F. R.; Baker, G. A.; Warner, I. M. Nontemplated approach to tuning the spectral properties of cyanine-based fluorescent nanoGUMBOS. *Langmuir* 2010, *26*, 12867-76.

27. Warner, I. M.; El-Zahab, B.; Siraj, N. Perspectives on Moving Ionic Liquid Chemistry into the Solid Phase. *Analytical Chemistry* 2014, 86, 7184-91.

28. Siraj, N.; Hasan, F.; Das, S.; Kiruri, L. W.; Steege Gall, K. E.; Baker, G. A.; Warner, I. M. Carbazole-Derived Group of Uniform Materials Based on Organic Salts: Solid State Fluorescent Analogues of Ionic Liquids for Potential Applications in Organic-Based Blue Light-Emitting Diodes. *Journal of Physical Chemistry C* 2014, *118*, 2312-2320.

29. Jordan, A. N.; Siraj, N.; Das, S.; Warner, I. M. Tunable near-infrared emission of binary nano- and mesoscale GUMBOS. *RSC Advances* 2014, *4*, 28471-28480;

30. Sarkar, A. K., K.; Jagadish, N.N.; Jordan, A.; Das, S.; Siraj, N.; Warner, I.M.; Daniels-Race, T. Electro-optical characterization of cyanine-based GUMBOS and nanoGUMBOS. *Electronic Materials Chemistry* 2014, *10,* 775-781.

31. Jordan, A. N.; Das, S.; Siraj, N.; de Rooy, S. L.; Li, M.; El-Zahab, B.; Chandler, L.; Baker, G. A.; Warner, I. M. Anion-controlled morphologies and spectral features of cyanine-based nanoGUMBOS--an improved photosensitizer. *Nanoscale* 2012, *4*, 5031-8.

32. Magut, P. K. S.; Das, S.; Fernand, V. E.; Losso, J.; McDonough, K.; Naylor, B. M.; Aggarwal, S.; Warner, I. M. Tunable Cytotoxicity of Rhodamine 6G via Anion Variations. *Journal of the American Chemical Society* 2013, *135*, 15873-15879.

33. Cole, M. R.; Li, M.; Jadeja, R.; El-Zahab, B.; Hayes, D.; Hobden, J. A.; Janes, M. E.; Warner, I. M. Minimizing human infection from Escherichia coli O157:H7 using GUMBOS. *Journal of Antimicrobial Chemotherapy* 2013, *68*, 1312-1318.

34. Regmi, B. P.; Monk, J.; El-Zahab, B.; Das, S.; Hung, F. R.; Hayes, D. J.; Warner, I. M. A novel composite film for detection and molecular weight determination of organic vapors. *Journal of Materials Chemistry C* 2012, *22*, 13732-13741.

35. Regmi, B. P.; Speller, N. C.; Anderson, M. J.; Brutus, J. O.; Merid, Y.; Das, S.; El-Zahab, B.; Hayes, D. J.; Murray, K. K.; Warner, I. M. Molecular weight sensing properties of ionic liquid-polymer composite films: theory and experiment. *Journal of Materials Chemistry C* 2014, *2*, 4867-4878.

36. Pileni, M. P. Reverse micelles as microreactors. *Journal of Physical Chemistry* 1993, *97*, 6961-6973.

37. de Loos, M.; Feringa, B. L.; van Esch, J. H. Design and Application of Self-Assembled Low Molecular Weight Hydrogels. *European Journal of Organic Chemistry* 2005, *2005*, 3615-3631.

38. D'Archivio, A. A.; Galantini, L.; Giglio, E.; Jover, A. x-ray and Quasi-Elastic Light-Scattering Studies of Sodium Deoxycholate. *Langmuir* 1998, *14*, 4776-4781.

39. Weber, G.; Farris, F. J. Synthesis and spectral properties of a hydrophobic fluorescent probe: 6-propionyl-2-(dimethylamino)naphthalene. *Biochemistry* 1979, *18*, 3075-8.

40. Weber, G., and Laurence, D.J.R. *Biochemistry* 1954, *56, xxxi.*

41. Murata, G. S.Y.; Nishikido, N.; Tanaka, M. In *Solution Behavior of Surfactants:Theoretical and Applied Aspects*, Fendler, K. L. M. a. E. J., Ed. Springer US: 1982; Vol. 1, pp 611-627.

42. Wanka, G.; Hoffmann, H.; Ulbricht, W. The aggregation behavior of poly-(oxyethylene)-poly-(oxypropylene)-poly-(oxyethylene)-block-copolymers in aqueous solution. *Colloid Polymer Science* 1990, *268*, 101-117.

43. Tan, H. M.; Chang, B. H.; Baer, E.; Hiltner, A. Relationship between crystallinity and thermoreversible gelation. *European Polymer Journal* 1983, *19*, 1021-1025.

44. Ruel-Gariépy, E.; Leroux, J.-C. In situ-forming hydrogels—review of temperature-sensitive systems. *European Journal of Pharmaceutics and Biopharmaceutics* 2004, *58*, 409-426.

45. Wu, D.-Q.; Wang, T.; Lu, B.; Xu, X.-D.; Cheng, S.-X.; Jiang, X.-J.; Zhang, X.-Z.; Zhuo, R.-X. Fabrication of Supramolecular Hydrogels for Drug Delivery and Stem Cell Encapsulation. *Langmuir* 2008, *24*, 10306-10312.

46. Schneider, J. P.; Pochan, D. J.; Ozbas, B.; Rajagopal, K.; Pakstis, L.; Kretsinger, J. Responsive Hydrogels from the Intramolecular Folding and Self-Assembly of a Designed Peptide. *Journal of the American Chemical Society* 2002, *124*, 15030-15037.

47. Breedveld, V.; Nowak, A. P.; Sato, J.; Deming, T. J.; Pine, D. J. Rheology of Block Copolypeptide Solutions: Hydrogels with Tunable Properties. *Macromolecules* 2004, *37*, 3943-3953.

48. Roos, A. A.; Edlund, U.; Sjöberg, J.; Albertsson, A.-C.; Stålbrand, H. Protein Release from Galactoglucomannan Hydrogels: Influence of Substitutions and Enzymatic Hydrolysis by β-Mannanase. *Biomacromolecules* 2008, *9*, 2104-2110.

49. Kobayashi, M.; Toguchida, J.; Oka, M. Preliminary study of polyvinyl alcohol-hydrogel (PVA-H) artificial meniscus. *Biomaterials* 2003, *24*, 639-647.

50. Li, J.; Ni, X.; Leong, K. W. Injectable drug-delivery systems based on supramolecular hydrogels formed by poly(ethylene oxide)s and α-cyclodextrin. *J. Biomedical Materials Research, Part A* 2003, *65A*, 196-202.

51. Jeong, B.; Bae, Y. H.; Lee, D. S.; Kim, S. W. Biodegradable block copolymers as injectable drug-delivery systems. *Nature (London)* 1997, *388*, 860-862.

CHAPTER 3.
SODIUM DEOXYCHOLATE/TRIS-BASED HYDROGELS FOR MULTIPURPOSE SOLUTE DELIVERY VEHICLES: AMBIENT RELEASE, DRUG RELEASE, AND ENANTIOPREFERENTIAL RELEASE*

3.1. Introduction

The study of controlled and sustained drug release vehicles has been a topic of increasing attention over the past several decades. Delivery vehicles are widely applied in many fields ranging from food production to agriculture to pharmaceuticals.[1] Drug delivery vehicles, specifically, are rapidly gaining importance as the focus of drug development shifts from small molecules to macromolecular biologics.[2] Biologics require higher delivery concentrations,[3] more protection from metabolic interactions,[4] and more targeted delivery than small molecule drugs.[5] Due to these requirements, more sophisticated delivery vehicles are needed. Hydrogels are often selected as drug delivery vehicles because of similarities to biological membranes[6] and beneficial characteristics[7] including high water content relative to other materials,[8] biocompatibility,[9] biodegradability,[10] stimuli-responsiveness,[11] and high porosity.[12] Low molecular weight (LMW), physical hydrogels have the benefits of facile processing[13] and lower toxicity due to the absence of crosslinkers.[14]

Hydrophobic domains within a hydrogel network can be used to increase

---

* This chapter previously appeared as "McNeel, K. E., Siraj, N., Negulescu, I., & Warner, I. M. Sodium deoxycholate/TRIS-based hydrogels for multipurpose solute delivery vehicles: Ambient release, drug release, and enantiopreferential release." Reproduced with permission from *Talanta*. *177*, 66-73. Copyright 2017 Elsevier B.V.

loadable drug concentration because most pharmaceuticals have low water solubility.[7,15,16] Hydrogel matrices are often used to protect drugs, specifically biologics such as proteins and antibodies, until the target is reached.[4] Injectable hydrogels are also often used for biologics to provide more targeted delivery. Protection of drugs also lowers the necessary dosage by reducing dilution of the drug in the body and retaining elevated local concentration through slow release.[7] Furthermore, frequency of administration can be reduced through the use of a hydrogel exhibiting sustained release properties.[17]

In addition to the rising number of biologic drugs, more than half of the molecular drugs on the market are chiral and exist as a mixture of enantiomers, making chirality an important consideration in the pharmaceutical industry.[18] In many cases, one enantiomer is less active than the other, making separation of enantiomers beneficial. In more severe cases, one enantiomer exhibits toxicity, which highlights the importance of enantiomeric separations. In order to formulate a pharmaceutical with a single enantiomer, a separation method such as chromatography or capillary electrophoresis is typically employed.[19,20,21] When these traditional methods of separations (chromatography, electrophoresis) are employed, enantiomeric separation must occur offline before the separated drug can be administered, thereby increasing cost and time for pre-processing. An ideal solution would involve racemic drug loading (i.e. equal amounts of each enantiomer) into a delivery vehicle from which only one enantiomer would be released.[22] Over the past decade, a few enantio-selective release hydrogels have been designed using a variety of methods and polymeric or LMW gelators. For example, Suedee et al. reported on chitosan-based transdermal patches for selective

delivery of S-propranolol.[23] This group later developed a pH-responsive system composed of poly(hydroxyethyl methacrylate) and polycaprolactone-triol for selective delivery of S-omeprazole.[24] In 2014, Suksuwan et al. demonstrated selective release of R-thalidomide from a polymer network composed of methacrylic acid, 2,6-bis(acrylamido)pyridine, and N,N' methylene-bis-acrylamide.[25] All three of these systems have excellent functionality in delivering the desired enantiomer. However, in all cases, synthesis of such systems required many steps, inclusive of chemical modification, polymerization, and molecular imprinting. Each of these steps takes technical ability and significant analysis, increasing the time and cost of development and production.

The Warner research group has recently studied the tunability of sodium deoxycholate (NaDC)/ tris(hydroxymethyl)aminomethane (TRIS) hydrogel systems.[26,27] Mechanical properties, sol-gel temperature, and release propeties were found to be tunable with modifications to pH and TRIS concentration. In the current study, I extend the preliminary findings of the previous work to explore the drug delivery capabilities of NaDC/TRIS hydrogels using model drugs of variable molecular weight and chirality. Analytes include fluorescein (a small molecule), bovine serum albumin (a 66 kDa protein), and the chiral molecules tryptophan and ibuprofen. The effect of shearing on the release of solutes was examined in order to simulate injection, as in subcutaneous drug delivery. Furthermore, other variables such as temperature, drug concentration, and hydrogel formulation were also explored as parameters affecting drug release. Each of these variables can be varied to tune drug release, indicating the broad tunability of NaDC/TRIS hydrogels as solute delivery systems. The specific application

of enantio-preferential drug release was examined in detail through release of both enantiomeric forms of model drugs. This NaDC/TRIS hydrogel system is a facilely synthesized, inexpensive candidate for injectable and enantio-selective drug delivery.

3.2. Materials and methods

3.2.1. Materials

Sodium deoxycholate (NaDC) (≥ 97%), tris(hydroxymethyl)aminomethane (TRIS) (≥ 99.9%), fluorescein sodium salt (≥ 97.5%), bovine serum albumin (BSA) (≥ 96%), α-lactalbumin (αLB) (≥ 85%), (S)-(+)-ibuprofen (≥ 99%), L-phenylalanine (≥ 98%), and L-tryptophan (≥ 98%) were purchased from Sigma Aldrich. (R)-(-)-ibuprofen (≥ 98%) was obtained from Enzo Life Sciences. D-phenylalanine (≥ 99.9%) and D-tryptophan (≥ 98%) were obtained from Bachem. γ-Cyclodextrin (≥ 98%) was obtained from Fluka. All chemicals were used as received. Triply deionized water (18 MΩ cm) was obtained from an Aries Filterworks high purity water system and used for all experiments.

3.2.2. Hydrogel selection and synthesis

Aqueous TRIS buffer solutions were prepared at 200, 250, and 300 mM. By use of hydrochloric acid, each TRIS solution was adjusted from an initial native pH value greater than 10 to an acidic pH value of 5.5. Solutions of 200 mM TRIS were also adjusted to a pH value of 6.8, generating a total of four formulations. These conditions of pH value and TRIS concentration were chosen because they were previously found to yield interesting rheological properties.[27] NaDC was added to the TRIS buffer solutions as a solid to produce a final concentration of 20 mM. NaDC addition was followed immediately with 30 seconds of vortexing and 20 minutes of bath sonication.

After sonication, samples were left to stabilize at 5 °C overnight before analyses. For drug delivery applications, it is useful to note that gelator is less than 1% of the system by weight. The hydrogel is composed of a maximum 6% TRIS (at 500 mM), while the remaining ≥ 93% is water.

3.2.3. Swelling Measurements

Swelling ratio is an important characteristic of hydrogel drug delivery vehicles due to drug loading and *in vivo* behavior dependence on these values. In order to measure swelling ratios, hydrogels were synthesized as previously outlined. Excess water was added to each gel after overnight stabilization, and samples were left to equilibrate for a week. After one week, any excess water not immobilized by the hydrogel was removed (leaving m_s). Dried gels were obtained by leaving exposed hydrogel samples in a desiccator (m_d). Swelling ratio was calculated as follows:

$$Swelling\ ratio = \frac{m_s - m_d}{m_d}$$

where m_s is the mass of the swollen hydrogel and m_d is the mass of the dry sample.

3.2.4. Viscoelastic measurements

A TA AR 1000 rheometer (TA Instruments, Inc., Waters Corp., New Castle, DE) with stainless steel plate geometry was used to investigate the rheological properties of these hydrogels, specifically the G' and G" moduli. This rheometer was also used to shear the hydrogels before solute release analyses.

3.2.5. Solute release measurements

Solute release measurements were performed using sets of identical hydrogels to measure different parameters within the same experiment. For example, if solute release was measured after one hour and after six hours, two hydrogels were prepared (one for each time of interest). At fixed time intervals, drug release was monitored by use of the absorbance of the supernatant. Absorbance was measured using a UV-vis-near-IR scanning spectrometer (Shimadzu, Columbia, MD). A 4 mm path length quartz cuvette (Starna Cells) was used for absorbance measurements with an identical cuvette filled with phosphate buffer as a blank. Fluorescein concentration was calculated using a linear calibration curve. Model drugs based on proteins and amino acids (BSA, α-lactalbumin, tryptophan) were analyzed at the absorbance wavelength of 280 nm. Ibuprofen was analyzed at 210 nm. Release experiments were performed at two different temperatures as noted with the corresponding data. All tryptophan and ibuprofen release experiments were performed at 37 °C. Room temperature experiments were performed under purely benchtop conditions. Experiments at 37 °C were performed in a temperature controlled incubator.

3.3. Results and discussion

3.3.1. Swelling capacity of hydrogels

Diffusion of drugs and other solutes from a hydrogel network is due in large part to the swelling capacity of the hydrogel system. Generally, an increased swelling ratio results in increased drug release. In the case of NaDC/TRIS-based hydrogels, swelling ratio was found to be dependent on TRIS concentration of hydrogel formulation (Table 3.1). Interestingly, the calculated swelling ratio decreased with increasing TRIS

concentration at pH 5.5. Hydrogels of pH 5.5, 200 mM TRIS had swelling ratios of 72.9 ± 0.9. An increase in TRIS concentration to 250 mM at pH 5.5 resulted in a significantly decreased swelling ratio of 57.0 ± 0.4. A further increase in TRIS concentration (i.e. to 300 mM) resulted in a smaller decrease in swelling ratio to 50.6 ± 0.2. Since TRIS has hydrogen bonding sites, it is likely that increased TRIS concentration reduced swelling by physically crosslinking the hydrogel to a further degree at higher concentrations. Previous work has also shown that this increase in [TRIS] enhanced the crystallinity, further supporting that increased [TRIS] restricted the hydrogel swelling.

Table 3.1. Swelling ratio of hydrogels with varied TRIS concentration

[TRIS] (mM)	Swelling ratio
200	72.9 ± 0.9
250	57.0 ± 0.4
300	50.6 ± 0.2

3.3.2. Viscoelasticity of solute-loaded hydrogels

I previously reported that several formulations of NaDC/TRIS-based hydrogels exhibit a unique rheological behavior.[27] The elastic modulus (G') of these materials showed two stable regions instead of the typical single region. The presence of two stable regions is interpreted as a rearrangement of internal gel structure upon application of sufficient shear rate.

Sun and colleagues[28] observed that the addition of certain amino acids to sodium deoxycholate hydrogels would disturb the hydrogel network enough to induce a gel-to-

sol transition. Since many target molecules for injectable systems are composed of proteins, it is of the utmost importance that this system retains its viscoelasticity upon addition of proteins. Figure 3.1A shows the elastic moduli of hydrogels of pH 5.5, 300 mM TRIS with 0, 1, 10, and 50 mg/mL BSA. As shown in this figure, increases in BSA concentrations (from 0-50 mg of BSA per mL of hydrogel) did not significantly change the observed elastic modulus of hydrogels within the range of angular shearing frequencies examined. It is important to note that the presence of two stable elastic regions is retained at all protein concentrations examined. The retention of viscoelastic properties with addition of BSA indicated that these hydrogels are good candidates for protein delivery systems.

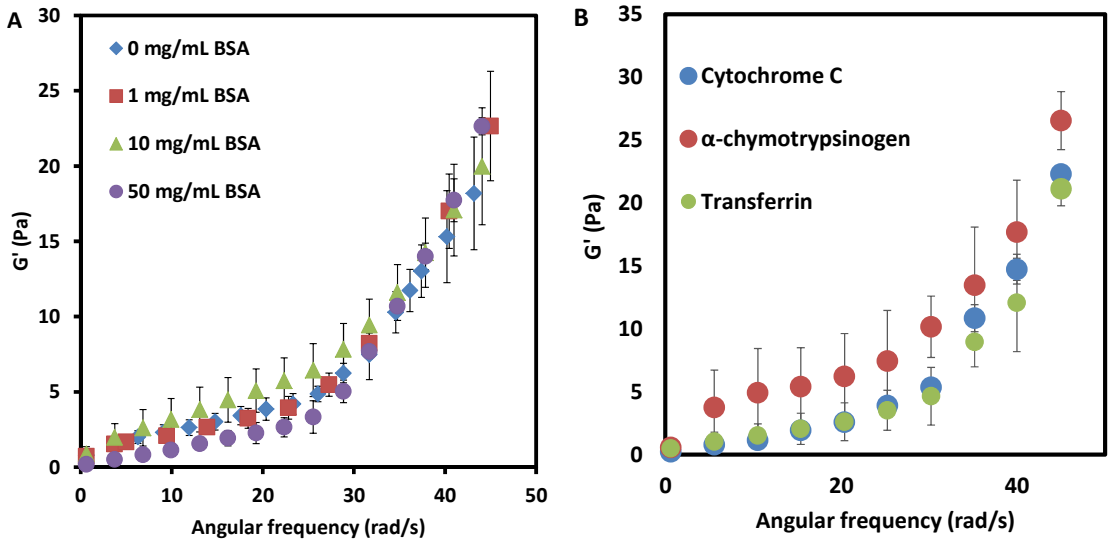

Figure 3.1. Angular frequency vs. G', storage modulus, of hydrogels pH 5.5 and 300 mM TRIS A) Four concentrations of BSA, i.e. 0, 1, 10, and 50 mg/mL. B) 3 proteins loaded at 10 mg/mL.

Three proteins of varying sizes were loaded into hydrogels of pH 5.5, 300 mM at 10 mg/mL (viz. cytochrome c – 12 kDa, α-chymotrypsinogen – 25.6 kDa, transferrin – 80 kDa). The elastic moduli of these protein-loaded gels were not significantly different

from those of native (i.e. non-loaded) hydrogels (Figure 3.1B). The unchanged moduli suggest that the hydrogel structure is highly resilient and can be used with a wide variety of loaded protein drugs.

3.3.3. Fluorescein release: effect of shearing, hydrogel formulation, loaded concentration, and temperature

Small molecule solutes, such as dyes, are often desirable for sustained release applications. The release of a small solute, fluorescein, was examined from sheared and non-sheared hydrogels of pH 5.5, 300 mM TRIS at room temperature and at 37 °C in order to analyze utility of this hydrogel system as a drug delivery vehicle (Figure 3.2). At room temperature, sheared and native gels completed fluorescein release in approximately 6 hours. Shearing resulted in a significant increase of total fluorescein released. Maximum release of fluorescein was increased from 175 μM to 303 μM, i.e. almost double. Disodium salt of fluorescein has significant water solubility. It is likely that upon shearing, the hydrogel structure becomes more porous in such a manner that fluorescein diffuses out in greater quantity. This significant increase in fluorescein release is critical to applicability of this system. To the best of our knowledge, this shearing effect on solute release has not been previously explored. The significant difference in release indicates that the mode of application (i.e. whether or not the hydrogel will be sheared before desired release) must be taken into consideration when calculating solute loading versus solute dosing concentrations for ambient temperature release.

Release of fluorescein at 37 °C was similarly found to plateau in ~6 hours (Figure 3.2B). Samples were allowed to release for 18 hours in order to ensure complete

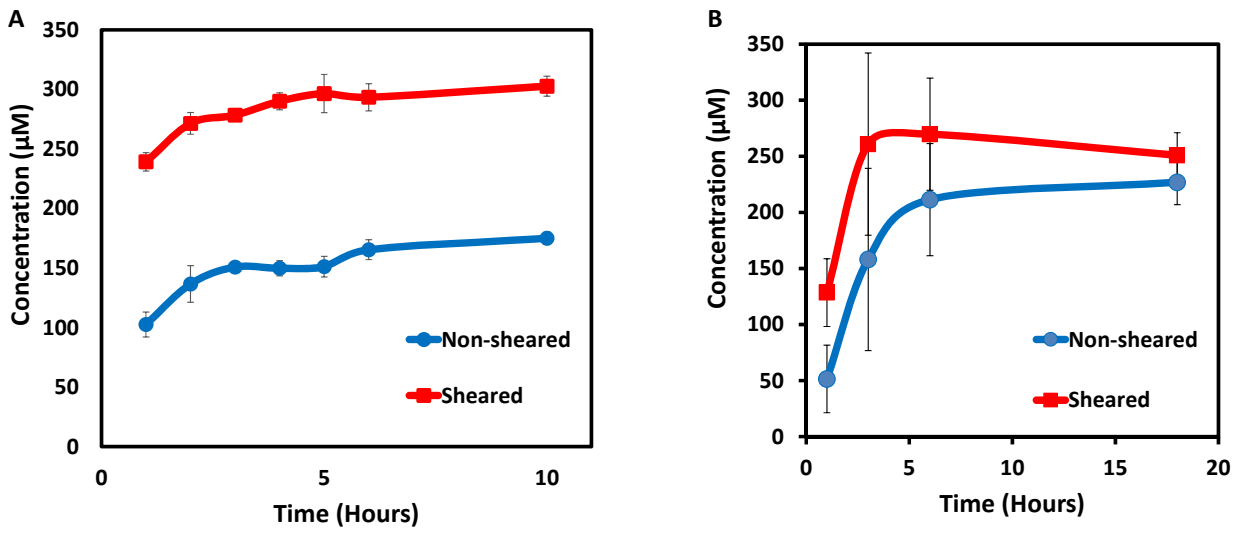

Figure 3.2. Release profiles of 500 µM disodium fluorescein from pH 5.5, 300 mM TRIS hydrogels that had and had not been sheared. A) Release at room temperature B) Release at 37 °C

release. Within the first hour, sheared hydrogels released significantly more fluorescein than a hydrogel that had not been sheared. As seen with room temperature release, shearing likely disrupted the crystalline packing of the hydrogel structure, which consequently lessened the hindrance of fluorescein release. At later time intervals, the difference was no longer as significant. However, within a single trial, sheared release was always higher than non-sheared release. Over longer periods of time at 37 °C, crystallinity of hydrogel structure likely began to reform (i.e. self-repair) from the disruption of shearing as evidenced by similarity in released fluorescein from sheared and non-sheared hydrogels at later times. The majority of release occurred within the first three hours, indicating that these materials are not suitable for prolonged release (> 6 hours) in their current form. For release over shorter time periods (< 6 hours) the mode of application (sheared or not) should still be considered. Long-term release applications can be loaded with less consideration of application mode for release at 37

°C. Thus, final solute release must be determined based on whether or not a shearing force will be applied to the gel before desired release and the temperature at which release will occur.

Three hydrogel formulations were investigated as sustained release vehicles. Specifically, solutions immobilized at a pH value of 5.5 were evaluated with three different TRIS concentrations, viz. 200 mM, 250 mM, and 300 mM. Increases in TRIS concentration has been previously shown to increase crystallinity of the materials, which may itself impact release.[26,27] As expected, formulation was determined to significantly affect total fluorescein release at room temperature (Figure 3.3A). It was found that at pH 5.5, an increase in TRIS concentration decreased the total amount of fluorescein released from hydrogels that had not been sheared. This decrease closely followed the decreased swelling ratio found between these hydrogel formulations. The decrease in fluorescein release also suggested that the closely related parameter of crystallinity impeded solute release. Interestingly, it was found that increased TRIS concentration also resulted in an increase of total fluorescein released from hydrogels that had been sheared. It is possible that shearing disrupted the crystalline packing of these materials, thereby reducing the impediment on solute release. Interestingly, at 37 °C average release of fluorescein decreased with increasing TRIS concentration (Figure 3.3B). As was seen at room temperature, decreased fluorescein release from gels that had not been sheared paralleled the decrease in swelling ratio. Unlike at room temperature, this trend was seen in both gels that had and had not been sheared. The decrease in amount of fluorescein released was likely due in part to crystallinity of the samples. While shearing is thought to disrupt crystallinity in these materials, examination of these

data suggested that at 37 °C, hydrogels reformed crystalline packing. Therefore, the amount of solute released from a hydrogel could be tuned simply by changing TRIS concentration when the mode (sheared or not) and temperature of delivery are known. The ease of this tunability is exceptionally useful for the applicability of this system.

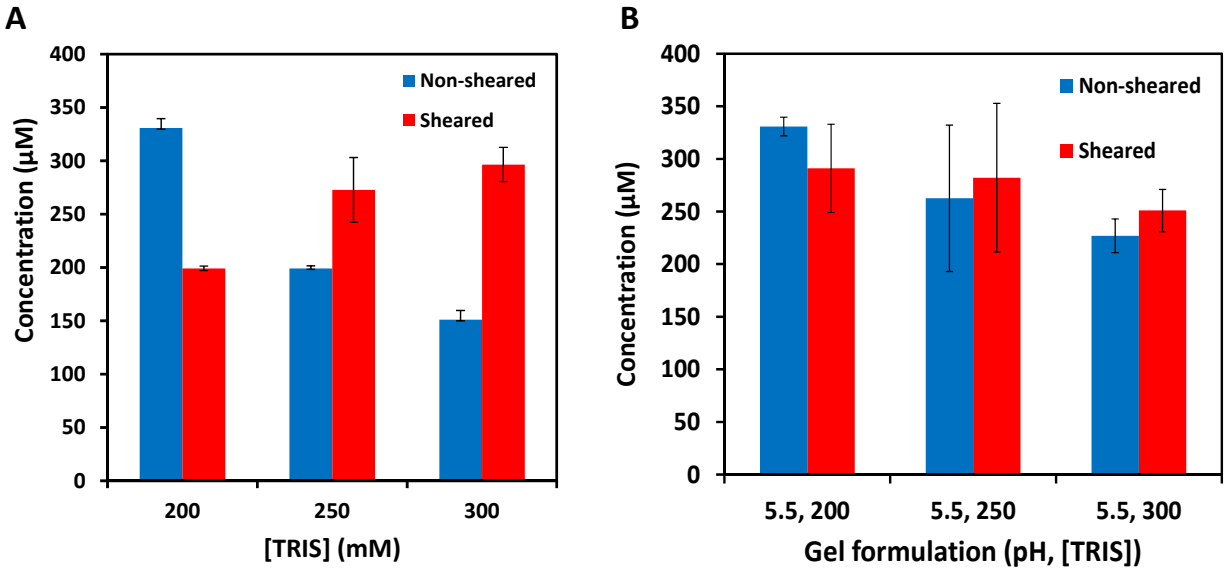

Figure 3.3. Effect of TRIS concentration in pH 5.5 hydrogels on release of fluorescein at A) room temperature B) 37 °C.

Several concentrations (viz. 100, 300, 500, 700, and 1000 μM) of fluorescein were loaded into hydrogels of pH 5.5, 300 mM. Total release at 37 °C was measured via absorbance after the plateau of release. A linear correlation was found between an increase in the concentration of fluorescein loaded and an increase in fluorescein released (Figure 3.4). Final concentration released was found to increase from 48.02 ± 18.03 μM (non-sheared) and 69.88 ± 32.29 μM (sheared) in gels loaded with 100 μM fluorescein to 458.00 ± 32.14 μM (non-sheared) and 449.30 ± 20.15 μM (sheared) in gels loaded with 1000 μM fluorescein with a linear correlation of $R^2 = 0.98$. This linear correlation is incredibly useful for solute delivery applications because it enables the

necessary loading concentration to easily be calculated when the required dosage is known.

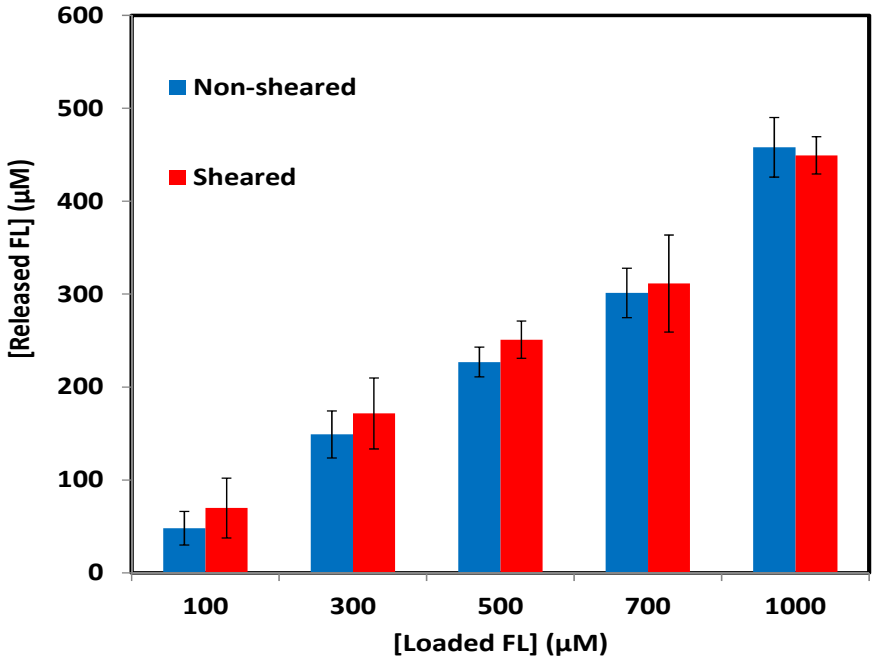

Figure 3.4. Total release of fluorescein from pH 5.5, 300 mM TRIS hydrogels at 37 °C when loaded with 100-1000 µM fluorescein.

3.3.4. BSA release: effect of shearing, hydrogel formulation, loaded concentration and temperature

Large molecules, often proteins and other biologics, are also useful as released agents from hydrogels. In order to examine the release of proteins, BSA –a protein of 66 kDa– was chosen as a large model solute. At room temperature, shearing of the hydrogel material had the opposite effect on this large solute than on the small solute fluorescein (Figure 3.5). At shorter time intervals (< 6 hours), BSA was released less from gels that had been sheared than from gels that had not been sheared. At longer time intervals (24-72 hours), there was no longer a significant difference in BSA release from sheared and non-sheared hydrogels. NaDC/TRIS hydrogels are formed primarily

through hydrophobic interactions and hydrogen bonding. This hydrogel formulation employed an acidic solution (pH 5.5) which may slightly denature BSA. Since BSA has many hydrophobic domains and hydrogen bond donors and acceptors, it is possible that applying a shear force to the gel may have increased protein/hydrogel interaction density. Shearing therefore inhibited initial release of BSA. Similarity of release at longer time intervals further supported the theory that the hydrogel network self-repairs after shearing.

Pharmaceutically relevant concentrations of protein-based drugs are typically between 10 and 100 mg of protein per mL of delivery matrix. For many hydrogel delivery systems, loading such a high concentration of protein is not feasible because drug loading is done through sorption or because such concentrations lead to a reversal of gelation. In the case of this NaDC/TRIS hydrogel system, solute loading occurs concurrently with gelation. Thus, protein is added to the buffer solution before gelator is added and before gelation begins. The result of this concurrent gelation is that high concentrations of protein can be added without disruption of the hydrogel structure. This high loading is of paramount importance to the true applicability of a hydrogel delivery system.

BSA was loaded to 50 mg/mL for examination of its release at 37 °C. It was found that at many time intervals, BSA was released more from gels that had been sheared than from gels that had not been sheared (Figure 3.7). However, at 24 and 72 hours, the release is not significantly different. At room temperature, shearing was found to decrease BSA release. Shearing increased release of BSA at 37 °C, indicating that increased temperature weakened hydrogen bonding sufficiently for BSA release to be

increased. Increased release was due to a more porous hydrogel network as seen in fluorescein release. However, the convergence of release profiles at 24 and 72 hours showed that release was controlled by multiple factors. Reforming of the hydrogel network apparently incorporated some the released BSA back into the hydrogel network (see decreased total release at 24 hours). It can be concluded that the type of hydrogel application (sheared or non-sheared) and the desired time of release should be considered when calculating loading and dosing concentrations for this set of conditions.

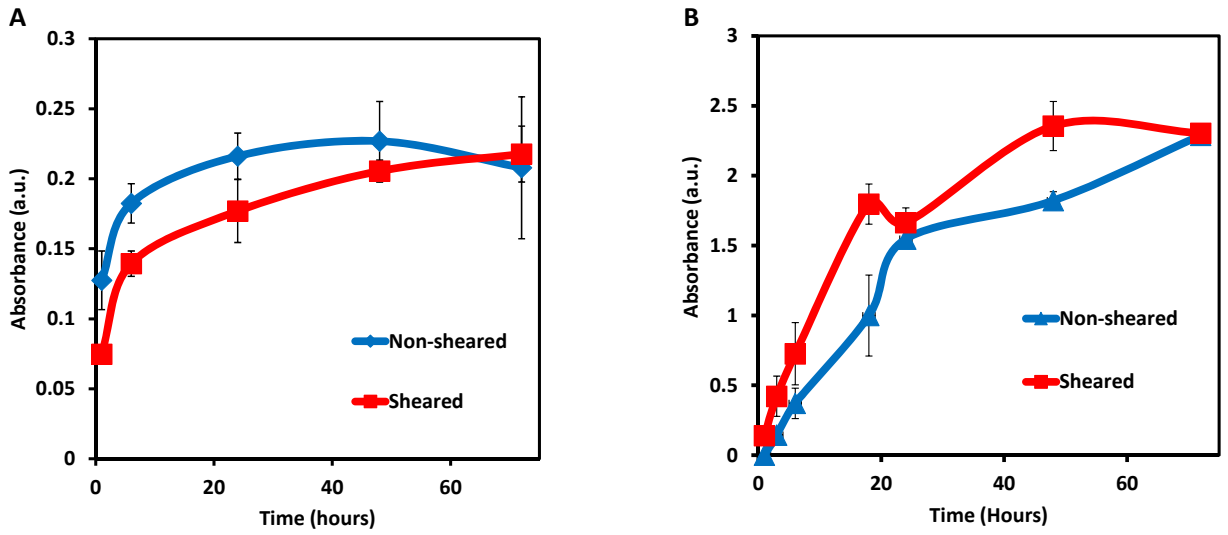

Figure 3.5. Release profiles of BSA from pH 5.5, 300 mM TRIS hydrogels that had and had not been sheared A) Room temperature release (loaded to 1.3 mg/mL) B) 37°C release (loaded to 50 mg/mL).

Three formulations of NaDC/TRIS hydrogels were examined in order to analyze the effect of modification on the release of BSA at room temperature (Figure 3.6A) and at 37 °C (Figure 3.6B). In the case of hydrogels of pH 5.5 with 200 mM TRIS, shearing significantly lowered the amount of BSA released at room temperature. This lower concentration of TRIS resulted in more hydrogen bonding sites for BSA, resulting in

increased effect of shearing. However, hydrogels of pH 5.5 with 250 mM and 300 mM TRIS did not yield a significant difference in BSA release from gels that had and had not been sheared. There is not a direct relationship between BSA released at room temperature and TRIS concentration. Hydrophobic domains and hydrogen bonding sites of BSA interacted with the hydrogel network resulting in a complex release mechanism. Therefore, hydrogel formulation and mode of application must both be considered before calculating solute loading concentrations of large molecules. Tunability of hydrogel formulation may still be utilized in cases where total release is not significantly affected. For example, the mechanical strength of a hydrogel of pH 5.5, 300 mM TRIS may be required for a specific application, while the final release of a pH 5.5, 200 mM TRIS hydrogel is known to be appropriate. In this case, hydrogel formulation can be altered without significantly changing solute release. Thus, the tunability in hydrogel properties, including amount of drug release and sol-gel temperature, can be used to design a hydrogel system which is well-suited to a particular application.

The total amount of BSA released at 37 °C was consistent between formulations and between gels that had and had not been sheared within a formulation. Thus, it is likely that BSA released at 37 °C was primarily diffusion controlled at long time intervals. This consistency in release can be very desirable for clinical application because hydrogel formulation can then be used to tune other properties of the hydrogel (e.g. mechanical strength) without significant impact to drug loading calculations.

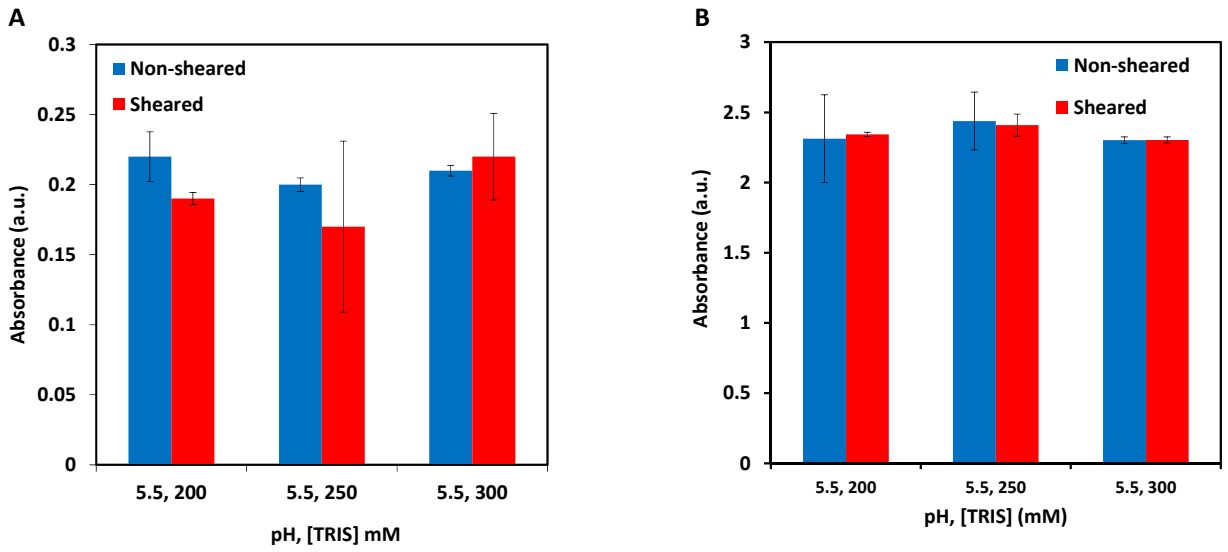

Figure 3.6. Comparison of BSA release from three hydrogel formulations that had and had not been sheared at A) room temperature and B) 37 °C.

Although pharmaceutically relevant concentrations of protein-based drugs are typically between 10-100 mg/mL, sustained release applications for food and agriculture often have substantially lower concentration requirements. For this reason, release profiles at three different concentrations of loaded BSA were examined (Figure 3.7). As

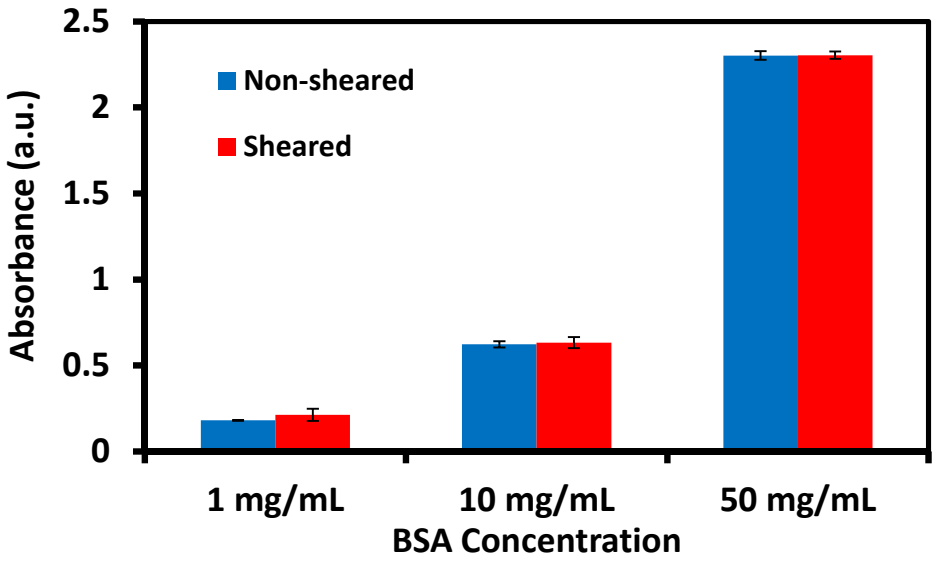

Figure 3.7. Effect of loaded BSA concentration on total release at 37 °C.

was determined with fluorescein, final release of BSA was found to increase with concentration of BSA loaded into the gel. BSA is known to be water soluble up to 40 mg/mL. A similar proportionality between concentration of solute loaded and amount of solute released suggested that solute release is not strongly dictated by solubility. This is an extremely useful property due to the low water solubility of many pharmaceuticals (especially biologics) and other desired solutes.

3.3.5. Release of three proteins at room temperature

Release of three model protein solutes of varied sizes, viz. cytochrome c (12 kDa), α-chymotrypsinogen (25.6 kDa), and transferrin (80 kDa) were analyzed from sheared and non-sheared hydrogels at room temperature. It was found that the effect of shearing a hydrogel varied significantly between different solutes (Figure 3.8). Cytochrome c (12 kDa) and transferrin (80 kDa) exhibited similar release. Sheared and non-sheared hydrogels exhibited significant release of both cytochrome c and transferrin proteins. Release from sheared hydrogels was slightly greater for both proteins. This is comparable to observed BSA release, indicating that protein size is not a primary factor in release. Notably, α-chymotrypsinogen (25.6 kDa) exhibited significantly lower release from non-sheared than from sheared hydrogels. While cytochrome c, transferrin, and (to a lesser extent) BSA are all somewhat water soluble (i.e. 40-200 mg/mL), α-chymotrypsinogen is only sparingly soluble. Therefore, without occurrence of shearing, the hydrogel network was a highly favorable environment for α-chymotrypsinogen. Upon shearing, however, α-chymotrypsinogen exhibited comparable release to other proteins examined. Therefore, in cases where desired solutes are not

water soluble, a sheared application (such as injection) could be used to stimulate release.

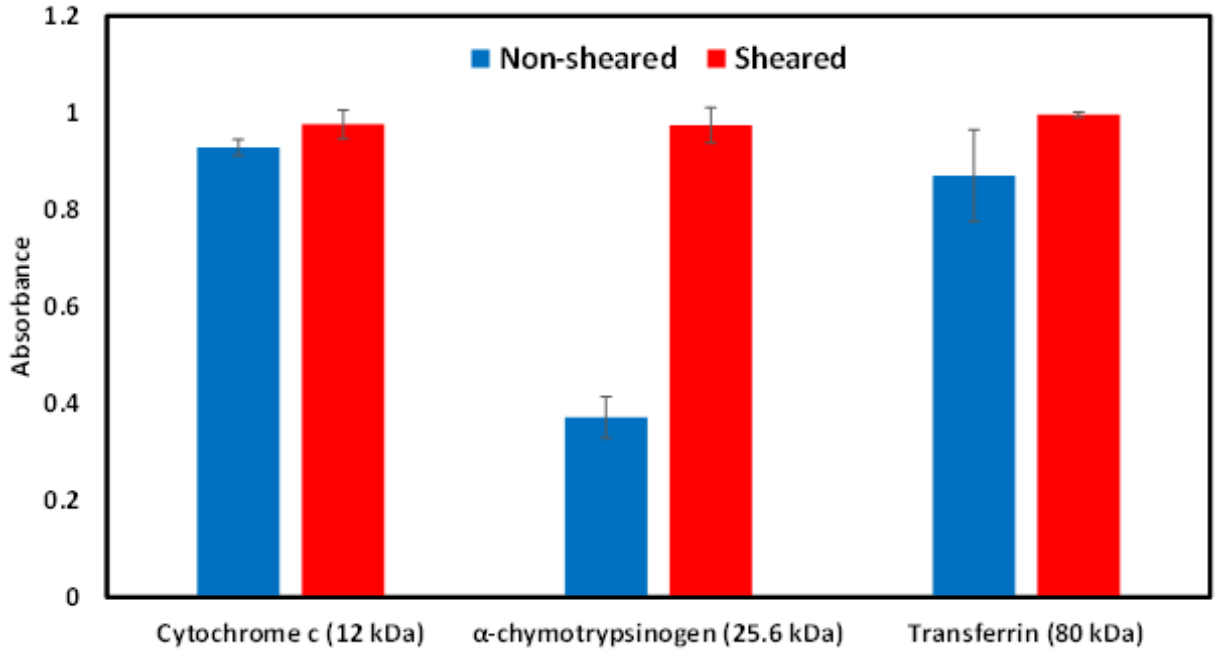

Figure 3.8. Release profiles of cytochrome c (12 kDa), α-chymotrypsinogen (25.6 kDa), and transferrin (80 kDa) from pH 5.5, 300 mM TRIS sheared and non-sheared hydrogels.

3.3.6. Enantio-preferential release of D-tryptophan at 37 °C

NaDC has long been known to form chiral micelles in aqueous solutions.[29,30] Tryptophan was chosen as a model chiral drug for investigating the chirality of NaDC/TRIS hydrogels. Hydrogels loaded with 5 mM L- or D- tryptophan released D-tryptophan with remarkable enantio-preference (Figure 3.9). D-tryptophan was substantially released from the hydrogel, while L-tryptophan had approximately zero release. Complete retention of one enantiomer is immensely desired in the case of molecules with a toxic enantiomer. It is useful to note that the enantio-preference of D-tryptophan released was from the native gel state with no additional chiral selectors or

modifiers. Known chirality of NaDC micelles was therefore retained or enhanced in formation of NaDC/TRIS hydrogels. Net chirality of the hydrogel network thereby facilitated enantio-preferential release of D-tryptophan.

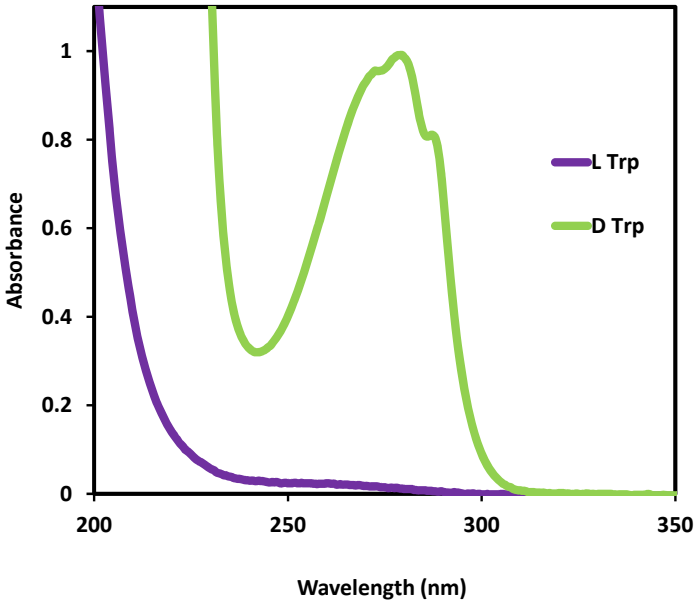

Figure 3.9. Absorbance of L- and D- tryptophan released from a hydrogel system at 37 °C.

3.3.7. Ibuprofen release: effect of loaded concentration and enantio-inversion

In addition to high water content and sustained release properties, hydrogels can also be useful to pharmaceutical applications due to the presence of hydrophobic domains in the hydrogel network. Although the human body is primarily an aqueous environment, most pharmaceuticals are water insoluble. The hydrophobic domains of a hydrogel can help to suspend hydrophobic drugs (if not dissolve them) and prevent crystallization and precipitation. In this regard, hydrogels can enhance bioavailability of drugs.

Ibuprofen, a common chiral analgesic, has very low water solubility (102 μM at 25 °C). Thus, ibuprofen was chosen to demonstrate the compatibility of this enantio-

preferential release system with the inherent benefit of hydrophobic domains in hydrogel delivery systems. Figure 3.10A shows the release of R- and S-ibuprofen at two different concentrations, viz. the maximum water soluble concentration (102 μM) and ten times the maximum water soluble concentration (1020 μM). Despite loaded concentration extending well beyond water solubility, enantio-preference was not lost in ibuprofen release. Chirality of the hydrogel network should be unaffected by loaded ibuprofen. Despite lack of solubility in water, ibuprofen was sufficiently dispersed throughout the hydrogel network to sample network chirality. Preservation of enantio-preferential release well above the level of solubility is of the utmost importance for practical use of NaDC/TRIS hydrogels as enantio-preferential drug delivery vehicles due to the low solubility of many pharmaceuticals.

Perhaps the most significant finding presented here is the ability to invert the enantio-preference of this release system. I found that through the addition of 5 mM γ-cyclodextrin to the hydrogel matrix, enantio-preference was reversed (Figure 3.10B). That is, with the addition of 5 mM γ-cyclodextrin, S-ibuprofen (loaded at 97 μM) was preferentially released. This preference was opposed to the preferential release of R-ibuprofen from the native gel. The amount of R-ibuprofen released from a native gel had an absorbance of 0.44 ± 0.039, whereas release from a gel with 5 mM γCD had an absorbance of 0.27 ± 0.0066. S-ibuprofen was quantitatively opposite. It was released to an absorbance of 0.24 ± 0.021 from a native gel and 0.49 ± 0.0075 from a gel with 5 mM γCD. Since γCD was added to the solution prior to gelation, it is likely incorporated into the hydrogel network upon gelation through hydrogen bonding, hydrophobic interactions, and other non-covalent interactions. Incorporation of γCD seemingly

reversed net chirality of the network in such a manner as to sufficiently reverse enantio-preference. Further investigation of this interesting quantitative similarity of enantiomeric releases may yield more information on the mechanism of the enantio-preferential release process.

Enantio-preference inversion is extremely significant due to the fact that the desired enantiomer may not be the enantiomer released from a native gel. For example, the S enantiomer may be beneficial while the R enantiomer is the one preferentially released. This monumental finding of facile enantio-inversion can greatly reduce the time, cost, and expertise required in the synthesis of enantio-selective drug delivery vehicles. To the best of our knowledge, the simplicity of this inversion is unprecedented.

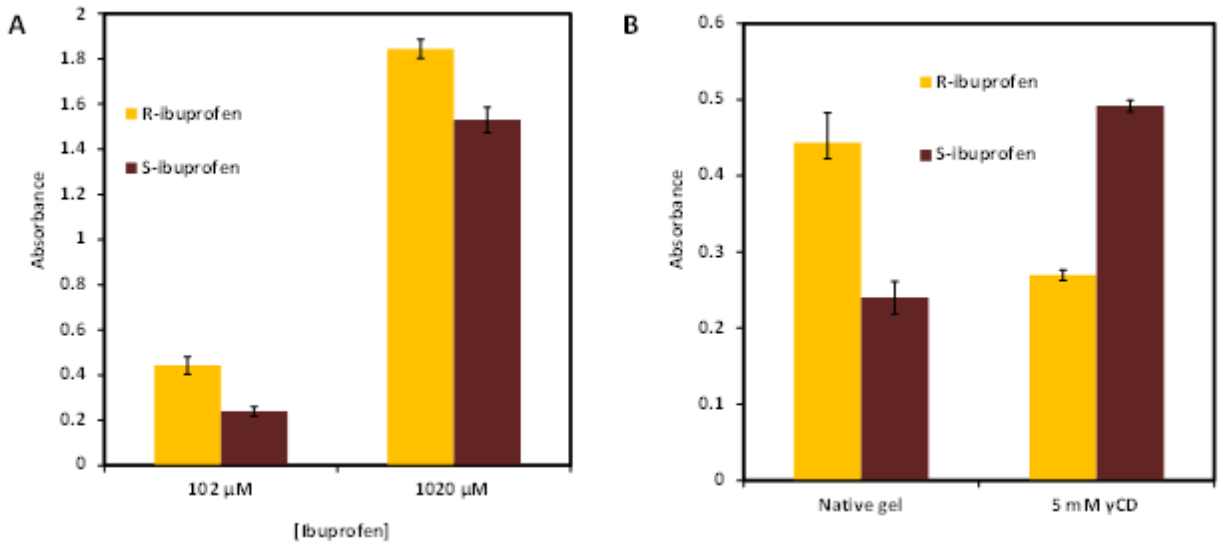

Figure 3.10. Release of ibuprofen at 37 °C. A) Two concentrations: 102 µM (maximum solubility) and 1020 µM (10x maximum solubility). Enantio-preference is retained well above water solubility of ibuprofen. B) Enantio-inversion of release from hydrogels modified with 5 mM γ-cyclodextrin.

3.4. Conclusions

NaDC/TRIS hydrogels were investigated for use as solute delivery vehicles. Temperature, hydrogel formulation, solute loading concentration, solute solubility, time, and application of shear force were all found to be factors in the amount of solute released. Increased temperature was found to reduce differences between release from sheared and non-sheared hydrogels. Hydrogel formulation was found to affect release differently at different temperatures and for different solute sizes. Solute release was found to be linearly proportional to concentration of solute loaded, ideal for calculating dosages. Sodium deoxycholate/TRIS-based hydrogels were also found to be useful as enantio-preferential release systems. With the addition of γ-cyclodextrin to the hydrogel network, I was able to invert enantio-preference: R-ibuprofen was preferentially released from a native gel, while S-ibuprofen was preferentially released from a modified gel. Ergo, the presented hydrogel system has exceptional potential for a wide variety of applications in which one enantiomer is desired over the other. When the inherent benefits of hydrogels are considered with the additional benefits of the presented system, these NaDC/TRIS hydrogels are a significant addition to the current library of solute delivery systems.

3.5. References

1. LinShu, L.; Joseph, K.; Marshall, L. F.; Kevin, B. H., A Review: Controlled Release Systems for Agricultural and Food Applications. In *New Delivery Systems for Controlled Drug Release from Naturally Occurring Materials*, American Chemical Society: 2008; Vol. 992, pp 265-281.

2. Ho, R. J. Y.; Chien, J. Y., Drug delivery trends in clinical trials and translational medicine: Growth in biologic molecule development and impact on rheumatoid arthritis, crohn's disease, and colitis. *Journal of Pharmaceutical Sciences* **2012,** *101* (8), 2668-2674.

3. Warne, N. W., Development of high concentration protein biopharmaceuticals: The use of platform approaches in formulation development. *European Journal of Pharmaceutics and Biopharmaceutics* **2011,** *78* (2), 208-212.

4. He, H.; Cao, X.; Lee, L. J., Design of a novel hydrogel-based intelligent system for controlled drug release. *Journal of Controlled Release* **2004,** *95* (3), 391-402.

5. Solaro, R.; Chiellini, F.; Battisti, A., Targeted delivery of protein drugs by nanocarriers. *Materials* **2010,** *3* (3), 1928-1980.

6. Ganji, F.; Vasheghani-Farahani, E., Hydrogels in controlled drug delivery systems. *Iranian Polymer Journal* **2009,** *18* (1), 63-88.

7. Hoare, T. R.; Kohane, D. S., Hydrogels in drug delivery: Progress and challenges. *Polymer* **2008,** *49* (8), 1993-2007.

8. Oh, J. K.; Drumright, R.; Siegwart, D. J.; Matyjaszewski, K., The development of microgels/nanogels for drug delivery applications. *Progress in Polymer Science* **2008,** *33* (4), 448-477.

9. Jhon, M. S.; Andrade, J. D., Water and hydrogels. *Journal of Biomedical Materials Research* **1973,** *7* (6), 509-21.

10. Kamath, K. R.; Park, K., Biodegradable hydrogels in drug delivery. *Advanced Drug Delivery Reviews* **1993,** *11* (1-2), 59-84.

11. White, E. M.; Yatvin, J.; Grubbs, J. B., III; Bilbrey, J. A.; Locklin, J., Advances in smart materials: Stimuli-responsive hydrogel thin films. *Journal of Polymer Science, Part B: Polymer Physics* **2013,** *51* (14), 1084-1099.

12. Nayak, S.; Kundu, S. C., Sericin-carboxymethyl cellulose porous matrices as cellular wound dressing material. *Journal of Biomedical Materials Research, Part A* **2014,** *102A* (6), 1928-1940.

13. Boucard, N.; Viton, C.; Domard, A., New Aspects of the Formation of Physical Hydrogels of Chitosan in a Hydroalcoholic Medium. *Biomacromolecules* **2005,** *6* (6), 3227-3237.

14. Gough, J. E.; Scotchford, C. A.; Downes, S., Cytotoxicity of glutaraldehyde crosslinked collagen/poly(vinyl alcohol) films is by the mechanism of apoptosis. *Journal of Biomedical Materials Research* **2002,** *61* (1), 121-130.

15. Yin, Y.; Yang, Y.-J.; Xu, H., Hydrophobically modified hydrogels containing azoaromatic cross-links: swelling properties, degradation in vivo and application in drug delivery. *European Polymer Journal* **2002,** *38* (11), 2305-2311.

16. Mullarney, M. P.; Seery, T. A.; Weiss, R., Drug diffusion in hydrophobically modified N, N-dimethylacrylamide hydrogels. *Polymer* **2006,** *47* (11), 3845-3855.

17. Li, Z.; Wen, T.; Su, Y.; Wei, X.; He, C.; Wang, D., Hollow hydroxyapatite spheres fabrication with three-dimensional hydrogel template. *CrystEngComm* **2014,** *16* (20), 4202-4209.

18. Nguyen, L. A.; He, H.; Pham-Huy, C., Chiral drugs: an overview. *International journal of biomedical science: IJBS* **2006,** *2* (2), 85.

19. Chen, J.; Korfmacher, W. A.; Hsieh, Y., Chiral liquid chromatography-tandem mass spectrometric methods for stereoisomeric pharmaceutical determinations. *Journal of Chromatography B* **2005,** *820* (1), 1-8.

20. Martins, L.; Yegles, M.; Chung, H.; Wennig, R., Simultaneous enantioselective determination of amphetamine and congeners in hair specimens by negative chemical ionization gas chromatography–mass spectrometry. *Journal of Chromatography B* **2005,** *825* (1), 57-62.

21. Iwata, Y. T.; Mikuma, T.; Kuwayama, K.; Tsujikawa, K.; Miyaguchi, H.; Kanamori, T.; Inoue, H., Applicability of chemically modified capillaries in chiral capillary electrophoresis for methamphetamine profiling. *Forensic Science International* **2013,** *226* (1), 235-239.

22. Cheong, W. J.; Ali, F.; Choi, J. H.; Lee, J. O.; Sung, K. Y., Recent applications of molecular imprinted polymers for enantio-selective recognition. *Talanta* **2013,** *106*, 45-59.

23. Suedee, R.; Bodhibukkana, C.; Tangthong, N.; Amnuaikit, C.; Kaewnopparat, S.; Srichana, T., Development of a reservoir-type transdermal enantioselective-controlled delivery system for racemic propranolol using a molecularly imprinted polymer composite membrane. *Journal of Controlled Release* **2008,** *129* (3), 170-178.

24. Suedee, R.; Jantarat, C.; Lindner, W.; Viernstein, H.; Songkro, S.; Srichana, T., Development of a pH-responsive drug delivery system for enantioselective-controlled delivery of racemic drugs. *Journal of Controlled Release* **2010,** *142* (1), 122-131.

25. Suksuwan, A.; Lomlim, L.; Rungrotmongkol, T.; Nakpheng, T.; Dickert, F. L.; Suedee, R., The composite nanomaterials containing (R)-thalidomide-molecularly imprinted polymers as a recognition system for enantioselective-controlled release and targeted drug delivery. *Journal of Applied Polymer Science* **2015,** *132* (18).

26. Das, S.; de Rooy, S. L.; Jordan, A. N.; Chandler, L.; Negulescu, II; El-Zahab, B.; Warner, I. M., Tunable size and spectral properties of fluorescent nanoGUMBOS in modified sodium deoxycholate hydrogels. *Langmuir* **2012,** *28* (1), 757-65.

27. McNeel, K. E.; Das, S.; Siraj, N.; Negulescu, I. I.; Warner, I. M., Sodium Deoxycholate Hydrogels: Effects of Modifications on Gelation, Drug Release, and Nanotemplating. *The Journal of Physical Chemistry B* **2015,** *119* (27), 8651-8659.

28. Sun, X.; Xin, X.; Tang, N.; Guo, L.; Wang, L.; Xu, G., Manipulation of the Gel Behavior of Biological Surfactant Sodium Deoxycholate by Amino Acids. *The Journal of Physical Chemistry B* **2014,** *118* (3), 824-832.

29. Reisinger, M.; Lightner, D., Bilirubin conformational enantiomer selection in sodium deoxycholate chiral micelles. *Journal of Inclusion Phenomena* **1985,** *3* (4), 479-485.

30. Xu, F.; Wang, H.; Zhao, J.; Liu, X.; Li, D.; Chen, C.; Ji, J., Chiral packing of cholesteryl group as an effective strategy to get low molecular weight supramolecular hydrogels in the absence of intermolecular hydrogen bond. *Macromolecules* **2013,** *46* (11), 4235-4246.

CHAPTER 4.
NOVEL FLUORESCENCE-BASED RATIOMETRIC NANOSENSOR FOR SELECTIVE IMAGNG OF CANCER CELLS

4.1. Introduction

Extracellular and intracellular pH sensing are important tasks due to fluctuation of pH with conditions such as cancer and bacterial infections. Healthy extracellular pH is generally between 5.5 and 7.4. However, extracellular pH in healthy individuals can be lowered due to renal failure, acidosis, COPD, and many other conditions.[1,2] Intracellular pH is tightly regulated by both normal and cancerous cells with typical values of 7.0-7.4.[3] Therefore, an extracellular pH sensor would be an effective diagnostic tool for pH-affecting conditions. Such pH sensors are also of great importance to agricultural,[4] environmental,[5] biological,[6] and food manufacturing applications. For instance, the dairy industry requires pH sensing for several processes such as to check freshness of milk, bacterial conversion of lactose to lactic acid in yogurt, cheese production, and so on.[7] The importance of pH sensing has led to development of many types of sensors such as potentiometric sensors,[8] electrolyte–insulator–semiconductor sensors,[9] and fluorescent sensors. Fluorescent pH sensors are of particular interest owing to high sensitivity, selectivity, and speed inherent to fluorescence measurements.[10,11] Nanomaterials can be used to enhance many such pH sensors by facilitating manipulation of solubility, fluorescence intensity, and combination of multiple beneficial components.[12] Furthermore, nanoscale pH sensors are important for intracellular pH sensing because they can be used with minimal invasion and can be synthesized in a size-controlled process for optimum cellular uptake.[13]

Common designs of nanoscale fluorescent pH sensors include incorporation of fluorescent moieties into different nanoparticle matrices made up of polymer,[14,15] silica,[16,17] etc. Microemulsion approach has also been applied for formation of pH-sensitive fluorescent nanoparticles.[18] Regardless of the method used to synthesize nanoparticles, several properties are required from an ideal nanoparticle-based pH sensor depending on the application. As an example, for cellular pH sensors, one of the important properties is that the range of pH sensing ability should encompass pH values relevant to the biological systems of interest.[19] Additionally, sensing should not be inhibited by components within the cell, such as calcium and sodium ions.[20] Typical fluorescence-based pH sensing techniques are impacted by variables such as source intensity, photobleaching, and path length of the measurement. These variables require calibration of sensing systems for accurate measurements.[21] The need for calibration is an especially large deficiency for cellular studies due to variation in path length between different parts of the cell and between different cells.[22]

Fluorophores with two emission peaks can be used to overcome calibration needs. Ratiometric responses (i.e. the emission intensity ratio between the two peaks) can be achieved using a single fluorophore with varied acidic and basic emission,[23] two fluorophores that exhibit pH-dependent Förster resonance energy transfer (FRET),[24] or one fluorophore with pH-dependent emission and one fluorophore with pH-independent emission.[25] Ratiometric measurements provide an intrinsic calibration that is inert to typical sensitivities of cellular fluorescent measurements.

Despite many and varied needs for pH sensors, there is still significant need for inexpensive pH sensors with straightforward synthesis.[26] A group of uniform materials

based on organic salts (GUMBOS) are solid phase ionic materials renowned for their tunability and broad applicability, possibly including as pH sensors.[27] Potential GUMBOS applications vary from photosensitizers in solar cells,[28] use in OLEDs,[29] sensing applications,[30,31] cancer treatment,[32] and beyond. In this study, I demonstrate a three-component, nanoscale, fluorescent GUMBOS as a pH sensor probe derived from fluorescein (FL), rhodamine B (RhB), and tetradecyltrihexyl phosphonium ions (P_{66614}), called [P_{66614}][RhB][FL]. Cationic P_{66614} was chosen for its significantly hydrophobic quality that is necessary for nanoparticle formation in aqueous media. Anionic fluorescein and cationic rhodamine B were selected for their satisfactory spectral overlap that is essential for FRET, where fluorescein serves as donor and rhodamine B works as acceptor. Intermolecular distance between donor and acceptor is critical and should be less than 10 nm for efficient FRET.[33] By incorporating these ions into a GUMBOS, the intermolecular distance between donor and acceptor is sufficiently reduced compared to mixing of two separately prepared solutions of fluorescein and rhodamine B. Different FRET efficiencies will result in different ratios of fluorescence emission peaks. Hence, ratiometric analysis can easily be performed on fluorescence emission peaks of [P_{66614}][RhB][FL]. Nanoparticles of [P_{66614}][RhB][FL] yielded an intrinsically calibrated fluorescence method for pH distinction between pH values of 4 and 7. This three-component nanoGUMBOS was also found to be preferentially taken up by cancer cells, providing a fast visual detection method. NanoGUMBOS of [P_{66614}][RhB][FL] are herein characterized and analyzed for use as pH-sensing and cancer imaging agents.

4.2. Materials and methods

4.2.1. Materials

Disodium fluorescein (≥97.5%), rhodamine B (≥95%), and tetradecyltrihexyl phosphonium chloride ([P_{66614}][Cl]) (≥95%) were purchased from Sigma Aldrich and used as received. Dichloromethane (DCM) (≥99.9%) was purchased from Fisher Scientific and used as received. Water used in all experiments is triply deionized (18 MΩ cm) and obtained from an Aries Filterworks high-purity water system.

4.2.2. Synthesis of GUMBOS

[P_{66614}][RhB][FL] GUMBOS was synthesized using a stepwise reaction. Initially, [P_{66614}][FL] GUMBOS was synthesized based on procedure described elsewhere.[34] Thereafter, the required [P_{66614}][RhB][FL] GUMBOS was synthesized by ion exchange. The comprehensive reaction scheme can be found in Figure 4.1. In brief, disodium fluorescein was dissolved in pH 5.5 citrate buffer resulting in a mono-anionic species. In a 1:1.1 molar ratio (P_{66614}:FL), [P_{66614}][Cl] in dichloromethane (DCM) was added to aqueous fluorescein and allowed to stir 48 hours. After stirring, fluorescein could be seen prominently in the DCM layer. Excess fluorescein remained unreacted as evidenced by slight coloration of the water layer. This transfer suggested that fluorescein ionically associated with the phosphonium cation to form a water insoluble salt. The DCM layer was washed several times with water to remove excess unreacted fluorescein and NaCl byproduct. Aqueous rhodamine B was added in a 1.1:1 molar ratio (rhodamine B:[FL][P_{66614}]) and left to stir 48 hours until rhodamine B was no longer prominent in the water layer. The water layer containing unreacted excess rhodamine B

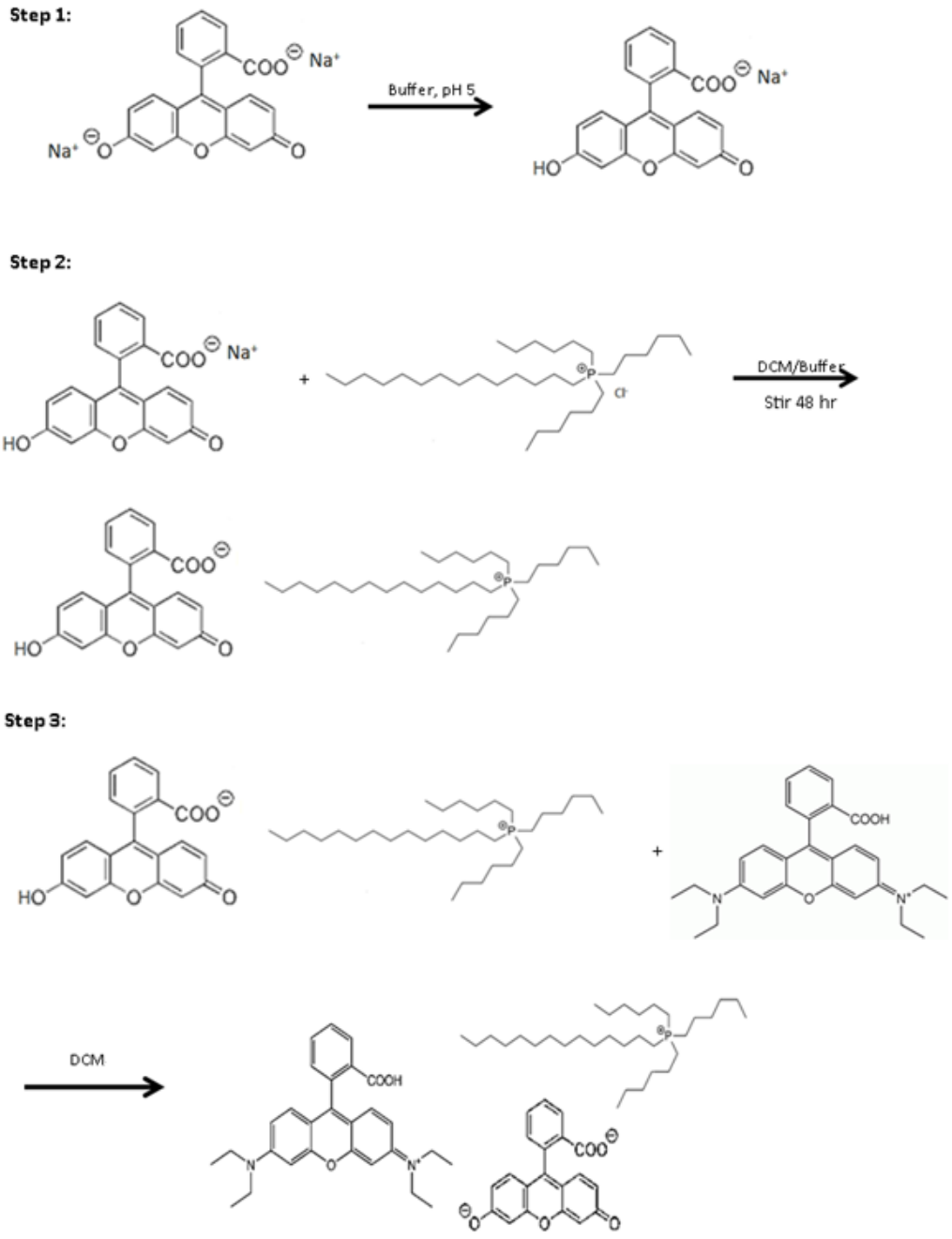

Figure 4.1. Reaction scheme of [P_{66614}][RhB][FL] GUMBOS synthesis. ESI-MS peaks with m/z 331, 443, and 521 confirmed the presence of the three expected components in the final product.

was removed. The DCM layer was washed with water several times to remove any unreacted rhodamine B and byproduct. The final product was obtained by removing

DCM through rotary evaporation. The sample was subsequently lyophilized to remove any water.

Synthesis of $[P_{66614}][RhB][FL]$ GUMBOS was confirmed by Bruker 400 Nanobay NMR (Figure 4.2). Thermal gravimetric analysis was performed using a TA Instruments TGA 2950 (TA Instruments, New Castle, DE).

4.2.3. Synthesis of nanoGUMBOS

NanoGUMBOS were synthesized using a reprecipitation method in which 60 µL of 1 mM ethanolic GUMBOS was added to 3 mL water under sonication. For pH studies, nanoGUMBOS synthesized in water were injected into buffer of desired pH for a final concentration of 2 µM. Size and morphology of resulting nanoGUMBOS were characterized using a JEOL1011CX transmission electron microscope (JEOL USA, Inc., Munich, Germany).

4.2.4. Spectroscopic studies of GUMBOS and nanoGUMBOS

Absorbance studies were performed using a Shimadzu UV-3101PC UV-vis-NIR scanning spectrometer (Shimadzu, Columbia, MD). Quartz cuvettes (Starna cells) with a 0.4 cm path length were used for all spectral analyses. For acquiring absorbance spectra, an identical cell was filled with water or buffer, as the case may be, and used as reference. Fluorescent emission spectra were obtained using a Fluorolog-3 spectrofluorimeter (model FL3-22TAU3; HORIBA Scientific, Edison, NJ) with 1 nm slit widths using right angle geometry.

4.2.5. Cell culture

Normal human breast fibroblast (Hs578BST, ATCC no. HTB-125) and human breast carcinoma (Hs578T, ATCC no. HTB-126) cell lines were obtained from American

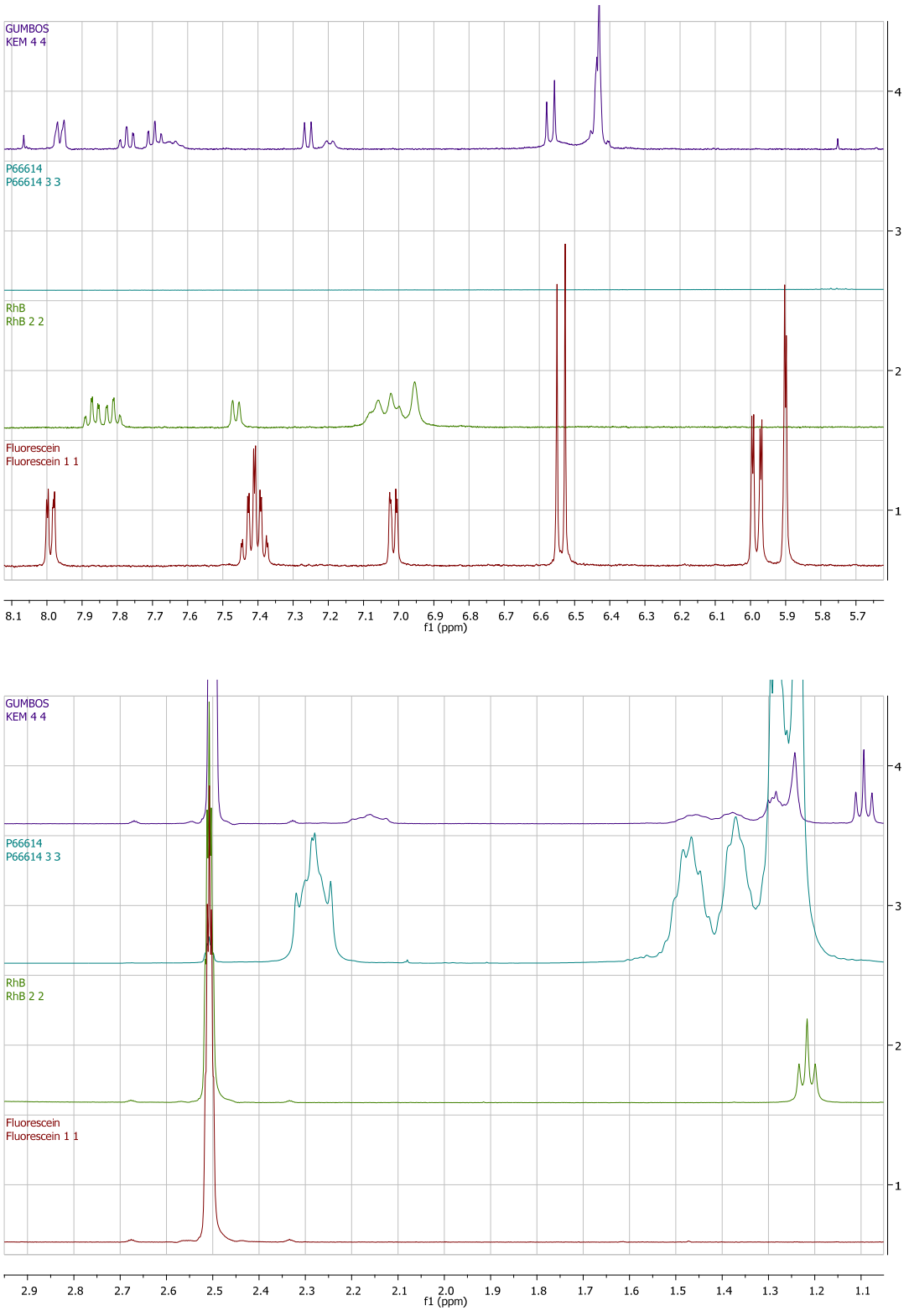

Figure 4.2. NMR comparison (expanded spectra) of [P_{66614}][RhB][FL] GUMBOS with parent compounds (DMSOd6 as solvent).

Type Culture Collection (ATCC, Manassas, VA) and grown to 90% confluence as per the instructions.

4.2.6. Fluorescence microscopy

Five thousand cells of each cell line (normal breast and breast carcinoma) were plated in 3 mL of cell media on a 25 mm glass bottom petri dish (10 mm micro cell; Ashland, MA, USA) and incubated for 24 h. Following incubation, the cell culture media was replaced by cell media containing suspended 25 nM [P_{66614}][RhB][FL] nanoGUMBOS and incubated for an additional 30 min. Fluorescence microscopy images were captured with a 40X dipping objective lens with a TRITC fluorescence filter and DIC polarization. All fluorescence images were captured with a 5000 s exposure time for consistency.

4.3. Results and discussion

4.3.1. Spectroscopic characterization of synthesized GUMBOS

In addition to NMR confirmation and supporting ESI (Figure 4.1 and 4.2), GUMBOS synthesis can be supported by comparing UV-vis absorbance and fluorescence spectra of parent dyes and GUMBOS. The absorbance spectrum of [P_{66614}][RhB][FL] GUMBOS retained all spectral features of parent dyes fluorescein and rhodamine B (Figure 4.3). However, the absorbance of FL at 505 nm is significantly reduced in [P_{66614}][RhB][FL] compared to native FL and shoulders in the absorption spectrum of [P_{66614}][RhB][FL] at approximately 430 and 450 nm were present. Absorbance of [P_{66614}][RhB][FL] between 400 and 520 nm corresponds to the known absorbance spectrum of mixed protolytic forms of FL (viz. cationic, neutral,

monoanionic, and dianionic).[35] Reduced absorbance at 505 nm further supports that multiple FL species (i.e. protolytic forms) exist within the three-component GUMBOS. Absorbance of parent dye RhB was not significantly impacted by incorporation into [P_{66614}][RhB][FL]. Stability of RhB absorbance in [P_{66614}][RhB][FL] indicates that GUMBOS formation is not likely to inhibit FRET acceptance.

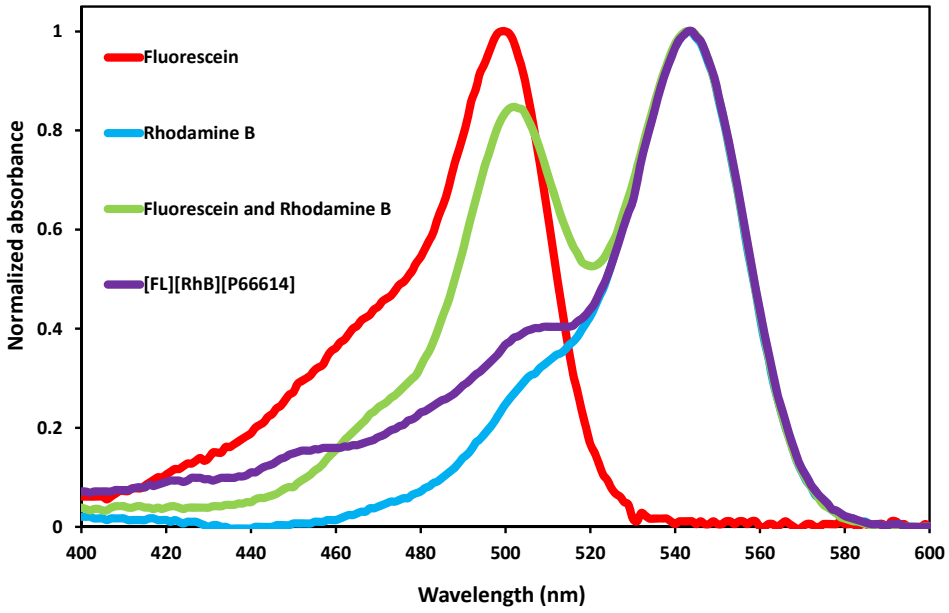

Figure 4.3. Normalized UV-vis absorbance spectra of ethanolic solutions: 10 μM of parent dye rhodamine B, 10 μM of the parent dye fluorescein, a mixture containing 10 μM each of rhodamine B and fluorescein, and 10 μM [P_{66614}][RhB][FL] GUMBOS.

Fluorescence spectroscopy was used to further verify synthesis of [P_{66614}][RhB][FL] GUMBOS (Figure 4.4). Fluorescence emission of individual parent dyes was somewhat affected by the presence of the other fluorophore in solution. That is, a solution with 10 μM each fluorescein and rhodamine B showed fluorescence emission in which the fluorescein peak intensity was slightly quenched while RhB emission was enhanced, indicating a slight occurrence of FRET. Fluorescence emission of the mixture exhibited no peak shift compared to separate fluorophore solutions of 10

μM each. When the two dyes were incorporated into a GUMBOS with P_{66614}, the fluorescence emission peak corresponding to fluorescein was reduced significantly, much more so than in free solution. This reduction in emission is likely due, in part, to reduced absorbance of $[P_{66614}][RhB][FL]$ GUMBOS at the excitation wavelength. Furthermore, emission of $[P_{66614}][RhB][FL]$ at 565 (band corresponding to rhodamine B) was more intense than at 520 nm (band corresponding to fluorescein). The change in intensity ratios suggested that formation of GUMBOS reduced the distance between fluorescein and rhodamine B sufficiently for significant FRET to occur.

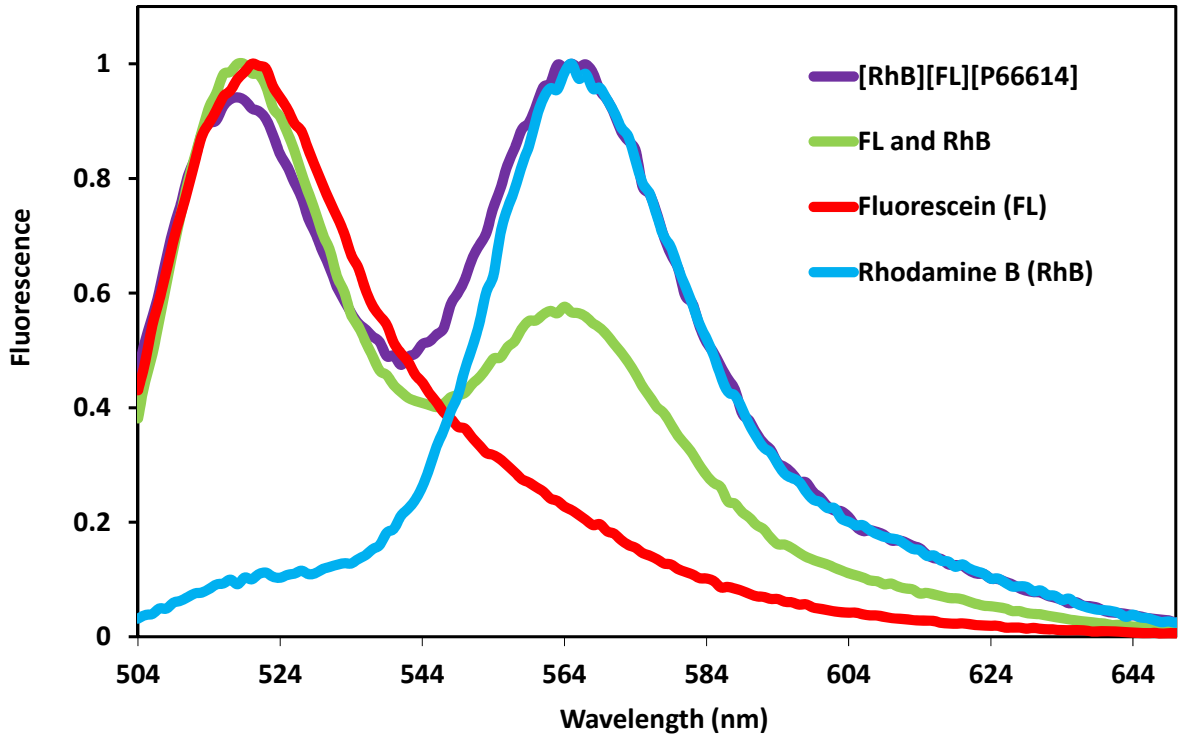

Figure 4.4. Normalized fluorescence spectra of 10 uM ethanolic solutions of fluorescein, rhodamine B, fluorescein and rhodamine B, and $[P_{66614}][RhB][FL]$ GUMBOS. λ_{ex} = 495 nm.

4.3.2. Spectral overlap integral of fluorescein and rhodamine B

In addition to limited spatial distance, another condition for FRET to occur is sufficient spectral overlap between emission spectrum of donor and absorbance

spectrum of acceptor. A high spectral overlap indicates the possibility of high FRET efficiency. Calculation of spectral overlap integral was performed using the following equation:

$$J(\lambda) = \frac{\int_0^\infty \varepsilon(\lambda) f(\lambda) \lambda^4 d\lambda}{\int_0^\infty f(\lambda) d\lambda}$$

where ε is the molar extinction coefficient of acceptor species ($cm^{-1}M^{-1}$), $f(\lambda)$ is the normalized emission intensity of donor, and λ is the wavelength. Fluorescein (donor) and rhodamine B (acceptor) were chosen because they have significant spectral overlap, calculated to be $J(\lambda) = 4.88 \times 10^{15}$ $M^{-1}cm^{-1}nm^4$ under studied experimental conditions (Figure 4.5).

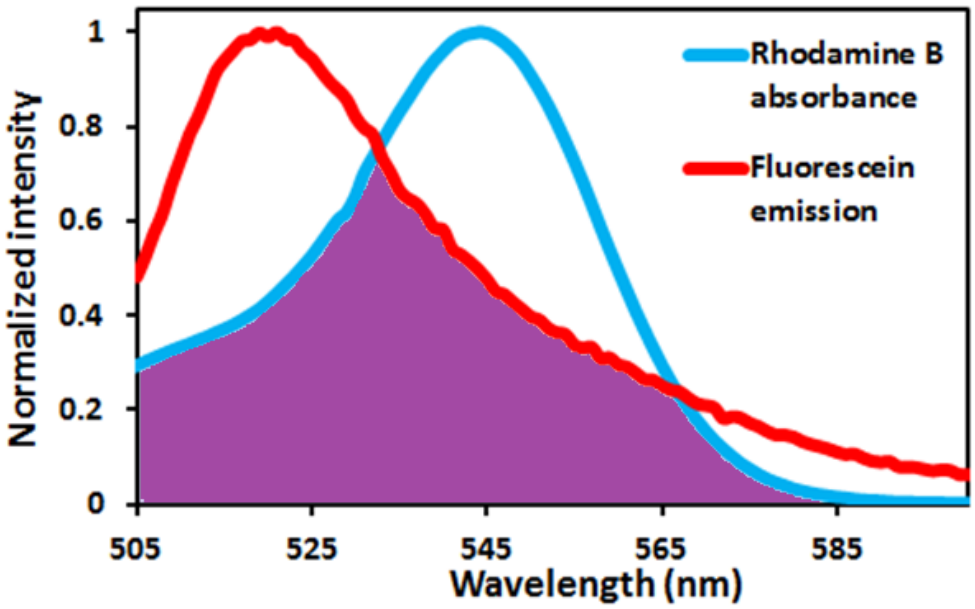

Figure 4.5. Spectral overlap of normalized fluorescein emission and rhodamine B absorbance. Shaded area indicates spectral overlap (J(λ)).

4.3.3. Energy transfer efficiency of [RhB][FL][P_{66614}] GUMBOS

Energy transfer efficiency (E) was calculated using the following equation:

$$E = (1 - \frac{F_{da}}{F_d}) \times 100\%$$

where F_{da} is the fluorescence intensity of donor in presence of acceptor and F_d is the fluorescence intensity of donor in absence of acceptor. E quantifies the percent of energy emitted by donor that is subsequently absorbed by acceptor. A higher value of E indicates a more efficient FRET pair. For calculation of E relevant to this study, ethanolic fluorescein was used for F_d determination, and [P_{66614}][RhB][FL] GUMBOS was used for F_{da} determination. Energy transfer efficiency was calculated to be 66% in [P_{66614}][RhB][FL] GUMBOS, further demonstrating occurrence of FRET.

4.3.4. Spectroscopic analysis of nanoGUMBOS

Spectroscopic analyses were performed on [P_{66614}][RhB][FL] nanoparticles suspended in pure water to understand the formation of nanoGUMBOS and for later comparison with pH-adjusted water. I found that in pure water, the nano[P_{66614}][RhB][FL] absorbance spectrum (Figure 4.6) retained all features of parent dyes. However, the absorbance value was significantly decreased in nanoGUMBOS compared to parent dyes. Decreased and broadened absorbance is not unexpected with nanoparticle formation and can be attributed to aggregation, absence of motional narrowing, and asymmetrical molecular arrangement (lattice disorder).[28,36,37,38]

Fluorescence emission spectra of parent dyes and nanoGUMBOS were obtained with an excitation wavelength of 495 nm, i.e. maximum absorbance of FL, in order for FRET to occur (Figure 4.7). As expected, RhB had a significantly lower fluorescence emission than FL due to low absorbance of RhB at 495 nm. When an aqueous solution containing FL and RhB was excited at this wavelength, FL emission was quenched approximately 9% (from 761,000 to 696,000 a.u.). Emission intensity corresponding to

RhB emission maximum (λ = 575 nm) is apparently enhanced from 25,500 to 91,100 a.u. this emission was purely the sum of molecular fluorescein and rhodamine B

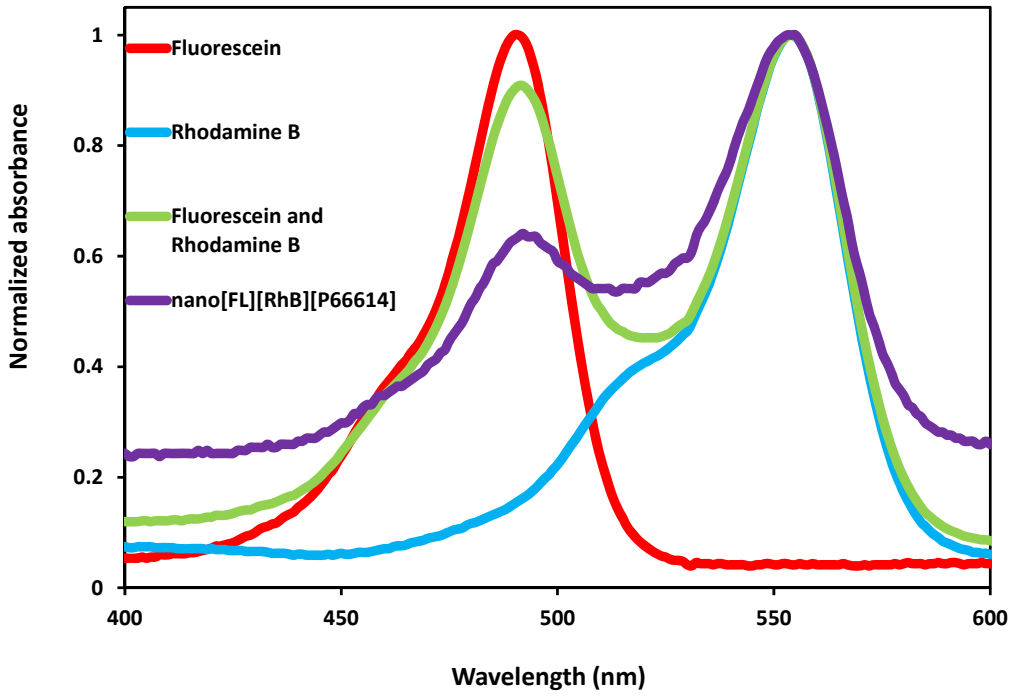

Figure 4.6. Normalized absorbance spectra of aqueous parent dyes fluorescein and rhodamine B in separate solutions, a solution containing both parent dyes, and $[P_{66614}][RhB][FL]$ nanoGUMBOS in water.

emissions. Lack of enhancement in rhodamine B emission suggested that an aqueous solution containing molecular fluorescein and rhodamine B did not undergo significant FRET. It can be discerned that FL and RhB were oriented in aqueous solution in a way that inhibited FRET. NanoGUMBOS suspended in water and excited at 495 nm exhibited significantly decreased fluorescein emission. Fluorescein incorporated into nanoGUMBOS had emission quenched to 78% of fluorescein emission in free solution. Rhodamine B emission was enhanced over 14 fold as a component of nanoGUMBOS (from 25,400 a.u. in free solution to 359,000 a.u. in nanoGUMBOS). Fluorescence of $[P_{66614}][RhB][FL]$ nanoparticles in water also featured a distinct emission band for

rhodamine B emission at 570 nm that was not seen in a solution with a mixture of fluorescein and rhodamine B when excited at 495 nm. Spectral properties thus indicated

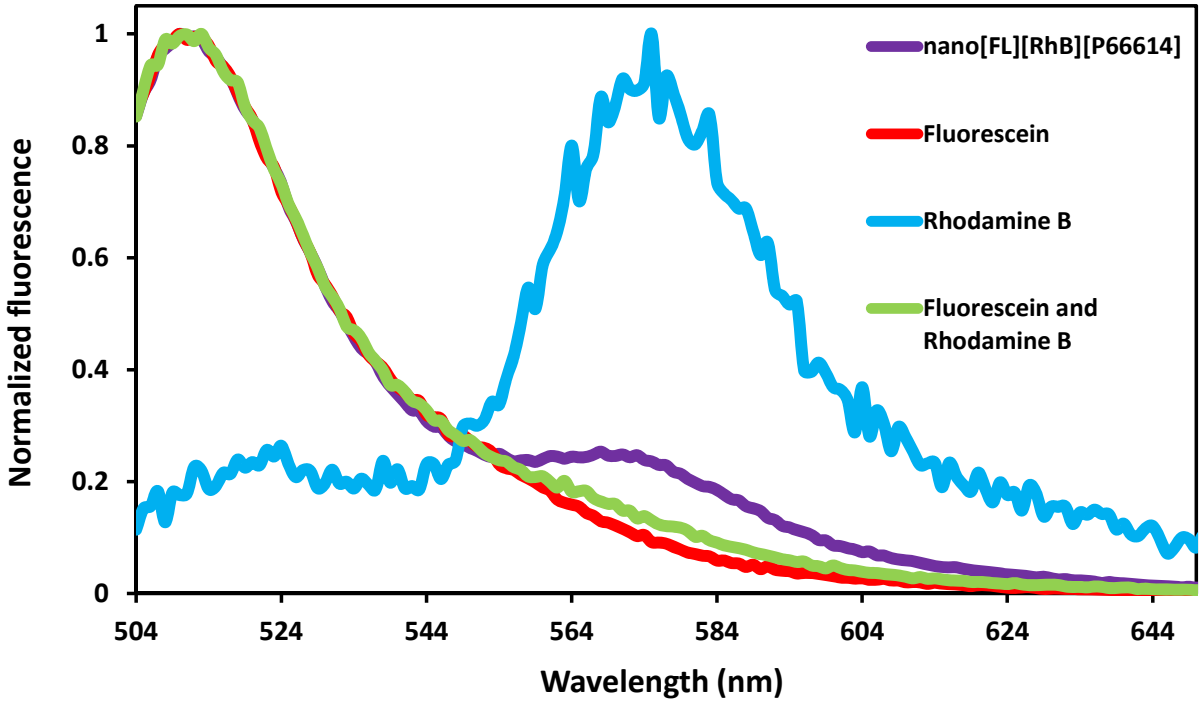

Figure 4.7. Normalized fluorescence emission spectra of aqueous parent dyes fluorescein and rhodamine B in separate solutions, a solution containing both parent dyes, and $[P_{66614}][RhB][FL]$ nanoparticles in water. λ_{ex} = 495 nm.

that in aqueous solutions, nanoparticles of $[P_{66614}][RhB][FL]$ underwent FRET. The occurrence of FRET suggested that this three-component GUMBOS may be suitable as a FRET-based sensor.

4.3.5. Effect of pH on spectral properties of $[P_{66614}][RhB][FL]$ nanoGUMBOS

Absorbance spectra of $[P_{66614}][RhB][FL]$ nanoparticles at a wide range of pH values yielded information about the form of fluorescein present at each pH (Figure 4.8A). The absorbance band at 550 nm corresponds to the rhodamine B component of the nanoGUMBOS and remains largely unchanged across all investigated pH values.

This pattern is comparable to known absorbance properties of molecular rhodamine B.[39] Therefore, any pH-dependent changes in rhodamine B emission can be attributed to association of rhodamine B with fluorescein and P_{66614}. In practical applications of fluorescence-based measurements, a single excitation wavelength with dual emission wavelengths is typically more feasible than a dual excitation wavelength.[40] For this reason, I excited [P_{66614}][RhB][FL] nanoparticles at a single wavelength, viz. 495 nm, and examined resulting emission at seven pH values (Figure 4.8B).

At pH 2, [P_{66614}][RhB][FL] nanoparticles yielded an absorbance band at 437 nm. This band was indicative of cationic fluorescein.[35] Interestingly, [P_{66614}][RhB][FL] nanoparticles at pH 2 did not exhibit any other absorbance bands attributed to fluorescein. This spectrum suggested that at pH 2, cationic fluorescein was the primary species in [P_{66614}][RhB][FL] nanoGUMBOS. The fluorescence emission band of [P_{66614}][RhB][FL] nanoparticles at pH 2 was significantly lower than at other pH values. This low emission was largely due to low absorbance of [P_{66614}][RhB][FL] at the selected excitation wavelength of 495 nm (characteristic of cationic fluorescein). The rhodamine B emission band in nano[P_{66614}][RhB][FL] was significantly higher than in the parent dye alone indicating occurrence of FRET. The fluorescein emission band of nano[P_{66614}][RhB][FL] in pH 2 buffer was approximately 15 nm red-shifted from that of the parent compound. This shift was most likely due to J-aggregation (i.e. head-to-tail stacking).[41]

Absorbance of [P_{66614}][RhB][FL] at pH 4 featured very little indication of fluorescein present. Molecular fluorescein with neutral charge is known to exhibit very low absorbance (relative to charged forms) between approximately 430 and 480 nm.[42]

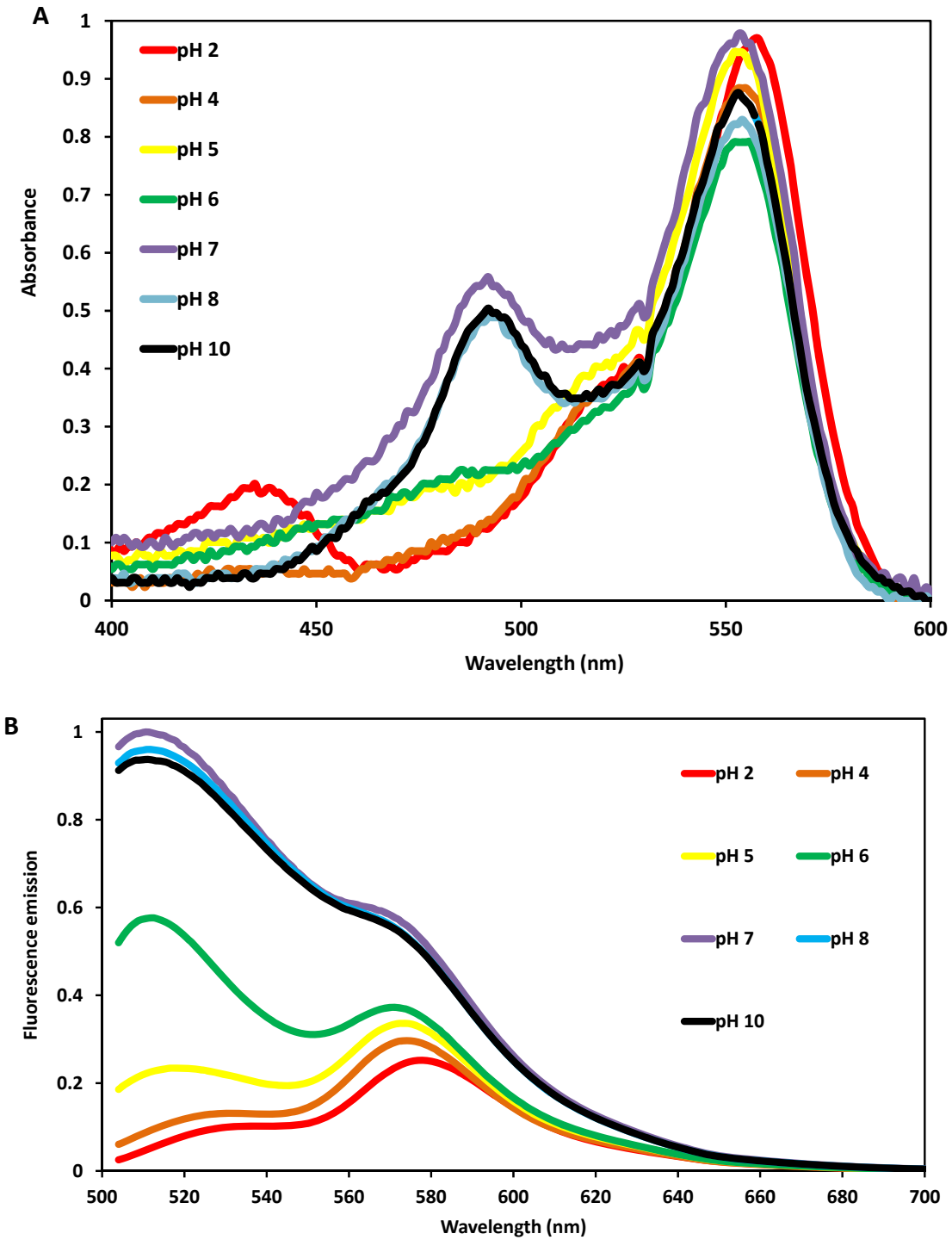

Figure 4.8. Spectral properties of [P_{66614}][RhB][FL] nanoGUMBOS in buffers of seven distinct pH values. A) Absorbance spectra B) Fluorescence emission spectra. λ_{ex} = 495 nm.

There was a broad absorbance band of very low intensity (between 0.05 and 0.1 units) from 460-490 nm that indicated slight absorbance of monoanionic fluorescein. Molecular fluorescein has a pKa of 4.31 for the transition from neutral to monoanionic form. Because pH 4 is close to the pKa of fluorescein it was not unexpected to see spectral contributions from both the neutral and monoanionic species. A previous study by Das et al. also demonstrated stable nanomaterials derived from fluorescein-based ionic materials with multiple protolytic forms of fluorescein present.[34] Emission of nano[P_{66614}][RhB][FL] at pH 4 was comparable to that at pH 2. The fluorescein band was again low intensity and red-shifted compared to the parent dye and to other pH values. Low emission was again due to low absorbance as described earlier.

The [P_{66614}][RhB][FL] nanoparticles absorbed broadly at pH 5. Absorbance was relatively low (viz. between 0.1 and 0.2) and broad across the known absorbance wavelengths of fluorescein. This spectrum and known fluorescein pKa values suggested that at pH 5, monoanionic form of fluorescein was present in nano[P_{66614}][RhB][FL].[43] Fluorescence emission at fluorescein band (515 nm) increased from that of more acidic pH values due to increased absorbance of the monoanionic form and correspondingly higher molar extinction coefficient at the chosen excitation wavelength.[42] Emission at rhodamine B band (575 nm) was also increased from the more acidic environment of pH 2. This emission is not expected to change with pH when excited at 495 nm. Therefore, this increase can be attributed to increased FRET resulting from more intense fluorescein emission. Emission at pH 5 was not significantly shifted from parent compound emission indicating that J-aggregates were not prevalent at this pH. It has

previously been demonstrated that the protolytic form of fluorescein participates in directing prevalence and type of aggregation (i.e. J or H). [34]

The absorbance spectrum of nano[P_{66614}][RhB][FL] at pH 6 was similar in broadness and intensity to the spectrum at pH 5 with two exceptions: At pH 6 there was a slight increase (0.02 units) in the absorbance band at 485 nm and a significant decrease in apparent shouldering from rhodamine B around 510 nm. Fluorescein has a pKa of 6.45 between mono- and di-anionic forms. Proximity of pH 6 to this pKa resulted in multiple fluorescein species as seen in the absorbance spectrum. Emission of nano[P_{66614}][RhB][FL] at pH 6 was significantly higher than at pH 5 for the fluorescein band despite comparable absorbance at the excitation wavelength. Dianionic fluorescein has significantly more intense fluorescence than monoanionic fluorescein.[43] Therefore, increased fluorescence intensity was likely due in part to the presence of dianionic fluorescein in nano[P_{66614}][RhB][FL] at pH 6. The emission band corresponding to rhodamine B was only slightly more intense than that of pH 5. This contrast in spectra strongly suggested that FRET decreased at pH 6. TEM images revealed that at pH 6, nano[P_{66614}][RhB][FL] had slight solubility. Expansion of nanoparticles at this pH increased distance between fluorescein and rhodamine B components to reduce the efficiency of FRET. Decreased FRET would also have contributed to a more intense (less quenched) emission at the fluorescein band.

Spectral properties of nano[P_{66614}][RhB][FL] did not differ significantly between pH values of 7 and 10. Between these pH values, molecular fluorescein remains dianionic. The intense absorbance band at 495 nm indicated that dianionic fluorescein was the primary species present in nanoGUMBOS at these pH values. As predicted,

intense absorbance at the excitation wavelength resulted in significantly more intense fluorescence emission at 510 nm than seen in other pH values. The fluorescence band corresponding to rhodamine B was almost twice the intensity of the band in more acidic environments. However, intensity of rhodamine band was only 60% of the fluorescein band. Varied absorbance of fluorescein within $[P_{66614}][RhB][FL]$ nanoparticles at different pH values and apparent differences in fluorescence intensities suggested that this GUMBOS can be used for pH-dependent emission using a single excitation wavelength.

Ratiometric calculations can be used for intrinsically calibrated determination of pH as previously discussed.[44,45] The ratio of intensities was calculated between 512 nm and 575 nm. As depicted in Figure 4.9, linearity of ratiometric pH response of $[P_{66614}][RhB][FL]$ nanoparticles was between approximate pH values of 5 and 7. This pH

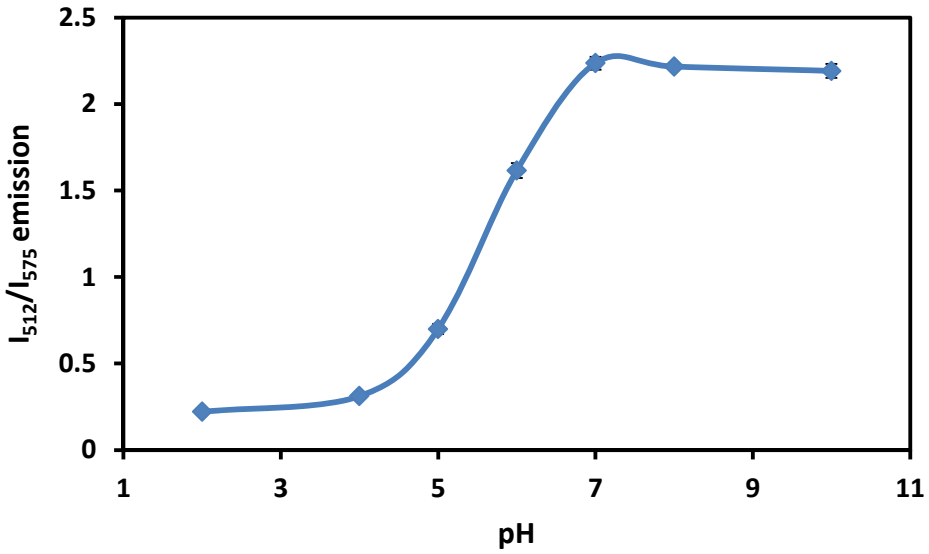

Figure 4.9. Ratio of fluorescence emission intensities at 512 nm and 575 nm. These wavelengths correspond to emission from the fluorescein component and rhodamine B component, respectively.

range aligns well with the desire for cellular pH determination. Ratiometric analysis cannot be used with this material to differentiate pH values between 2 and 4, or between 7 and 10. However, this material can be used for qualitative analysis of pH values lower or higher than the linear range. For example, a ratio of 0.22 could indicate acidity too high for normal cells, but not quantify pH of the cells.

4.3.6. Size analysis of [P_{66614}][RhB][FL] nanoGUMBOS

Nanoparticles derived from [P_{66614}][RhB][FL] were synthesized in pure water using a reprecipitation method. As can be seen from Figure 4.10A, uniform size distribution of nanoparticles with average size 4.4 ± 0.7 nm was observed from TEM micrograph analysis. When these particles were injected into buffer solutions at various pH values, size distribution of nanoparticles was found to differ between different environmental acidities, especially at extreme pH values (viz. 2 and 10). It has previously been shown that both the protolytic form of fluorescein[34] (where applicable) and several types of interactions (covalent and noncovalent)[46] impact molecular arrangement of nanoparticles and can impart pH-induced size changes. At pH 2, molecular fluorescein exists in in the cationic form.[42] [P_{66614}][RhB][FL] nanoparticles injected into pH 2 buffer coalesce into significantly larger particles of 69.7 ± 8.1 nm (Figure 4.10B). Relatively large nanoparticles suggested that presence of cationic fluorescein (as seen in absorbance spectrum, Figure 4.8A) exhibited sufficient repulsion with P_{66614} cations to increase particle size. Such changes in size due to intraparticle interactions with pH were previously described in detail.[34] Despite this significant size and repulsion increase, particles are uniformly sized with spherical shape.

Between pH 4 and 8, [P_{66614}][RhB][FL] nanoparticle size was not significantly altered upon injection into buffer solutions (relative to suspension in water). Nanoparticles at pH 4 were found to be 4.3 ± 0.7 nm (Figure 4.10C). Molecular fluorescein would be neutral at this pH value. The presence of neutral fluorescein species is supported by the absorbance spectrum (Figure 4.8A). Interestingly, no significant size difference was observed at pH 4 compared to pure water. Neutral fluorescein would not be expected to have significant intraparticle repulsion effects with cationic components. Therefore, size preservation further supported the theory that nanoparticle size is partially driven by the protolytic form of fluorescein and the resulting intraparticle interactions.

Between pH values of 5 and 6 molecular fluorescein would be monodeprotonated. Nanoparticles of [P_{66614}][RhB][FL] were found to aggregate into a network of material at these pH values (Figure 4.10D, E). Within many of these networks of material, particles of approximately 4-5 nm were retained. However, boundaries of nanomaterials were indistinct. At these pH values, [P_{66614}][RhB][FL] appeared to be slightly soluble, thereby decreasing nanoparticle stability. A buffer of pH 7 resulted in distinct particles embedded in a network of material (Figure 4.10F). However, at pH 7 particles could be more clearly distinguished from surrounding network than at pH 5 and 6. Average particle size found in the network of pH 7 were found to be 4.2 ± 0.5 nm, statistically equivalent in size to particles in pure water. A pH value of 8 also resulted in particles of similar size and shape (Figure 4.10G) to those formed in pure water (viz. 3.8 ± 0.6 nm). Molecular fluorescein is dianionic at both pH 7 and 8. The two negative charges strongly interacted with cationic rhodamine B and

P_{66614} to retain GUMBOS and nanoparticle association at these pH values. Interestingly, this size stability was not seen at pH 10 (Figure 4.10H). Basic pH 10 resulted in coalescence of [P_{66614}][RhB][FL] nanoparticles into larger particles of 71.0 ± 11.0 nm. The substantial increase in hydroxide ions between a pH 8 solution and a pH 10 solution resulted in a more favorable environment for combination of 4 nm [P_{66614}][RhB][FL] particles into larger diameter particles.

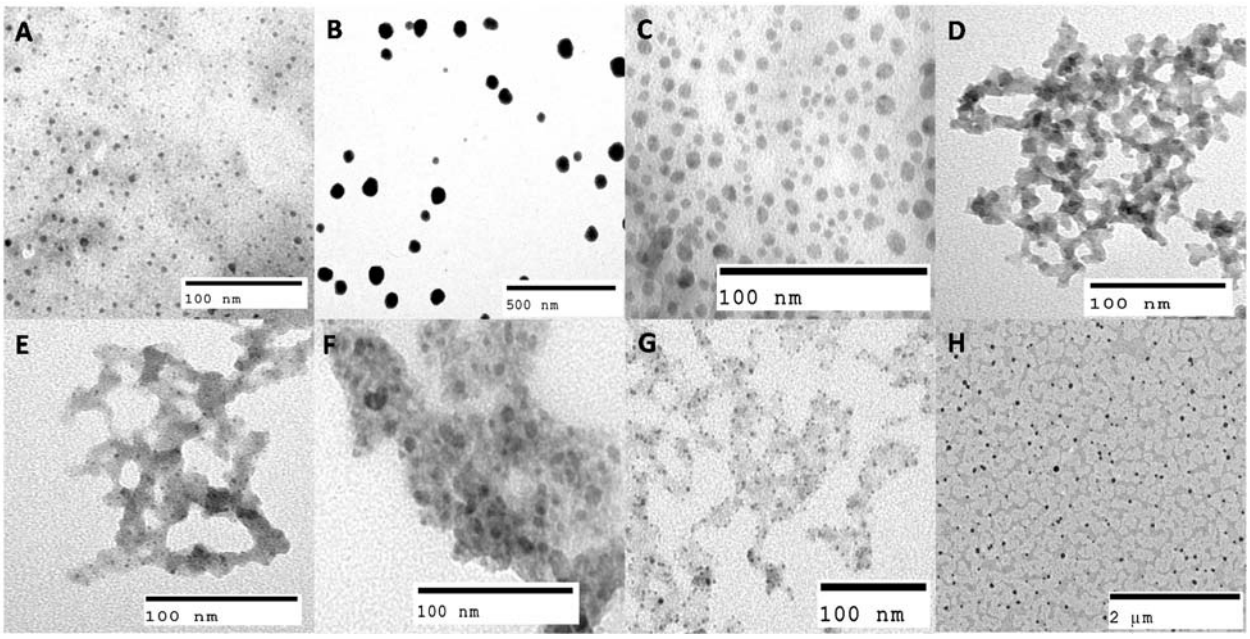

Figure 4.10. TEM micrographs of [P_{66614}][RhB][FL] nanoGUMBOS in A) pure water, B) pH 2, C) pH 4, D) pH 5, E) pH 6, F) pH 7, G) pH 8, H) pH 10.

4.3.7. [P_{66614}][RhB][FL] nanoGUMBOS for fluorescence microscopy imaging of cancer cells

The significant difference between fluorescent peak ratios at pH 5 and pH 7 (0.70 and 2.2, respectively) implied that [P_{66614}][RhB][FL] nanoparticles could be useful for cancer imaging applications. Fluorescence microscopy filters can be selected to pass fluorescein emission and rhodamine B emission separately. In this case, measured intensities (from each filter) can be used to ratiometrically determine pH in situ. This

analysis is strongly beneficial, not only in cancer detection, but for many human conditions involved in pH change (e.g. acidosis).

Two cell lines, normal human breast cells and cancerous human breast cells, were incubated with 25 nM [P_{66614}][RhB][FL] nanoparticles. Control studies were done with equivalent concentrations of parent dyes (Figure 4.11 A-B). Fluorescence microscopy images were obtained using a TRITC filter and a DIC polarizing filter. A clear visual distinction could be made between normal and cancer cells incubated with nano[P_{66614}][RhB][FL] (Figure 4.11C). Cancer cells exhibited intense fluorescence throughout the entirety of the cell, except for the nucleus. Normal cells exhibited significantly less distribution of fluorescence than cancer cells, where only scattered fluorescence can be seen. Studies of parent dye fluorescein showed that incubation in normal and cancer cells both resulted in fluorescence throughout the cell. Studies of parent dye rhodamine B showed that incubation in normal and cancer cells both resulted in localized fluorescence in the nucleus. Comparison of [P_{66614}][RhB][FL] nanoGUMBOS to parent dyes revealed that formation of nanoGUMBOS serviceably causes differentiation of cellular uptake between cancerous and normal cells and, effectually, observed fluorescence. This substantial visual difference indicated that [P_{66614}][RhB][FL] nanoGUMBOS can be useful in imaging of cancer cells, especially due to ease and speed required for visual diagnostic analyses.

4.3.8. Photostability and thermostability of [P_{66614}][RhB][FL]

Photostability is an important characteristic of dyes developed for biomedical imaging.[47,48] High photostability in a material results in longer shelf-life and more

reproducible measurements over time. As depicted in Figure 4.12A, an exceptional photostability of [P_{66614}][RhB][FL] GUMBOS was observed with an increase of 170% over the first 11000 s. From 11000 to 36000 s, photostability was nearly constant at

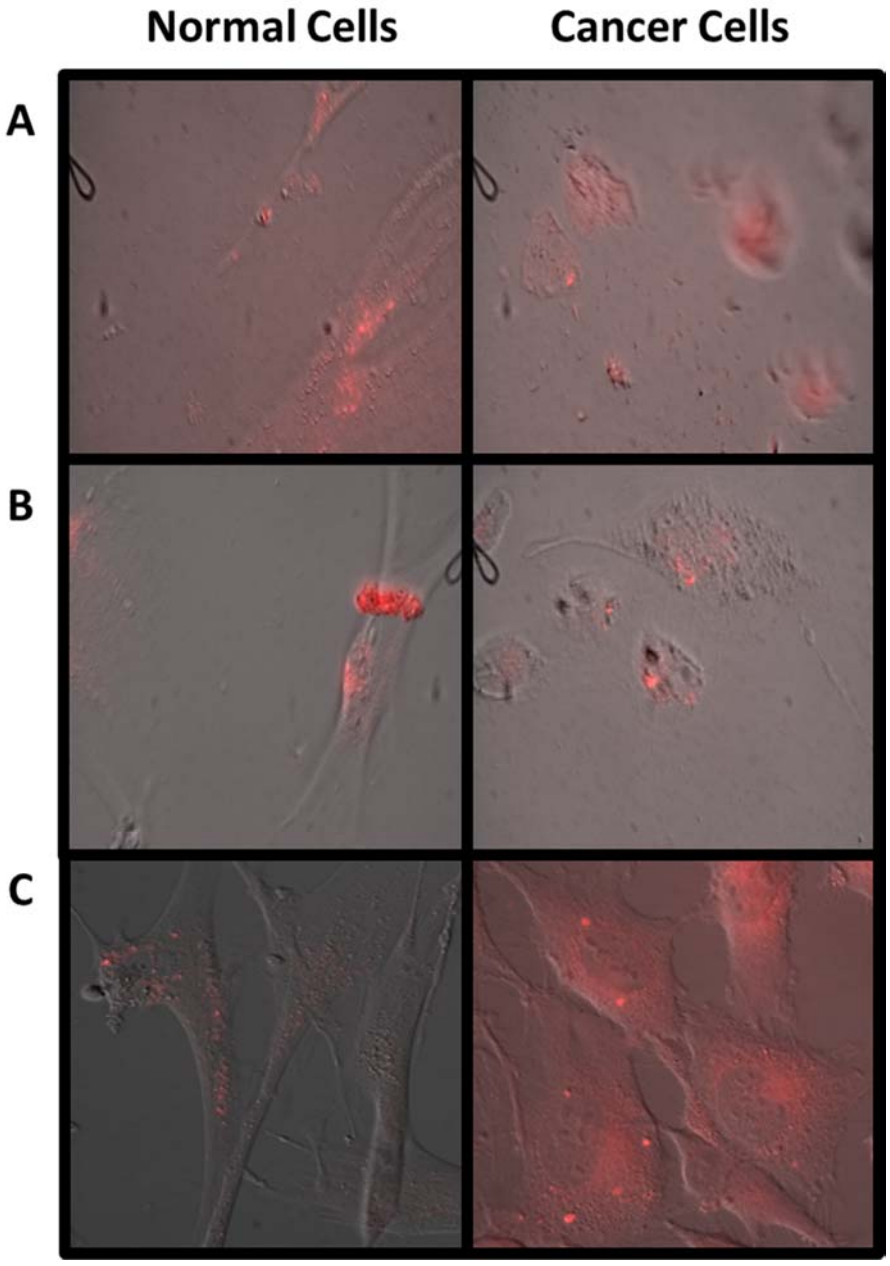

Figure 4.11. Fluorescence microscopy images of 25 nM parent dyes and sensor in normal and cancerous breast cells. All images have TRITC and DIC filters applied for visualization of cells. A) FL, B) RhB, and C) [P_{66614}][RhB][FL] nanoGUMBOS.

170%. Fluorescein was reduced to 74%, and rhodamine B remained at 98% over the same time period (Figure 4.12B). However, the lack of photobleaching in case of RhB is presumably due to insignificant absorbance at the chosen excitation wavelength. Increased photostability was also observed in previous studies where Lu et al. ascribed this increase in photostability to laser-induced J-aggregation.[34,49] This increase in fluorescence emission with light exposure is a strong advantage for practical utility of [P_{66614}][RhB][FL], especially in the case of fluorescence imaging. Thermal stability is another important characteristic of materials exposed to lasers. Bulk [P_{66614}][RhB][FL] was found to be thermally stable (90% weight retention) up to 299 °C (Figure 4.12C).

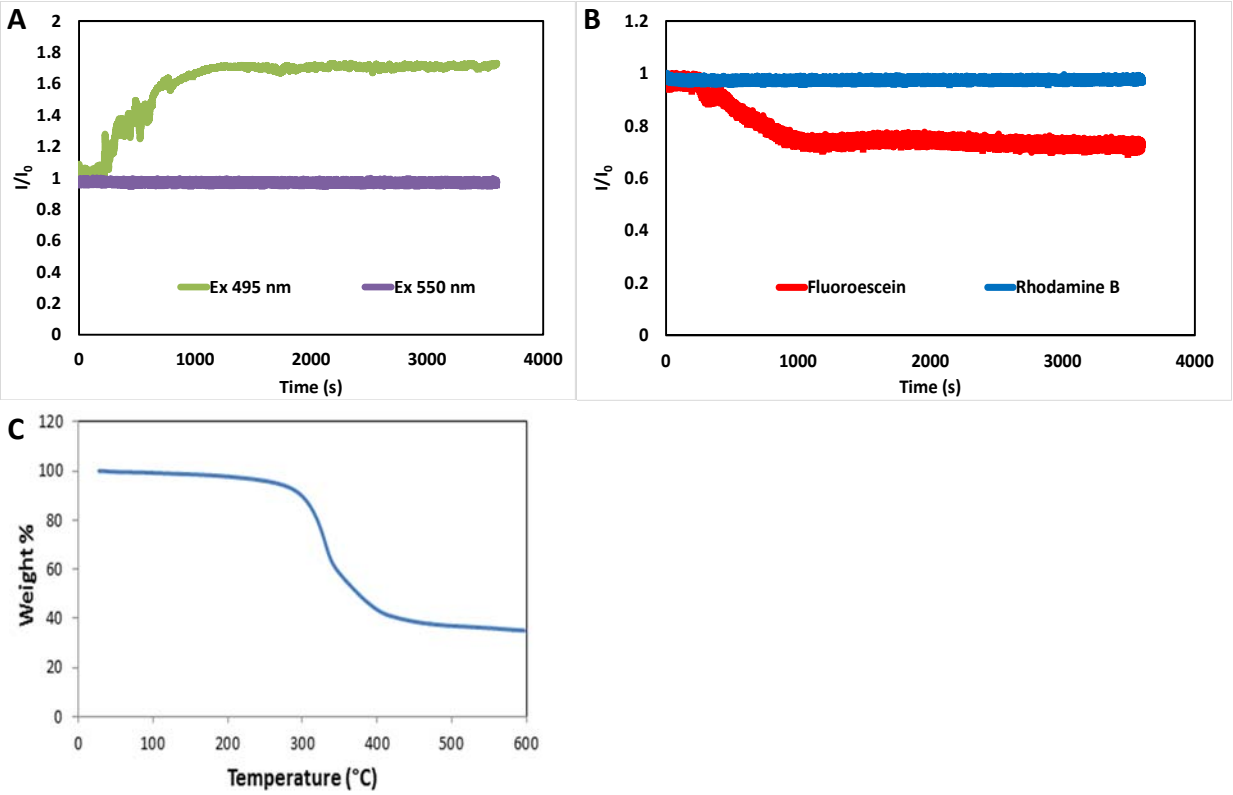

Figure 4.12. Photostability A) fluorescein and rhodamine B (λex=495 nm). B) [P_{66614}][RhB][FL] (λex = 495 nm, 550 nm). C) Thermogravimetric analysis of [P_{66614}][RhB][FL] GUMBOS.

4.4. Conclusions

In this work, I have shown synthesis of [P_{66614}][RhB][FL], a three-component GUMBOS derived from fluorescein, rhodamine B, and tetradecyltrihexyl phosphonium. NanoGUMBOS were found to have consistent size of approximately 4 nm with changes in pH. However, in the case of very acidic or very basic conditions (i.e. pH 2 and 10 respectively), particles were significantly larger (approximately 70 nm). Nano[P_{66614}][RhB][FL] exhibited pH-dependent spectral properties. Absorbance spectra of the nanoGUMBOS indicated that the protolytic form of fluorescein within the nanoparticle corresponded to that of fluorescein in solution. Fluorescence emission of nano[P_{66614}][RhB][FL] exhibited two bands corresponding to fluorescein and rhodamine B. Both bands increased with increasing pH due to enhanced absorbance in more anionic forms of fluorescein and increased FRET, with the exception of pH 6. FRET was slightly decreased at this pH due to slight solubility. Intramolecular FRET yielded a fluorescent peak ratio that varied significantly between pH 5 and pH 7, an essential range for cellular pH sensing. Cancer cells incubated with [P_{66614}][RhB][FL] nanoparticles were found to have a greater selective distribution of fluorescence over normal cells incubated with equivalent experimental conditions. Such differentiation could not be made with equivalently analyzed parent compounds. This visual difference shows incredible potential for use of [P_{66614}][RhB][FL] nanoGUMBOS in visual diagnosis of cancer.

4.5. References

1. Gillies, R. J.; Raghunand, N.; Garcia-Martin, M. L.; Gatenby, R., pH imaging. *Engineering in Medicine and Biology Magazine, IEEE* **2004,** *23* (5), 57-64.

2. Robey, I. F.; Baggett, B. K.; Kirkpatrick, N. D.; Roe, D. J.; Dosescu, J.; Sloane, B. F.; Hashim, A. I.; Morse, D. L.; Raghunand, N.; Gatenby, R. A., Bicarbonate increases tumor pH and inhibits spontaneous metastases. *Cancer Research* **2009,** *69* (6), 2260-2268.

3. Damaghi, M.; Wojtkowiak, J. W.; Gillies, R. J., pH sensing and regulation in cancer. *Frontiers in Physiology* **2013,** *4*, 370.

4. Mahmood, H. S.; Hoogmoed, W. B.; van Henten, E. J., Sensor data fusion to predict multiple soil properties. *Precision Agriculture* **2012,** *13* (6), 628-645.

5. Dutta, S.; Sarma, D.; Nath, P., Ground and river water quality monitoring using a smartphone-based pH sensor. *AIP Advances* **2015,** *5* (5), 057151.

6. Schreml, S.; Meier, R. J.; Weiß, K. T.; Cattani, J.; Flittner, D.; Gehmert, S.; Wolfbeis, O. S.; Landthaler, M.; Babilas, P., A sprayable luminescent pH sensor and its use for wound imaging in vivo. *Experimental Dermatology* **2012,** *21* (12), 951-953.

7. John, G. T.; Goelling, D.; Klimant, I.; Schneider, H.; Heinzle, E., pH-sensing 96-well microtitre plates for the characterization of acid production by dairy starter cultures. *Journal of Dairy Research* **2003,** *70* (03), 327-333.

8. Kang, T.-F.; Xie, Z.-Y.; Tang, H.; Shen, G.-L.; Yu, R.-Q., Potentiometric pH sensors based on chemically modified electrodes with electropolymerized metal-tetraaminophthalocyanine. *Talanta* **1997,** *45* (2), 291-296.

9. Schöning, M. J.; Brinkmann, D.; Rolka, D.; Demuth, C.; Poghossian, A., CIP (cleaning-in-place) suitable “non-glass” pH sensor based on a Ta2O5-gate EIS structure. *Sensors and Actuators B: Chemical* **2005,** *111–112*, 423-429.

10. Gao, F.; Tang, L.; Dai, L.; Wang, L., A fluorescence ratiometric nano-pH sensor based on dual-fluorophore-doped silica nanoparticles. *Spectrochimica Acta Part A: Molecular and Biomolecular Spectroscopy* **2007,** *67* (2), 517-521.

11. Zhang, X.; Jing, S.-Y.; Huang, S.-Y.; Zhou, X.-W.; Bai, J.-M.; Zhao, B.-X., New fluorescent pH probes for acid conditions. *Sensors and Actuators B: Chemical* **2015,** *206*, 663-670.

12. Sapsford, K. E.; Berti, L.; Medintz, I. L., Materials for fluorescence resonance energy transfer analysis: beyond traditional donor–acceptor combinations. *Angewandte Chemie International Edition* **2006,** *45* (28), 4562-4589.

13. Lu, F.; Wu, S. H.; Hung, Y.; Mou, C. Y., Size effect on cell uptake in well-suspended, uniform mesoporous silica nanoparticles. *Small* **2009,** *5* (12), 1408-1413.

14. Zhou, K.; Wang, Y.; Huang, X.; Luby-Phelps, K.; Sumer, B. D.; Gao, J., Tunable, Ultrasensitive pH-Responsive Nanoparticles Targeting Specific Endocytic Organelles in Living Cells. *Angewandte Chemie International Edition* **2011,** *50* (27), 6109-6114.

15. Brasuel, M.; Kopelman, R.; Miller, T. J.; Tjalkens, R.; Philbert, M. A., Fluorescent nanosensors for intracellular chemical analysis: decyl methacrylate liquid polymer matrix and ion-exchange-based potassium PEBBLE sensors with real-time application to viable rat C6 glioma cells. *Analytical Chemistry* **2001,** *73* (10), 2221-2228.

16. Burns, A.; Sengupta, P.; Zedayko, T.; Baird, B.; Wiesner, U., Core/Shell Fluorescent Silica Nanoparticles for Chemical Sensing: Towards Single-Particle Laboratories. *Small* **2006,** *2* (6), 723-726.

17. Gao, F.; Wang, L.; Tang, L.; Zhu, C., A Novel Nano-Sensor Based on Rhodamine-β-Isothiocyanate – Doped Silica Nanoparticle for pH Measurement. *Microchim Acta* **2005,** *152* (1-2), 131-135.

18. Qiao, Y.; Xu, T.; Zhang, Y.; Zhang, C.; Shi, L.; Zhang, G.; Shuang, S.; Dong, C., Green synthesis of fluorescent copper nanoclusters for reversible pH-sensors. *Sensors and Actuators B: Chemical* **2015,** *220*, 1064-1069.

19. Shi, W.; Li, X.; Ma, H., A Tunable Ratiometric pH Sensor Based on Carbon Nanodots for the Quantitative Measurement of the Intracellular pH of Whole Cells. *Angewandte Chemie* **2012,** *124* (26), 6538-6541.

20. Wu, Y.-X.; Zhang, X.-B.; Li, J.-B.; Zhang, C.-C.; Liang, H.; Mao, G.-J.; Zhou, L.-Y.; Tan, W.; Yu, R.-Q., Bispyrene–Fluorescein Hybrid Based FRET Cassette: A Convenient Platform toward Ratiometric Time-Resolved Probe for Bioanalytical Applications. *Analytical Chemistry* **2014,** *86* (20), 10389-10396.

21. Han, J.; Burgess, K., Fluorescent indicators for intracellular pH. *Chemical Reviews* **2009,** *110* (5), 2709-2728.

22. Shaked, N. T.; Rinehart, M. T.; Wax, A., Dual-interference-channel quantitative-phase microscopy of live cell dynamics. *Optics Letters* **2009,** *34* (6), 767-769.

23. Kermis, H. R.; Kostov, Y.; Harms, P.; Rao, G., Dual Excitation Ratiometric Fluorescent pH Sensor for Noninvasive Bioprocess Monitoring: Development and Application. *Biotechnology Progress* **2002,** *18* (5), 1047-1053.

24. Hong, S. W.; Jo, W. H., A fluorescence resonance energy transfer probe for sensing pH in aqueous solution. *Polymer* **2008,** *49* (19), 4180-4187.

25. Wang, X.-d.; Meier, R. J.; Wolfbeis, O. S., Fluorescent pH-Sensitive Nanoparticles in an Agarose Matrix for Imaging of Bacterial Growth and Metabolism. *Angewandte Chemie* **2013,** *125* (1), 424-427.

26. Meier, R. J.; Simbürger, J. M.; Soukka, T.; Schäferling, M., A FRET based pH probe with a broad working range applicable to referenced ratiometric dual wavelength and luminescence lifetime read out. *Chemical Communications* **2015,** *51* (28), 6145-6148.

27. Warner, I. M.; El-Zahab, B.; Siraj, N., Perspectives on Moving Ionic Liquid Chemistry into the Solid Phase. *Analytical Chemistry* **2014**.

28. Jordan, A. N.; Das, S.; Siraj, N.; de Rooy, S. L.; Li, M.; El-Zahab, B.; Chandler, L.; Baker, G. A.; Warner, I. M., Anion-controlled morphologies and spectral features of cyanine-based nanoGUMBOS--an improved photosensitizer. *Nanoscale* **2012,** *4* (16), 5031-8.

29. Siraj, N.; Hasan, F.; Das, S.; Kiruri, L. W.; Steege Gall, K. E.; Baker, G. A.; Warner, I. M., Carbazole-Derived Group of Uniform Materials Based on Organic Salts: Solid State Fluorescent Analogues of Ionic Liquids for Potential Applications in Organic-Based Blue Light-Emitting Diodes. *Journal of Physucal Chemistry C* **2014,** *118* (5), 2312-2320.

30. Regmi, B. P.; Monk, J.; El-Zahab, B.; Das, S.; Hung, F. R.; Hayes, D. J.; Warner, I. M., A novel composite film for detection and molecular weight determination of organic vapors. *Journal of Materials Chemistry* **2012,** *22* (27), 13732-13741.

31. Galpothdeniya, W. I. S.; Regmi, B. P.; McCarter, K. S.; de Rooy, S. L.; Siraj, N.; Warner, I. M., Virtual Colorimetric Sensor Array: Single Ionic Liquid for Solvent Discrimination. *Analytical Chemistry* **2015,** *87* (8), 4464-4471.

32. Magut, P. K. S.; Das, S.; Fernand, V. E.; Losso, J.; McDonough, K.; Naylor, B. M.; Aggarwal, S.; Warner, I. M., Tunable Cytotoxicity of Rhodamine 6G via Anion Variations. *Journal of the American Chemical Society* **2013,** *135* (42), 15873-15879.

33. Saini, S.; Singh, H.; Bagchi, B., Fluorescence resonance energy transfer (FRET) in chemistry and biology: Non-Förster distance dependence of the FRET rate. *Journal of Chemical Sciences* **2006,** *118* (1), 23-35.

34. Das, S.; Magut, P. K.; de Rooy, S. L.; Hasan, F.; Warner, I. M., Ionic liquid-based fluorescein colorimetric pH nanosensors. *RSC Advances* **2013,** *3* (43), 21054-21061.

35. Margulies, D.; Melman, G.; Shanzer, A., Fluorescein as a model molecular calculator with reset capability. *Nature Materials* **2005,** *4* (10), 768-771.

36. An, B.-K.; Kwon, S.-K.; Jung, S.-D.; Park, S. Y., Enhanced emission and its switching in fluorescent organic nanoparticles. *Journal of the American Chemical Society* **2002,** *124* (48), 14410-14415.

37. Eisfeld, A.; Briggs, J. S., The J-band of organic dyes: lineshape and coherence length. *Chemical Physics* **2002,** *281* (1), 61-70.

38. Knapp, E., Lineshapes of molecular aggregates, exchange narrowing and intersite correlation. *Chemical Physics* **1984,** *85* (1), 73-82.

39. Coppeta, J.; Rogers, C., Dual emission laser induced fluorescence for direct planar scalar behavior measurements. *Experiments in Fluids* **1998,** *25* (1), 1-15.

40. Hanson, G. T.; McAnaney, T. B.; Park, E. S.; Rendell, M. E.; Yarbrough, D. K.; Chu, S.; Xi, L.; Boxer, S. G.; Montrose, M. H.; Remington, S. J., Green fluorescent protein variants as ratiometric dual emission pH sensors. 1. Structural characterization and preliminary application. *Biochemistry* **2002,** *41* (52), 15477-15488.

41. Würthner, F.; Kaiser, T. E.; Saha-Möller, C. R., J-Aggregates: From Serendipitous Discovery to Supramolecular Engineering of Functional Dye Materials. *Angewandte Chemie International Edition* **2011,** *50* (15), 3376-3410.

42. Klonis, N.; Sawyer, W. H., Spectral properties of the prototropic forms of fluorescein in aqueous solution. *Journal of Fluorescence* **1996,** *6* (3), 147-157.

43. Sjöback, R.; Nygren, J.; Kubista, M., Absorption and fluorescence properties of fluorescein. *Spectrochimica Acta Part A: Molecular and Biomolecular Spectroscopy* **1995,** *51* (6), L7-L21.

44. Lan, M.; Zhang, J.; Chui, Y.-S.; Wang, P.; Chen, X.; Lee, C.-S.; Kwong, H.-L.; Zhang, W., Carbon nanoparticle-based ratiometric fluorescent sensor for detecting mercury ions in aqueous media and living cells. *ACS Applied Materials and Interfaces* **2014,** *6* (23), 21270-21278.

45. Yang, C. J.; Jockusch, S.; Vicens, M.; Turro, N. J.; Tan, W., Light-switching excimer probes for rapid protein monitoring in complex biological fluids. *Proceedings of the National Academy of Sciences of the United States of America* **2005,** *102* (48), 17278-17283.

46. Min, Y.; Akbulut, M.; Kristiansen, K.; Golan, Y.; Israelachvili, J., The role of interparticle and external forces in nanoparticle assembly. *Nature Materials* **2008,** *7* (7), 527-538.

47. Shaner, N. C.; Steinbach, P. A.; Tsien, R. Y., A guide to choosing fluorescent proteins. *Nature Methods* **2005,** *2* (12), 905-909.

48. Liu, Q.; Guo, B.; Rao, Z.; Zhang, B.; Gong, J. R., Strong two-photon-induced fluorescence from photostable, biocompatible nitrogen-doped graphene quantum dots for cellular and deep-tissue imaging. *Nano Letters* **2013,** *13* (6), 2436-2441.

49. Lu, C.; Das, S.; Magut, P. K.; Li, M.; El-Zahab, B.; Warner, I. M., Irradiation induced fluorescence enhancement in PEGylated cyanine-based NIR nano-and mesoscale GUMBOS. *Langmuir* **2012,** *28* (40), 14415-14423..

Chapter 5.
Conclusions and Future Work

5.1. Conclusions

In this dissertation, I have outlined the development and exploration of sodium deoxycholate(NaDC)/TRIS-based hydrogels and a fluorescein/rhodamine B-based GUMBOS for biomedical applications. In the first chapter, I provide a broad outline of hydrogels including classification and properties and a brief outline of GUMBOS applications. Stimuli-responsive hydrogels and drug delivery applications are discussed, highlighting the idea that each application of hydrogels requires a distinct set of properties: A hydrogel perfectly suited for one application may be useless in another. To this point, I discuss a tunable hydrogel system and its potential for applications.

In the second chapter, NaDC/TRIS hydrogels were modified through changes in pH and [TRIS] of the immobilized solution. It was found that these modifications significantly affected the properties of this system. For example, by increasing [TRIS] the number of hydrogen bonding sites is increased. This resulted in increased crystallinity, mechanical strength, and sol-gel temperature. Structural rigidity of the hydrogel network was also found to be affected by changes in pH. Fewer hydrogen bonding sites are present when above the pKa of NaDC, resulting in lower mechanical strength. Near-IR dyes were used to form GUMBOS. The tunability of these hydrogel materials allowed for tunable synthesis of nanoparticles from these GUMBOS. Especially when coupled with the inherent biocompatibility of hydrogels, this could be particularly useful in imaging applications. Characterization in this chapter can be used to determine the suitability of these materials to a desired application.

In the third chapter of this dissertation, I thoroughly examined the application of solute release. It was found that at room temperature, there is a substantial difference in the amount of solute released from gels that had and had not been sheared. At the physiologically relevant temperature of 37 °C, these significant differences were reduced. This indicates that the mode of delivery must be considered when calculating the dosage of a gel. Hydrogel formulation, loaded solute concentration, solute solubility, and time were also found to impact solute release. Drug release was found to increase linearly with the amount of drug loading, facilitating dosing calculations. NaDC/TRIS-based hydrogels were found to have inherent enantio-preferential release. One enantiomer of model chiral molecules was found to be preferentially released from the hydrogels when loaded in equal amounts in sister samples. This is extremely beneficial for drug delivery applications in which the racemic mixture is commercially available but one enantiomer has unfavorable effects in the body. Through addition of cyclodextrin, enantiopreferential inversion was possible. This is exceptionally important in cases where the less desirable enantiomer is released by the native gel. In conjunction with the inherent biocompatibility of hydrogels and the tunability of this system, native enantioselectivity provides great potential for the use of these hydrogels in drug delivery applications.

In the fourth chapter of this dissertation I explored synthesis, characterization, and potential applications of a three-component nanoGUMBOS, nano[P_{66614}][RhB][FL]. NanoGUMBOS were uniform in size between pH values of 4 and 8 after facile synthesis. Fluorescein and rhodamine B components of the nanoGUMBOS contributed to pH-dependent spectral properties. Two fluorescence emission bands were observed

and increased in intensity with increasing pH due to the protolytic forms of fluorescein and rhodamine B components. Intramolecular FRET resulted in ratiometric differences between the emission bands at varied pH levels. Significant ratiometric variation was found between pH values of 5 and 7, a range highly relevant for cellular pH. In vitro fluorescence microscopy revealed that cancer cells incubated with nano[P_{66614}][RhB][FL] had significantly greater fluorescence distribution than normal cells incubated equivalently. Such obvious visual differentiation indicates pronounced potential for use of these nanoGUMBOS in visual cancer diagnosis.

5.2. Future work

Thus far, the potential of these hydrogel materials for use in drug delivery applications has been discussed at length. However, several more studies must be performed before their clinical use. Toxicity studies will be critical to ensure successful use. The components of the hydrogels are deoxycholate (a bile acid), TRIS (a medically used buffer), and water. Thus, toxicity is expected to be very low. One potential concern is the surfactant properties of deoxycholate. However, it is anticipated that the assembly of a gel network will prevent surfactant action. Biodegradation studies will also be required before clinical application of NaDC/TRIS hydrogels. Particularly due to the absence of polymers and the natural presence of deoxycholate in the body, I anticipate that biodegradation will occur acceptably. Finally, in vivo studies will need to be performed. Drug release profiles may be affected by substituents in the body and therefore need to be analyzed thoroughly before being used pharmaceutically.

Several modes of delivery were discussed in this work. Future work could include exploration of nanogels as delivery systems. As the name suggests, nanogels are

crosslinked (physically in this case) networks on the nanoscale. They typically retain the beneficial properties of macroscale hydrogels with the additional benefits of bioavailability. For example, nanogels can be used to transport drugs to difficult places such as across the blood brain barrier. There are currently many methods for synthesis of such materials, so it is expected that a suitable method could be found to further enhance these tunable materials.

Drug delivery was a focus of this dissertation, but it is important to note that hydrogels can be applied in a wide variety of fields. Especially due to the tunability of this system, several applications can be explored in the future. Hydrogels can be used in sensing applications, for example. I have shown that these materials are sensitive to their environment, can be loaded with many different solutes of different sizes and properties, and are highly tunable in mechanical strength, crystallinity, and other properties. This is strong evidence that they may be used effectively in sensing applications. The biocompatibility and ability to load solutes easily also suggest that they may be useful in imaging applications. Whether in drug delivery, sensing, or imaging, future work on NaDC/TRIS hydrogels can involve the choosing of a specific application. When a desired application is specifically defined, the hydrogels can be tuned to fit the requirements of that particular application.

Due to the high potential for nano[P_{66614}][RhB][FL] to be used in cancer diagnoses, future work should be aimed at further understanding the uptake properties and development of this approach for clinical applications. Primary efforts should be towards analysis of pH within the cells and in media surrounding the cells. Such analysis could significantly further the diagnostic ability of this material. Uptake

mechanism and cytotoxicity studies may reveal further uses of nano[P_{66614}][RhB][FL]. Synthesis of nano[P_{66614}][RhB][FL] was demonstrated to be facile at small scale. However, for commercial use, scalability studies should be performed. While photostability and thermostability were found to be favorable, practical storage and shelf-life studies should be performed for better stability understanding.

APPENDIX: LETTERS OF PERMISSION

Title of publication: *Sodium Deoxycholate Hydrogels: Effects of Modifications on Gelation, Drug Release, and Nanotemplating*

Authors: Kelsey E. McNeel, Susmita Das, Noureen Siraj, Ioan I. Negulescu, Isiah M. Warner

Publication: The Journal of Physical Chemistry B

Publisher: American Chemical Society, Copyright 2015.

RE: Permission request confirmation

E EIC Office Journal of Physical Chemistry <eic@jpc.acs.org> Reply all

Mon 10/9, 8:54 AM

Kelsey McNeel

Inbox

Dear Kelsey:

Permission is granted with the understanding that the appropriate citations of the published work must be made.

Sincerely,
Davine for
George C. Schatz
Editor-in-Chief

From: Kelsey McNeel [mailto:kem07f@my.fsu.edu]
Sent: Sunday, October 08, 2017 7:06 PM
To: EIC Office Journal of Physical Chemistry <eic@jpc.acs.org>
Subject: Permission request confirmation

Dear Dr. Schatz,

In accordance with the ACS blanket permission guidelines, I am writing to request that you confirm permission for me to use my previously published article:

McNeel, K. E.; Das, S.; Siraj, N.; Negulescu, I. I.; Warner, I. M., Sodium Deoxycholate Hydrogels: Effects of Modifications on Gelation, Drug Release, and Nanotemplating. *The Journal of Physical Chemistry B* **2015**, *119* (27), 8651-8659

in my PhD dissertation. It will be reproduced in whole and will be available online. It will be included following the ACS requirements.

Thank you, and please let me know if you need any further information from me.

Title of publication: *Sodium deoxycholate/TRIS-based hydrogels for multipurpose solute delivery vehicles: Ambient release, drug release, and enantiopreferential release*

Authors: Kelsey E. McNeel, Noureen Siraj, Ioan I. Negulescu, Isiah M. Warner

Publication: Talanta

Publisher: Elsevier

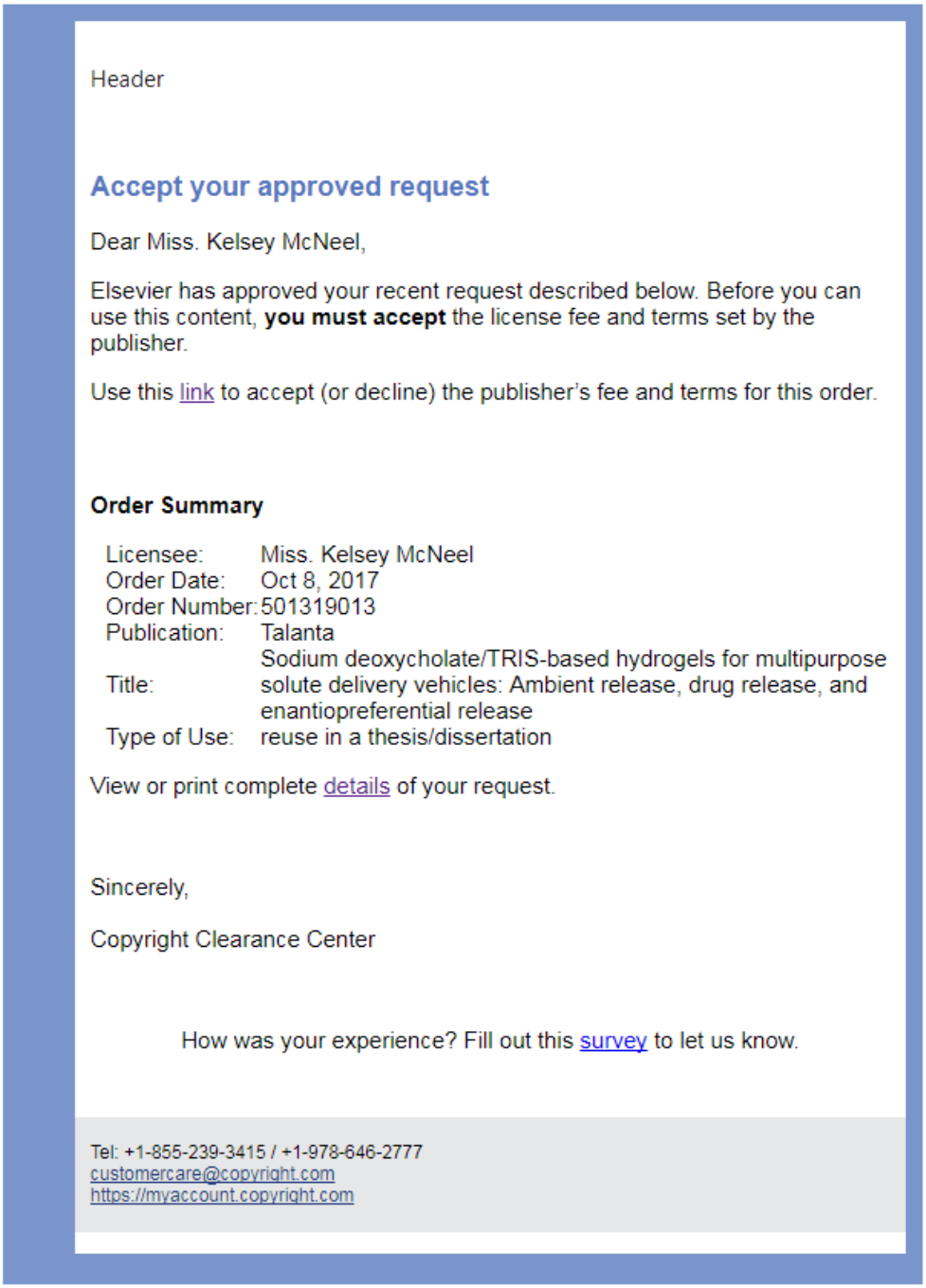

Header

Accept your approved request

Dear Miss. Kelsey McNeel,

Elsevier has approved your recent request described below. Before you can use this content, **you must accept** the license fee and terms set by the publisher.

Use this link to accept (or decline) the publisher's fee and terms for this order.

Order Summary

Licensee:	Miss. Kelsey McNeel
Order Date:	Oct 8, 2017
Order Number:	501319013
Publication:	Talanta
Title:	Sodium deoxycholate/TRIS-based hydrogels for multipurpose solute delivery vehicles: Ambient release, drug release, and enantiopreferential release
Type of Use:	reuse in a thesis/dissertation

View or print complete details of your request.

Sincerely,

Copyright Clearance Center

How was your experience? Fill out this survey to let us know.

Tel: +1-855-239-3415 / +1-978-646-2777
customercare@copyright.com
https://myaccount.copyright.com

VITA

Kelsey Elizabeth McNeel was born in Las Vegas, Nevada where she attended Elbert B. Edwards, Selma F. Bartlett, and Nate Mack Elementary Schools before moving to Palmdale, California where she attended Ana Verde Plaza for middle school. At Ana Verde, Kelsey was fortunate to be taught by Karyl Bruhn, a woman who expanded Kelsey's way of thinking in a way critical to her current success. In 2007, Kelsey graduated from Countryside High School in Clearwater, Florida. She earned her Bachelor of Science with Honors (Cum Laude) with a major in Biochemistry and a minor in Biology from Florida State University in 2011. For her sophomore and junior years as an undergraduate, Kelsey was a resident assistant. This was a pivotal experience for her communication, relationship building, and leadership skills. Kelsey also had the opportunity to do research for Dr. Andre Striegel. This opportunity shaped her as a researcher and prepared her for success in graduate work. Kelsey began her graduate studies in 2011 at Louisiana State University on the Board of Regents Fellowship, where Prof. Isiah Warner provided support and guidance as her adviser. With his mentorship, Kelsey honed experimental design, problem solving, and mentorship skills. As a culmination of these experiences, Kelsey plans to graduate with a Doctor of Philosophy from Louisiana State University in 2018.